

UNIVERSIDADE FEDERAL DE SANTA CATARINA
DEPARTAMENTO DE ENGENHARIA MECÂNICA

Thiago de Jesus de Araujo Rios

**DEVELOPMENT OF A FUEL-SAVING
ALGORITHM FOR A VEHICLE'S DRIVER
ASSISTANT SYSTEM**

Florianópolis

2018

Thiago de Jesus de Araujo Rios

**DEVELOPMENT OF A FUEL-SAVING ALGORITHM FOR A
VEHICLE'S DRIVER ASSISTANT SYSTEM**

Dissertação submetida ao Programa de Pós-Graduação em Engenharia Mecânica para a obtenção do Grau de Mestre em Engenharia Mecânica.

Orientador: Prof. Henrique Simas, Dr. Eng.

Coorientador: Prof. Lauro Cesar Nicolazzi, Dr.Eng.

Florianópolis

2018

Ficha de identificação da obra elaborada pelo autor,
através do Programa de Geração Automática da Biblioteca Universitária da UFSC.

Rios, Thiago de Jesus de Araujo
DEVELOPMENT OF A FUEL-SAVING ALGORITHM FOR A
VEHICLE'S DRIVER ASSISTANT SYSTEM / Thiago de Jesus
de Araujo Rios ; orientador, Henrique Simas,
coorientador, Lauro Cesar Nicolazzi, 2018.
163 p.

Dissertação (mestrado) - Universidade Federal de
Santa Catarina, Centro Tecnológico, Programa de Pós
Graduação em Engenharia Mecânica, Florianópolis, 2018.

Inclui referências.

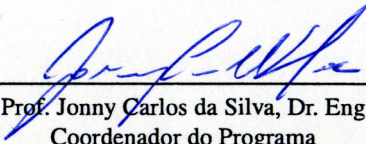
1. Engenharia Mecânica. 2. Dinâmica Veicular. 3.
Controle Automotivo. 4. Otimização. 5. Redes Neurais
Artificiais. I. Simas, Henrique . II. Nicolazzi,
Lauro Cesar . III. Universidade Federal de Santa
Catarina. Programa de Pós-Graduação em Engenharia
Mecânica. IV. Título.

Thiago de Jesus de Araujo Rios

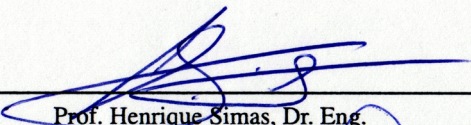
**DEVELOPMENT OF A FUEL-SAVING ALGORITHM FOR A
VEHICLE'S DRIVER ASSISTANT SYSTEM**

Esta Dissertação foi julgada aprovada para a obtenção do Título de "Mestre em Engenharia Mecânica", e aprovada em sua forma final pelo Programa de Pós-Graduação em Engenharia Mecânica.

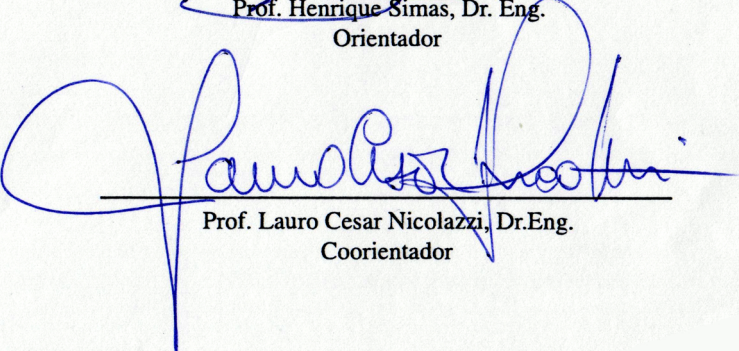
Florianópolis, 07 de Maio de 2018.



Prof. Jonny Carlos da Silva, Dr. Eng
Coordenador do Programa




Prof. Henrique Simas, Dr. Eng.
Orientador

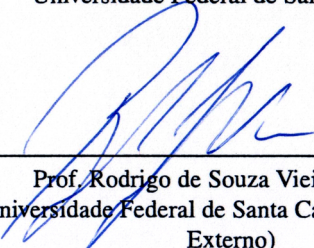


Prof. Lauro Cesar Nicolazzi, Dr.Eng.
Coorientador

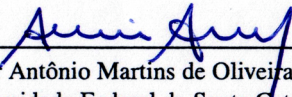
Banca Examinadora:



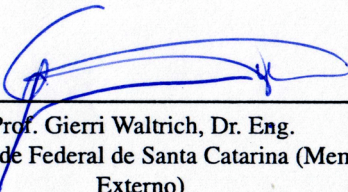
Prof. Henrique Simas, Dr. Eng.- Presidente
Universidade Federal de Santa Catarina



Prof. Rodrigo de Souza Vieira, Dr. Eng
Universidade Federal de Santa Catarina (Membro
Externo)



Prof. Amir Antônio Martins de Oliveira Jr., Ph.D.
Universidade Federal de Santa Catarina



Prof. Gierri Waltrich, Dr. Eng.
Universidade Federal de Santa Catarina (Membro
Externo)

AGRADECIMENTOS

A dissertação, apesar de autorada por somente uma pessoa, depende do trabalho e contribuição de muitos. Meus sinceros agradecimentos a todos que colaboraram e possibilitaram que mais essa etapa fosse concluída.

Primeiramente aos meus pais e irmã por todos esses anos de apoio e carinho, inclusive nos dias e horários completamente não usuais de trabalho. Aos colegas mais próximos, Abreu, André, Apolo, Artur, João Dudy e Pedro (Bahia), por todo apoio e bons momentos de descontração.

Aos meus colegas de LabCET, LRRG e Grante, com os quais tive o prazer de trabalhar em diferentes momentos ao longo do mestrado. Em especial ao Thiago Batista, Flávia Artuso, Jônatas Vicente e Frederico Baumgratz, pelo apoio em todas as atividades no LabCET, e aos colegas de sala, Eduardo, Rafael, Abílio, Letícia e Diogo (Poca), pela companhia e boas conversas ao longo de todo esse tempo.

Aos professores Lauro Nicolazzi e Henrique Simas, por terem aceito a proposta de orientação e acreditado no potencial do trabalho, além de todo o suporte ao longo da pesquisa, bancas e coorientações de trabalhos de conclusão. Muito obrigado por tantas oportunidades de aprendizado e pela contribuição tão significativa na minha formação.

Agradeço também ao professor Amir Oliveira e ao Ricardo Hartmann pelo convite para entrar no LabCET e poder aprender tanto com a equipe, além da oportunidade de contribuir para o desenvolvimento dos projetos e do laboratório.

Muito obrigado também aos colegas de Baja SAE, em especial Joseph, Richard (Aspira) e Gustavo, veteranos da época de equipe e que me convenceram a voltar às competições, dessa vez junto à organização.

Finalmente, ao CNPQ pelo fomento fornecido para o desenvolvimento da pesquisa.

“There are no two words in the English language more harmful than ‘good job’”. (Whiplash, 2014)

RESUMO

A fim de reduzir o consumo de combustível em sistemas de propulsão automotivos, a implementação de conjuntos motrizes híbridos, o *downsizing* de motores à combustão interna e a automatização do câmbio têm crescido no mercado de veículos de passeio. No entanto, as melhorias individuais em sistemas de um veículo não necessariamente aproximam a sua operação do ponto de ótima eficiência, e a adição de diferentes fontes de energia deve ser feita de forma metódica e estruturada, a fim de proporcionar ganhos consideráveis em consumo de combustível. Ademais, o comportamento do condutor e as trajetórias percorridas pelo veículo são características extremamente dependentes da região em análise, dificultando ainda mais o desenvolvimento de uma estratégia única de redução de consumo de combustível. Assim, a partir de um modelo de dinâmica longitudinal com três graus de liberdade para um veículo genérico, desenvolvido utilizando as equações de Euler-Lagrange do segundo tipo, essa dissertação tem como objetivo principal a proposta de um algoritmo para um assistente de direção automotivo, o qual promove a redução do consumo de combustível a partir do ajuste da relação de transmissão e abertura da válvula borboleta, em função da demanda de torque imposta pelo condutor, dinâmica do *powertrain* e características da fonte de potência. As características de desempenho do motor foram modeladas utilizando Redes Neurais Artificiais do tipo *Feedforward Multi-Layer Perceptron*, viabilizando a simulação de ciclos urbanos em tempo hábil e a inserção de propriedades relacionadas ao gradiente dos mapas estáticos no algoritmo do assistente de direção. O sistema foi implementado e simulado em Matlab™, e seu desempenho avaliado através de um estudo de caso, utilizando modelos da literatura como referência.

Palavras-chaves: Assistente de Direção, Dinâmica Veicular Longitudinal, Consumo de Combustível, Redes Neurais Artificiais, Otimização.

RESUMO EXPANDIDO

INTRODUÇÃO

A criação de novas leis ambientais tornou a emissão gases poluentes de veículos automotores mais restritiva. Logo, muito esforço tem sido empregado para o desenvolvimento de alternativas de sistemas de propulsão mais eficientes e de fontes de energias renováveis e limpas, que possam ser empregadas em veículos.

Entretanto, a emissão de gases, mais especificamente o dióxido de carbono (CO_2), em veículos com combustível de origem fóssil não pode ser evitada, visto que é um produto natural da reação de oxidação do combustível. Portanto, a única forma viável de se reduzir a produção de CO_2 é diminuir a demanda por combustível através de modificações tanto no projeto veicular quanto na forma de condução.

O estado da arte, em termos de projeto veicular, aponta modificações que vão do processo de queima do combustível ao refinamento do projeto aerodinâmico. Dentre as novas tecnologias, destacam-se:

- Processos de ignição de carga homogênea por compressão, *Homogeneous Charge Compression Ignition* (HCCI) e *Reactivity Controlled Compression Ignition* (RCCI), os quais aliam vantagens dos ciclos Otto e Diesel, porém ainda encontram-se em estágio de testes em bancada;
- Hibridização do trem-de-força, visando a associação de diferentes fontes de potência para suprir a demanda de potência de forma complementar e controlada, aumentando a eficiência global do sistema e possibilitando a recuperação de energia. O principal desafio de sistemas híbridos está na definição do leiaute de motores e transmissão, de forma que a economia de combustível seja atingida mesmo com o aumento de massa;
- Sistemas de transmissão continuamente variáveis (CVT), que proporcionam infinitas relações de transmissão em uma faixa de valores determinados por projeto. Assim, enquanto o veículo varia de velocidade,

o motor de combustão interna (ICE) permanece com velocidade aproximadamente constante e, idealmente, próximo de uma região ótima eficiência. Entretanto, as CVTs têm limitações em relação à transmissão de torque e desgaste, que afetam severamente a sua eficiência.

A fim de avaliar o cenário brasileiro, diversos carros de passeio com motorização semelhante foram classificados quanto ao consumo, emissão de CO_2 , tipo de transmissão e quantidade de marchas, como mostrado na Figura 1. Primeiramente, nota-se a correlação entre consumo de combustível e emissão de dióxido de carbono, justificada pela reação de combustão, como discutido anteriormente. Ademais, vê-se que não há uma relação clara entre o tipo de transmissão ou o número de marchas com o consumo de combustível, apesar de se esperar que os veículos com transmissões automáticas e com maior número de marchas apresentassem melhores resultados.

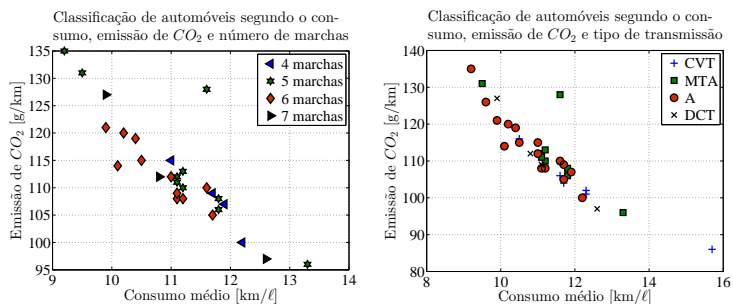


Figure 1 – Classificação de veículos do mercado nacional de acordo com o consumo médio, emissão de CO_2 , número de marchas (esquerda) e tipo de transmissão (direita). As siglas "A", "MTA", "DCT" e "CVT" significam "automático", "manual", "dual-clutch" e "transmissão continuamente variável", respectivamente. Dados disponíveis em (INMETRO, 2017).

A dispersão dos dados em função da transmissão pode ser justificada por diversos fatores, como as diferenças de funcionamento de catalisadores, condições de teste e comportamento do motorista. Portanto, o problema de redução do consumo de combustível não deve ser tratado somente a nível de projeto mecânico, mas deve levar também aspectos relacionados ao controle do trem

de força e influência do modo de operação do veículo.

Objetivos

O objetivo principal do trabalho é propor um algoritmo de redução de consumo de combustível, o qual possa ser implementado em um sistema de assistência de direção e que não afete severamente o desempenho do veículo. A fim de atingir o objetivo principal, foram definidos os seguintes objetivos específicos:

- Desenvolver de um modelo matemático da dinâmica longitudinal e do trem de força do veículo;
- Definir a abordagem matemática para modelagem do comportamento da fonte de potência e, conseqüentemente, do consumo de combustível;
- Revisar as estratégias de redução de consumo de combustível e de controle automotivo disponíveis na literatura;
- Propor um algoritmo de redução de consumo de combustível, o qual possa ser integrado com o desenvolvimento matemático anterior;
- Realizar análises de verificação e validação dos modelos e algoritmo propostos, a fim de comparar os resultados com outras estratégias disponíveis na literatura.

METODOLOGIA

Modelagem da Dinâmica Veicular

O comportamento dinâmico veicular pode ser modelado em diferentes graus de complexidade, sendo a abordagem quase-estática a mais simples e usual. O desenvolvimento do modelo de dinâmica longitudinal a partir dessa abordagem considera o movimento longitudinal do veículo completamente acoplado ao da transmissão e motor, logo, admite-se ausência de escorregamento na embreagem e pneus.

Apesar de razoável para condições de movimento com pequenas acelerações, a hipótese de adesão completa dos pneus ao solo é falha em situações de

arrancada, bastante comuns em situações de tráfego urbano. Além disso, o modelo não prevê o funcionamento estacionário do motor quando o veículo está parado, gerando uma fonte de erro no cálculo do consumo de combustível nessas situações. Assim, foi proposto um modelo mais complexo, com três graus de liberdade, que leva em consideração a transmissão do movimento através do atrito na embreagem e interface do pneu com o solo.

A modelagem matemática do sistema encontra-se descrita no Capítulo 2 e a abordagem escolhida para obtenção das equações do movimento foi o método energético de Euler-Lagrange. A principal hipótese adotada foi a de escorregamento desprezável nas rodas não motrizes, e a dinâmica de frenagem foi simplificada, visto que não é de interesse deste trabalho. Ademais, os modelos de transmissão de torque na embreagem e de força ao solo pelo pneu foram adaptados da literatura (PICA et al., 2016; PACEJKA, 2006), de forma que se adequassem às informações disponíveis acerca das características do veículo e método numérico de solução das equações. As forças de arrasto aerodinâmico, resistência ao aclave e de rolamento foram retiradas da literatura (HUCHO, 1998; HEIBING; ERSOY, 2011; LEAL; ROSA; NICOLAZZI, 2012) e ajustadas para o veículo de interesse.

As equações obtidas foram implementadas utilizando os *software* MatlabTMe Simulink, e verificadas a partir dos resultados obtidos com um modelo de referência, desenvolvido utilizando o software AdamsTMView. A comparação entre os resultados obtidos apontou diferenças de no máximo 0,82% no resultado de velocidade angular do motor e 0,5% para a transferência de carga, demonstrando que o modelo desenvolvido é coerente e capaz de representar os fenômenos desejados.

Algoritmo de Economia de Combustível

Para o desenvolvimento do algoritmo de economia de combustível, detalhado no Capítulo 3, foi realizada uma revisão da literatura com ênfase em ferramentas matemáticas para modelagem do ICE, técnicas de controle e fatores de influência associados ao consumo de combustível, bem como .

O motor de combustão interna foi modelado utilizando modelos substitutos do tipo Rede Neural Artificial (ANN), em função da sua flexibilidade de representação de sistemas não lineares e custo computacional. Já em relação à estratégia de controle, utilizou-se como base o método de controle preditivo (MPC), já que sua estrutura sequencial facilita a implementação em controladores automotivos e as ações de controle podem ser determinadas a partir da minimização de uma função objetivo.

Os requisitos de projeto considerados para desenvolvimento do algoritmo levam em consideração a segurança dos ocupantes como maior prioridade, seguida da manutenção do desempenho dinâmico e possibilidade de implementação em diferentes veículos (grau de generalização). O algoritmo proposto encontra-se ilustrado na Figura 2.

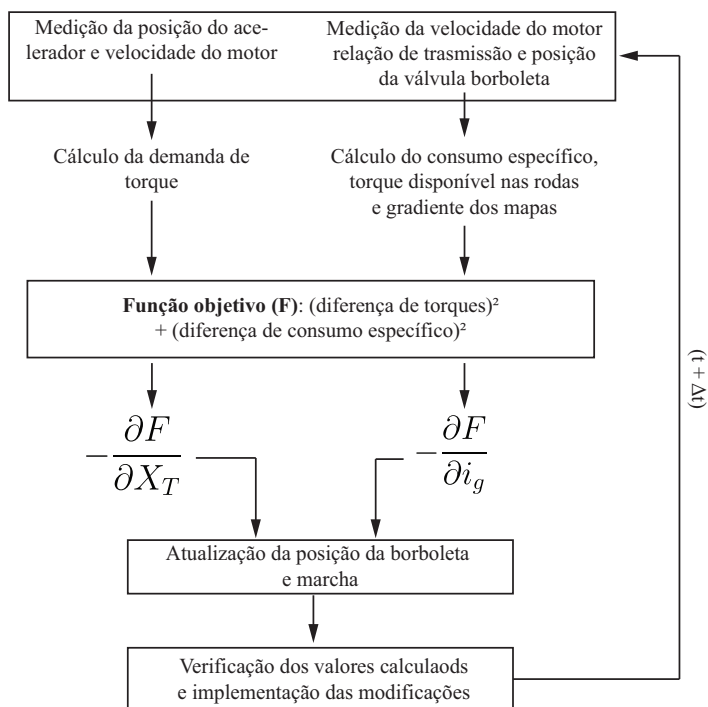


Figure 2 – Algoritmo genérico de redução do consumo de combustível.

Para fins de verificação, o algoritmo foi implementado em Simulink, acoplado ao sistema de equações desenvolvido no Capítulo 2, e testado utilizando funções analíticas de torque e consumo de combustível. O veículo considerado para a simulação foi um FIAT Punto™2008, 1.4L, o qual também foi utilizado em simulações posteriores. Como resultado, verificou-se que a região de operação do ICE tornou-se mais próxima do ponto de mínimo consumo específico de combustível, quando comparada à estratégia de operação sugerida pelo fabricante.

RESULTADOS

Simulação da NBR6601

Uma vez que os modelos foram verificados, o algoritmo foi testado utilizando condições mais realistas de condução, utilizando como referência o ciclo urbano proposto na norma NBR6601, como explorado no Capítulo 4. As simulações foram divididas em três estratégias: "FIAT", com aceleração e troca de marchas conforme proposto pelo fabricante; "Eckert", com aceleração padrão e troca de marchas segundo a estratégia otimizada proposta em (ECKERT, 2017); e "DA", com aceleração e troca de marchas assistidas pelo algoritmo proposto no trabalho.

Além da divisão segundo as estratégias de operação, foram feitas comparações com os resultados experimentais apresentados em (ECKERT, 2017), sendo que foram encontrados desvios inferiores a 2%. Em relação às simulações, os principais resultados obtidos encontram-se resumidos na Tabela 1.

Table 1 – Principais resultados dos modelos simulados

Estratégia	Dist. [km]	Cons. total [ℓ]	(1-R)	Média [km/ ℓ]
FIAT	11,993	1,035	0,0007	11,587
Eckert	11,993	0,874	0,0008	13,724
DA	11,969	0,876	0,0003	13,663

Analisando os resultados das simulações feitas no estudo de caso, nota-se convergência dos valores de consumo de combustível obtidos com o método

proposto e com a estratégia otimizada apresentada por Eckert (2017). Visto que os cálculos de validação demonstraram-se satisfatórios, nota-se que o algoritmo proposto tem potencial para economia de combustível sem alteração significativa em termos de desempenho longitudinal.

Por fim, o modelo proposto não depende de características do trajeto ou de propriedades específicas do veículo simulado, as quais possam impedir a sua implementação em outros automóveis. Portanto, os objetivos de modificação do comportamento do sistema e capacidade de generalização do algoritmo foram atingidas, bem como o trabalho trouxe contribuições acadêmicas importantes tanto para as áreas de dinâmica veicular quando controle automotivo.

Palavras-chaves: Assistente de Direção, Dinâmica Veicular Longitudinal, Consumo de Combustível, Redes Neurais Artificiais, Otimização.

ABSTRACT

The adoption of hybrid powertrain systems in passenger vehicles, as well as downsized engines and automatic transmissions, has been increasing in the last years as solutions to reduce the fuel consumption. However, the individual optimization of components or layout does not necessarily approximates the operation to conditions of maximum efficiency, and the addition of power sources should be done methodically, such that improvements of fuel efficiency can actually be achieved. Furthermore, the behavior of the driver and traffic conditions, factors which have major influence on the fuel consumption, vary with the geographic region, increasing the difficulty to develop a single solution to minimize the fuel consumption. Given such complex scenario, this dissertation proposes an algorithm for a Fuel-saving Driver Assistant System, which actuates on the throttle valve and gearbox, based on the demand of torque imposed by the driver, powertrain dynamics and characteristics of the power sources. In order to do so, a mathematical model of powertrain and longitudinal dynamics with 3 Degrees of Freedom was developed, which allows the simulation of urban traffic conditions. The performance of the engine was modeled using Artificial Neural Networks (ANN), which allies a flexible representation of the nonlinear characteristics of the power source, low computational costs and possibility to derive gradient information from the static maps, which is used by the Driver Assistant Algorithm. The system was implemented on Matlab™ and its performance compared to different models available in the literature.

Key-words: Driver Assistance, Vehicle Dynamics, Powertrain Dynamics, Fuel Consumption, Artificial Neural Networks, Optimization.

LIST OF FIGURES

Figure 1 – Classificação de veículos do mercado nacional de acordo com o consumo médio, emissão de CO_2 , número de marchas (esquerda) e tipo de transmissão (direita).	14
Figure 2 – Algoritmo genérico de redução do consumo de combustível. 17	
Figure 3 – History of CO_2 average emissions according to the vehicle’s fuel	42
Figure 4 – Average power flow for a gasoline mid-size vehicle in urban driving mode. The parasitic systems are auxiliary equipment connected to the engine, e.g. alternator and oil pump.	43
Figure 5 – (a) The target region of operation of a HCCI process, in terms of air-fuel rate and temperature. (b) Comparison between fuel injection strategies in conventional and HCCI engines.	44
Figure 6 – Diagram for a geometric progression of gear ratios; (b) Diagram for progressive gear ratios, where the velocity span is kept constant.	46
Figure 7 – Classification of vehicles according to their fuel consumption, emissions, number of gears (left) and transmission concept (right).	47
Figure 8 – Vehicle fixed coordinate system according to (SAE, 1976). 52	
Figure 9 – Force diagram for a vehicle in generic ride conditions. The CP is the center of aerodynamic pressure.	53
Figure 10 – Torque delivered by the powertrain and maximum achievable traction torques according to the envelope and vehicle layout.	58
Figure 11 – Layout of the powertrain considered as reference for the development of the model. The white arrows indicate the direction of power flow.	60

Figure 12 – Schematic of the crank-slide mechanism. (a) Main dimensions; (b) Reference angles; (c) Inertial properties. 61

Figure 13 – Crankshaft’s velocity result for different values of inertia for the flywheel using a multibody dynamic model in Adams™View. 62

Figure 14 – Structural representation of an automotive transmission. The components highlighted in red are the ones which transmit power when the first gear is selected 64

Figure 15 – Tangential velocities at the contact surface between clutch and flywheel. R_i and R_o are the inner and outer radius of the contact surface. 66

Figure 16 – Comparison between the models of equivalent radius. The adjusted model corresponds to the simplified equation multiplied by the scale factor. 68

Figure 17 – Behavior of the friction coefficient, according to the *Magic Formula*, as a function of the side-slip angle and longitudinal slip velocity. 69

Figure 18 – Common shape of an efficiency map for a automotive transmission. The plots in the right show the behavior of the resistance torque and efficiency for constant load and speed, respectively. 71

Figure 19 – Top view of the complete vehicle model developed in Adams™View. On the right, a detailed schematic of the transmission layout used in the model. 73

Figure 20 – Results of velocity for the main reservoirs of kinetic energy, obtained with the reference model and developed system. 77

Figure 21 – Comparison between the results of longitudinal load transfer obtained with both models 78

Figure 22 – Frequency of relative deviation between results and deviation over simulation time, for the three reservoirs of kinetic energy, in the simulation with plain road 78

Figure 23 – Frequency of relative deviation between results and deviation over simulation time, for the three reservoirs of kinetic energy	79
Figure 24 – Shape of a typical fuel consumption map as function of the engine speed and throttle position.	82
Figure 25 – Generic flow chart of the MPC algorithm.	87
Figure 26 – Representation the method used to interpolate intermediary conditions using Look-up Tables.	90
Figure 27 – Representation of a multi-layer perceptron, with n inputs and a single output.	91
Figure 28 – Schematic of an ICE indicating the main sensors for controlling the AF ratio.	93
Figure 29 – Structure of the proposed driver assistant algorithm, based on the method proposed in (KAMAL et al., 2010)	96
Figure 30 – Evaluation of the torque demand function for $X_G \in [0, 1]$ and $\dot{\theta}_e \in [900, 4500]min^{-1}$ and $s_v = 5$	97
Figure 31 – Block diagram of the driver model for controlling the accelerator pedal, brake and clutch forces.	103
Figure 32 – Block diagram of the complete model, including the driver assistant and model of the driver behavior.	103
Figure 33 – Velocity profile used to adjust the gains of the driver model and the response of the vehicle for the best obtained configuration.	104
Figure 34 – Values of (1-R) obtained for each iteration of the procedure used to adjust the driver model (PI Controller)	105
Figure 35 – Throttle pedal input using the PI controller with minimum (1-R) and filtered signal.	106
Figure 36 – Comparison between the reference velocity profile and results achieved with the DA, for different levels of velocity.	107
Figure 37 – Gear ratio over simulation time for different velocities and both validation maps.	107
Figure 38 – Throttle opening for both maps and different velocity profiles.	108

Figure 39 – Regions of the BSFC Maps achieved during the simulation of a ramp to 80 km/h.	108
Figure 40 – Comparison of the results of velocity and gear ratio obtained with 10% and 50% of tolerance for the DA correction.	109
Figure 41 – Indicator of fuel economy in the instrumentation panel of a passenger vehicle. Adapted from (SANDOVAL, 2008) . .	111
Figure 42 – Velocity profile for measuring vehicle emissions according to the standard NBR6601 (ABNT, 2016).	114
Figure 43 – Maps generated using the trained ANN models.	115
Figure 44 – Engine velocity oscillations due to shifting gears for a time frame of the NBR6601 simulation with the standard gearshift strategy.	117
Figure 45 – Maps of BSFC with operating points obtained with the proposed model (left) and by the literature reference (right, adapted from (ECKERT, 2017)).	118
Figure 46 – Example of two populations sampled from a bidimensional space with LHS with different number of samples	119
Figure 47 – Results of LHS for the gains $K_{t,\phi}$, $K_{t,T}$ and K_i of the Driver Assistant.	120
Figure 48 – Results of average fuel consumption and correlation between the reference and achieved velocities	121
Figure 49 – Size and color of the bubbles according to the value of K_i .	121
Figure 50 – Size and color of the bubbles according to the value of $K_{t,T}$	122
Figure 51 – Size and color of the bubbles according to the value of $K_{t,\phi}$	122
Figure 52 – Gear ratio and velocity results for the first section of the urban cycle	124
Figure 53 – Gear ratio and velocity results for the section of highest velocity of the cycle	124
Figure 54 – Gear ratio and velocity results for the section of multiple start and stop events during the cycle	125
Figure 55 – Throttle angle and engine velocity results for the first section of the urban cycle	125

Figure 56 – Throttle angle and engine velocity results for the section of highest velocity	126
Figure 57 – Throttle angle and engine velocity results during multiple start-and-stop events	126
Figure 58 – Zoom of a section in sector 3, which presented intense oscillations of the throttle valve.	127
Figure 59 – Fuel consumption results for the first section	127
Figure 60 – Fuel consumption during the section of highest velocity .	128
Figure 61 – Fuel consumption in the section with multiple stops . . .	128
Figure 62 – BSFC Maps for different operation strategies.	129
Figure 63 – Histogram indicating the level of occurrence for possible distances between points of operation and the point of minimum BSFC	130
Figure 64 – (a) Structural representation of the crank-slid mechanism of an ICE; (b) Schematic of a plane mechanism for an ICE with 2 cylinders.	153
Figure 65 – Schematic of a crank-slide mechanism with multiple prismatic joints and their respective crankshaft angles for a given position.	156
Figure 66 – ADAMS Model	158
Figure 67 – Results of angular velocity calculated using Adams™View and Simulink in different time intervals of the simulation.	160
Figure 68 – On the left, the position of the connecting rod’s center of gravity is shown as a function of its coordinates. On the right, it is shown the behavior of the coordinates x and y within a time interval	160
Figure 69 – Position of the piston represented as a function of the simulation time	161

LIST OF TABLES

Table 1 – Principais resultados dos modelos simulados	18
Table 2 – Characteristics of some Hybrid Electric Vehicles according to the U.S. Environmental Protection Agency (2017). . . .	45
Table 3 – List of coordinates according to (SAE, 1976).	52
Table 4 – Values of f_0 for different road conditions. Adapted from (JAZAR, 2008a; GILLESPIE, 1992).	54
Table 5 – Efficiency range for different types of transmission. Adapted from (NAUNHEIMER et al., 2011).	55
Table 6 – Additional properties used to calculate the resistant forces and traction limits (GILLESPIE, 1992; JAZAR, 2008a). .	57
Table 7 – Set up parameters for the model in Adams TM View.	74
Table 8 – Assigned values for the properties of the friction models. .	74
Table 9 – Parameters adopted for the simulations in Simulink and Adams TM View.	75
Table 10 – Characteristics of the simulated vehicle, adapted from (ECKERT, 2017).	100
Table 11 – Final configuration of the ANN and results of the training and verification procedures	102
Table 12 – Parameters adopted for the simulations in Simulink. . . .	105
Table 13 – Results of the training and verification procedures to develop the engine maps of a FIAT TM Punto.	114
Table 14 – Comparison between the results obtained experimentally by Eckert (2017) and the ones calculated using the proposed model.	116
Table 15 – Boundary values for the gains during the design exploration	119
Table 16 – Summary of the main results obtained with the experiments	123
Table 17 – Summary of the simulated models	123
Table 19 – Geometric and inertial properties of the reference engine model	158

Table 20 – Parameters adopted for the simulations in Simulink and
Adams/View 159

LIST OF ABBREVIATIONS AND ACRONYMS

AFV	Alternative Fuel Vehicles
ANN	Artificial Neural Network
CG	Center of Gravity
CP	Center of Pressure
CVT	Continuously Variable Transmission
DA	Driver Assistant
DoE	Design of Experiments
DoF	Degree of Freedom
ECU	Engine Control Unit
GPS	Global Positioning System
HCCI	Homogeneous Charge Compression Ignition
HV	Hybrid Vehicle
ICE	Internal Combustion Engine
ITS	Intelligent Transportation System
LHS	Latin Hypercube Sampling
MAF	Manifold Air-Flow Sensor
MAP	Manifold Absolute Pressure
MPC	Model Predictive Control
OBD	On-board Diagnosis

PI	Proportional-Integral
PID	Proportional-Integral-Derivative
RCCI	Reactivity Controlled Compression Ignition
VSP	Vehicle Specific Power

LIST OF SYMBOLS

AF	Air-to-fuel ratio [-]
A_f	Projected frontal area of the vehicle [m ²]
A_t	Throttle opening area [m ²]
$B_{d,L}$	Viscous damping factor of the drivetrain [-]
C_D	Aerodynamic drag coefficient [-]
C_{env}	Constant of the torque envelope [kg m ² / s]
F_{ax}	Clutch's clamping force [N]
F_D	Force due to the aerodynamic drag [N]
F_G	Weight of the vehicle [N]
$F_{R,j}$	Force due to rolling friction at axle j [N]
F_S	Force due to the grade of the road [N]
F_t	Driving force [N]
F_z	Reaction of the tire, normal to the road [N]
H_l	Lower heating value of the fuel [kJ/kg]
J_c	Inertia of the clutch [kg m ²]
J_e	Inertia of the internal combustion engine [kg m ²]
J_d	Inertia of the differential [kg m ²]
J_g^i	Inertia of the gearbox for the i -th gear [kg m ²]
J_w	Inertia of the tire assembled to the wheel [kg m ²]

K_c	Sensitivity factor of the axial force of the clutch to the engine speed
K_I	Gain of the integral term of the driver's model
K_i	Gain related to the adjustment of the gear ratio
$K_{t,T}$	Gain related to the adjustment of the throttle based on the torque demand
$K_{t,\Phi}$	Gain related to the adjustment of the throttle based on the fuel consumption
K_P	Gain of the proportional term of the driver's model
L	Wheelbase of the vehicle [m]
M_i	Molar mass of the substance i [kg/kmol]
N	Number of revolutions per cycle [-]
N_s	Number of Samples [-]
P_i	Power delivered by the part/system i [kW]
R	Correlation factor (R^2) [-]
R_g	Ideal gas constant [kJ/kmol-K]
R_i	Inner radius of the clutch
R_o	Outer radius of the clutch
R_w	Radius of the wheel [m]
R_μ	Equivalent friction radius of the clutch [m]
S_f	Scale factor of the clutch's equivalent radius [-]
T_{clt}	Torque due to friction at the clutch [N m]
T_d	Dissipation torque of the drivetrain [N m]

$T_{e,b}$	Brake torque of the ICE [N m]
$T_{f,c}$	Friction torque at the clutch [N m]
T_j^*	Kinetic energy of a component j [kJ]
T_{Ref}	Reference torque, defined by the driver [N m]
V	Potential energy [kJ]
V_d	Displacement volume of the ICE [m ³]
V_m	Volume of the intake manifold [m ³]
V_R	Velocity of Reference [km/h]
X_G	Position of the throttle pedal, $X_G \in [0, 1]$ [-]
X_T	Throttle valve position, $X_T \in [0, 1]$ [-]
$c_{\mu,ct}$	Sensibility of clutch's coefficient of friction to the slip [-]
$c_{\mu,t}$	Sensibility of the tire's coefficient of friction to the slip [-]
e	Thermodynamic efficiency of the ICE [-]
f_r	Rolling friction coefficient [-]
h_{CG}	Height of the center of gravity [m]
i_j	j -th gear ratio or of a system j [-]
l_x	Rear weight distribution of a vehicle [-]
m_v	Mass of the vehicle [kg]
\dot{m}_i	Mass flow rate of the fluid i [kg s ⁻¹]
n_f	Number of contact pairs at the clutch [-]
p	Pressure [Pa]
p_{me0}	Pressure related to the pumping losses of the ICE [Pa]

q_j	Minimum coordinate associated to the reservoir j
s_v	Sensibility factor of the throttle pedal position to the engine velocity [-]
x	Longitudinal displacement [m]
$\Phi(X_T, \dot{\theta}_e)$	Brake Specific Fuel Consumption [kg / s-kW]
Ω	Temperature [K]
δ_M	Scaled equivalent inertia of the rotational parts [-]
γ	Road grade [rad]
η_j	Ratio between the input and output power of a system j [-]
η_T^*	Adjusted efficiency of the drivetrain [-]
η_V	Volumetric efficiency of the ICE [-]
$\mu_{d,clt}$	Dynamic coefficient of friction of the clutch [-]
$\mu_{d,t}$	Dynamic coefficient of friction of the tires [-]
μ_t	Coefficient of friction between tires and road [-]
ρ_{air}	Density of the air [kg/m ³]
σ	Stoichiometric air-to-fuel ratio [kmol _{air} / kmol _{fuel}]
τ	Nonlinear term of inertia associated to the ICE [kg m ²]
θ_e	Angular position of the engine's crankshaft [rad]
θ_d	Angular position of the primary drivetrain shaft [rad]
\cdot	Representation of the time derivative (d/dt)
$\ddot{}$	Representation of the second time derivative (d^2/dt^2)
\mathcal{L}	Lagrangian operator

\mathbf{F}_j	Vector of forces applied to the DoF j
\mathbf{D}_j	Vector of dissipation forces applied to the DoF j
∇F	Gradient vector of the function F

CONTENTS

1	INTRODUCTION	41
1.1	THE CHALLENGE OF MINIMUM FUEL CONSUMPTION	41
1.2	OBJECTIVES	48
1.3	WORK OUTLINE	48
2	MATHEMATICAL MODEL OF LONGITUDINAL DYNAMICS	51
2.1	QUASI-STATIC ANALYSIS OF LONGITUDINAL MOTION	51
2.2	3-DoF MODEL OF POWERTRAIN AND VEHICLE LONGITUDINAL DYNAMICS	59
2.2.1	Equations of Motion for Longitudinal Dynamics	59
2.2.2	Verification Analyses	72
2.3	SUMMARY AND CONCLUSIONS	76
3	DEVELOPMENT OF THE DRIVER ASSISTANT	81
3.1	LITERATURE REVIEW	81
3.1.1	Automotive Controllers and Driver Assistance Systems	84
3.2	DRIVER ASSISTANT FOR FUEL CONSUMPTION IMPROVEMENT	88
3.2.1	Torque and Fuel Consumption Maps	89
3.2.2	Algorithm of the Driver Assistant	95
3.2.3	Preliminary Analysis	99
3.3	IMPLEMENTATION ON REAL SYSTEMS	109
3.4	SUMMARY AND CONCLUSIONS	111

4	PERFORMANCE ASSESSMENT OF THE DRIVER ASSISTANT	113
4.1	METHODOLOGY	113
4.2	RESULTS AND DISCUSSION	116
4.2.1	Simulations with reference strategies	116
4.2.2	Simulations considering the DA	117
4.3	SUMMARY AND CONCLUSIONS	130
5	CONCLUSIONS	133
5.1	Future Developments	135
	BIBLIOGRAPHY	137
	APPENDIX	147
	APPENDIX A – CHARACTERISTICS OF VEHICLES	149
	APPENDIX B – EQUATIONS FOR THE ENGINE CRANKSHAFT’S DYNAMICS	153

1 INTRODUCTION

1.1 THE CHALLENGE OF MINIMUM FUEL CONSUMPTION

The new environmental regulations added new design requisites for automotive development, specially concerning the fuel efficiency and pollutant emissions. In the European Union, for example, the goal for fleet average of Carbon Dioxide (CO_2) emissions was set to 95g/km by 2021, which corresponds to a fuel consumption around 4,1l/100km, for gasoline vehicles (EUROPEAN COMMISSION, 2016).

The emission of CO_2 cannot be completely avoided, if hydrocarbon fuels are used, since it is a natural product of the combustion reaction. Therefore, developing methods to reduce the fuel consumption play an important role in the industry. However, decreasing the demand of fuel while maintaining the performance of a vehicle becomes a significant challenge for the engineering teams (SERRARENS; VELDPAUS, 1999).

Hence, automotive manufacturers are gradually moving from the conventional concept of powertrain to new layouts with multiple power sources and energy recovery systems, as in HV. As observed in Figure 3, the European panorama of CO_2 emissions indicate that Alternative Fuel Vehicles (AFV) have significant lower levels of emission than the systems with conventional fuels, which is justified by the capacity of the powertrain of those vehicles to operate within a close region of optimum efficiency during most of the time, and application of renewable energy sources, e.g. ethanol and biofuel.

Additionally to the optimality of the operation condition, identifying the inefficiencies is an important task to improve the energetic efficiency of a vehicle. In (KOBAYASHI; PLOTKIN; RIBEIRO, 2009), it is presented an average power flow for a gasoline light-duty vehicle, in urban driving mode, illustrated in Figure 4. According to the reference, about 15% of the energy

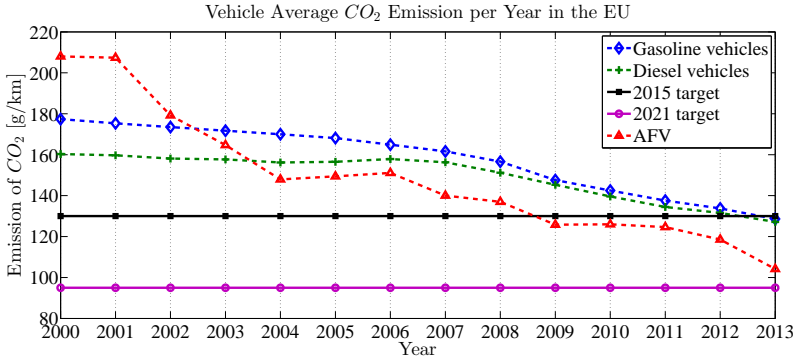


Figure 3 – History of CO_2 average emissions according to the vehicle's fuel. The acronym *AFV* stands for "Alternative Fuel Vehicles". Adapted from (EUROPEAN ENVIRONMENT AGENCY, 2015).

delivered by the fuel is actually used to move the car, and most of it is lost through thermal energy in the exhaust and cooling systems. However, it is important to remember that part of the losses are inherent to the thermodynamic cycle, and the remaining can be used in energy recovery systems or even avoided by the minimizing the friction.

Similarly, Schultze e Lienkamp (2016) investigate the potential for energetic improvements in the chassis' components. The analyses of the authors considered the losses of the tires, wheel bearings, drive shafts and brake calipers drag. This study points out that the chassis is responsible for about 25% of the vehicle's power losses, mostly due to the rolling resistance, which is comparable to the losses due to aerodynamic drag.

In the work presented by Ting (2010), the author investigates the effects of weight reduction on the energetic efficiency of automobiles, considering also economic and manufacturing effects during the product's life-cycle. The main results indicate that weight saving is beneficial, but it demands a significant effort to achieve considerable gains in fuel economy (about 0,39 $\ell/100\text{km}$ for each 100kg of weight reduction). Moreover, the conclusions also indicate the requirement to implement alternative powertrain technologies, such as hybrid concepts, and that the consumers have to be willing to accept that no

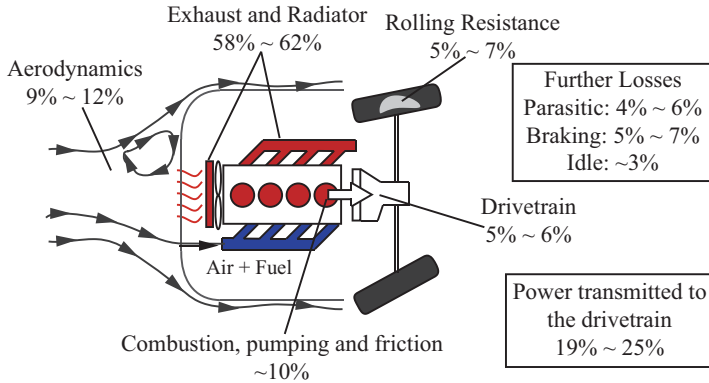


Figure 4 – Average power flow for a gasoline mid-size vehicle in urban driving mode. The parasitic systems are auxiliary equipment connected to the engine, e.g. alternator and oil pump. Adapted from (TRANSPORTATION; QUALITY, 1995) and (KOBAYASHI; PLOTKIN; RIBEIRO, 2009).

considerable improvement in acceleration performance can be achieved within certain fuel consumption constraints.

The presented scenario motivated several attempts to improve the efficiency of engine and drivetrain systems. One of the explored fields contemplates the modification of conventional thermal processes in the Internal Combustion Engines (ICE). Some of the results are the Homogeneous Charge Compression Ignition Cycle (HCCI) and Reactivity-Controlled Compression Ignition (RCCI), explored in (ZHANG; ZHAO, 2014), (DEMPSEY; CURRAN; WAGNER, 2016) and (MILES; GHANDHI, 2016). The goal of homogeneous charge combustion is to reduce the temperature, in order to avoid the production of Nitrous Oxide (NO_X) and fuel-rich areas in the chamber ($\lambda < 0,8$), preventing the formation of soot (MERKER et al., 2006), as illustrated in Figure 5. The proposal of RCCI is to mix fuels with different reactivities in a HCCI cycle, in order to increase the degree of control over the ignition process.

Although the previous works presented promising results in terms of

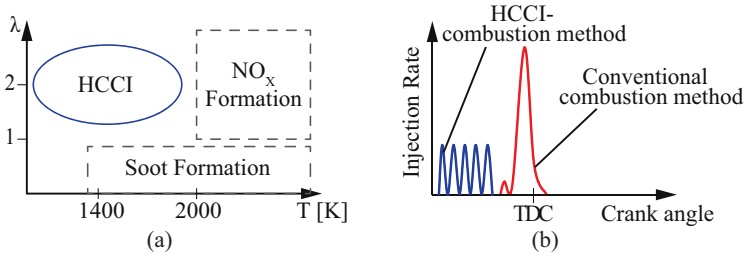


Figure 5 – (a) The target region of operation of a HCCI process, in terms of air-fuel rate and temperature. (b) Comparison between fuel injection strategies in conventional and HCCI engines. Adapted from (MERKER et al., 2006).

efficiency, for engines operating with HCCI, a few drawbacks still unsolved, such as lack of direct control over the ignition, low specific power output and narrow range of operating conditions (SHARMA; RAO; MURTHY, 2016). Further solutions are still being explored, such as engine downsizing, shown in (RICARDO; APOSTOLOS; YANG, 2011), and design modifications in two-stroke engines, as in (HOOPER; AL-SHEMMERI; GOODWIN, 2011; MATTARELLI; CANTORE; RINALDINI, 2013).

Parallel to engine development, the hybridization of powertrain systems is an alternative to improve the energetic efficiency of a vehicle. A hybrid vehicle (HV) is defined as a vehicle with more than one energy storage system capable of providing forces to drive the vehicle, either together or independently (SAE, 2007 apud WU; ZHANG; DONG, 2015). In Table 2 are listed some hybrid vehicles available in the market and their respective mileage.

Nevertheless, the design of a hybrid powertrain is more complex than of a conventional system, because the number of variables increases with the number of added power sources. Wu, Zhang e Dong (2015) propose a classification of hybrid electric vehicles, based on the level of electrification and architecture of the system. The work includes a review of the state of art and the objective of the authors is to simplify the comparison between systems and, therefore, the definition of a layout during the design phase of a vehicle.

Table 2 – Characteristics of some Hybrid Electric Vehicles according to the U.S. Environmental Protection Agency (2017).

Vehicle Model	Engine Volume [ℓ]	Kilometer per Liter [km/ℓ]
Acura NSX Hybrid	3.5	8.92
Infiniti Q50 Hybrid	3.5	11.47
Toyota Prius C	1.5	20.40
Ford Fusion Hybrid FWD	2.0	18.28
Honda Accord Hybrid	2.0	20.83

In addition to the layout, the management of the power sources is also important. It affects not only the performance, but also the level of CO_2 emissions, driving range and further aspects related to battery life and integrity of electronic components. A MAny-Objective optimization (MAO) for a 6-rule based controller is presented in (RODEMANN et al., 2015), which has 7 objectives that include vehicle emissions, battery operation conditions and level of noise. Similarly, Rodemann e Nishikawa (2016) present a comparison between evolutionary algorithms and dynamic programming, as optimization methods to find the best sequences of control actions for hybrid vehicles.

Although hybridization shows promising results of fuel consumption and emissions, the drivetrain developed for the vehicle has to suit the power sources, such that they can operate in optimum efficiency conditions. Moreover, it is the transmission that conciliates the power delivered by the engine to the road loads and velocity. Therefore, a vehicle designed to ride in a wide range of conditions demands high flexibility of operation from the drivetrain.

The gear ratios for a discrete gearbox can be defined in order to fulfill specific requirements, such as optimum start or fuel economy. Usually the first gears (highest ratios) are designed to provide the maximum torque at the wheel, which is defined by the maximum slope the vehicle must climb. The last gears (lowest gear ratios) are defined according to the engine's optimum efficiency operation point, considering highway velocities (GILLESPIE, 1992).

For intermediate gears, there are two traditional approaches: geometric and progressive ratios (JAZAR, 2008a). In the first, the span of engine speed

between two successive gears is constant, while in the second it is the span of vehicle's velocity between gears that is approximately constant. The engine/vehicle - velocity diagrams for both approaches are shown in Figure 6, where the variable ω_{eng} is the angular velocity of the engine and $V_{vehicle}$ is the velocity of the vehicle.

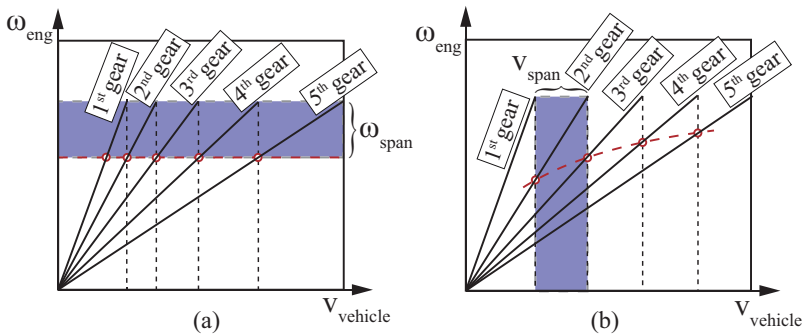


Figure 6 – (a) Diagram for a geometric progression of gear ratios; (b) Diagram for progressive gear ratios, where the velocity span is kept constant. The red dashed line indicates how the engine velocity behaves with the vehicle speed and gearshift. Adapted from (NAUNHEIMER et al., 2011).

If the number of gears is increased, the engine is allowed to work closer to an optimum performance point, while the velocity range of the vehicle is unaffected. Nevertheless, the mass and size of the gearbox is also greater, which affects the vehicle acceleration performance (NAUNHEIMER et al., 2011).

A Continuously Variable Transmission (CVT) provides to the power-train the enough flexibility, such that the engine can operate close to a desired condition (NAUNHEIMER et al., 2011; LEE; KIM, 2005). Nevertheless, such control strategies cause a different response to accelerations, which makes the driver feel uncomfortable (PATEL, 2006 apud SUN; LUO; QIN, 2012). Control strategies considering the improvement of comfort and drivability levels are proposed in (SUN; LUO; QIN, 2012) and (SERRARENS; VELDPAUS, 1999). Ryu et al. (2009) analyze the performance of a CVT for a hybrid electric

vehicle and Zheng, Lim e Cha (2011) presents a performance optimization for a CVT used in two-wheeled vehicles.

Finally, the scenario presented above can be summarized into Figure 7. Based on the data available in (INMETRO, 2017), a sample of the vehicles available in the Brazilian market were classified according to the number of gears (left) and type of transmission (right). A table with the samples used for the analysis can be found in the Appendix A.

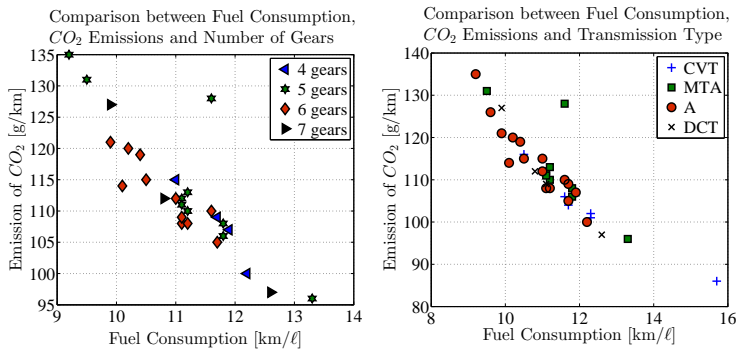


Figure 7 – Classification of vehicles according to their fuel consumption, emissions, number of gears (left) and transmission concept (right). The acronyms "A", "MTA" and "DCT" mean "Automatic", "Automated" and "Dual Clutch", respectively. Adapted from (INMETRO, 2017)

The results show a strong correlation between the emission of CO₂, fuel consumption, which was already expected, since the gas is a natural product of the combustion reaction and its production is proportional to the amount of burned fuel. However, there is not a clear correlation between the number of gears or type of transmission and fuel economy, as shown in the same Figure, suggesting that improving only the design of the drivetrain should not lead the vehicle to the optimum fuel efficiency. In fact, the problem of fuel consumption depends on many more aspects than the design of the powertrain and in this work the solution proposed to improve the fuel economy focus on the control of some parameters of the engine and transmission systems.

1.2 OBJECTIVES

The objective of this work is to propose a method to adapt the driver's actions, such as throttling and gear shifting, to powertrain inputs, which reduce the fuel consumption without severely affecting the longitudinal performance of the vehicle.

In order to reach the main objective, specific objectives were set as follows:

- to develop a mathematical model of powertrain and longitudinal dynamics;
- to define an approach to model the engine behavior, i.e. fuel consumption and mean brake torque, which can be coupled to the dynamic model for the simulations of urban cycles;
- to review strategies of vehicle control focused on fuel saving and longitudinal dynamics;
- to propose an algorithm for a driver assistent system, which helps the driver to reduce the fuel consumption and that can be integrated to the mathematical model;
- to compare the performance of the proposed algorithm to fuel saving strategies available in the literature.

1.3 WORK OUTLINE

This dissertation is divided into three main chapters, organized according to the order that the models were developed and implemented.

Chapter 2 concerns the development of the mathematical model that represents the dynamics of a vehicle in the longitudinal direction. A brief description of the quasi-static approach is given, in order to set a theoretical background, and then, the equations of motion for the vehicle are defined.

Closing the chapter, a verification analysis of the mathematical model is presented.

In Chapter 3, the algorithm of the Driver Assistant is presented. It begins with a review of the literature concerning automotive controllers and strategies to reduce the fuel consumption. Then, the models of torque delivered by the engine and fuel consumption are explored, since the algorithm considers different information of these models. Closing the chapter, the algorithm is mathematically developed and integrated with the previous system of equations, followed by a preliminary analysis of the system's performance.

In Chapter 4 a performance assessment of the proposed method is carried, adopting the solution proposed in (ECKERT, 2017) as baseline. Also, the behavior of the system is verified for urban traffic conditions, simulated according to the cycle NBR6601, which are more complex than the ones considered in the previous chapter.

Finally, the conclusions of the researcher are presented, as well as the considerations regarding future developments in this field of study.

2 MATHEMATICAL MODEL OF LONGITUDINAL DYNAMICS

In this chapter the mathematical model developed to simulate the longitudinal and powertrain dynamics of a generic vehicle is presented. The first section concerns the quasi-static approach and the fundamentals of the longitudinal dynamics analysis. Based on this approach, in the following section it is presented an enhanced model with 3 Degrees of Freedom (DoF), which was adopted for the simulations in this work.

The mathematical model presented in the second section was developed according to the methodology of the Euler-Lagrange Equations of 2^{nd} kind. The formulation of the terms that describe the forces acting on the system and energy dissipation was withdrawn from the literature and adapted according to the purposes of this work. Finally, the verification of the model was performed by comparing the results obtained with the solution of the proposed equations to the ones obtained with a comparable model developed in a commercial software, AdamsTMView.

2.1 QUASI-STATIC ANALYSIS OF LONGITUDINAL MOTION

The quasi-static approach is the most simple analysis to be carried out, with respect to the vehicle's longitudinal performance. The vehicle is considered to operate close to steady-state conditions and the results of the analysis point out the limits of operation of the vehicle and can be used to verify the gearbox and differential design.

The motion of a vehicle is described using a reference coordinate system, which is attached to the vehicle's CG (Center of Gravity). In order to keep the conformity with the literature, it is adopted the convention proposed in the (SAE, 1976), shown in Figure 8, with the corresponding coordinates

listed in Table 3.

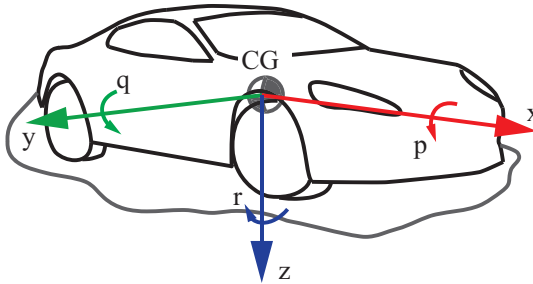


Figure 8 – Vehicle fixed coordinate system according to (SAE, 1976).

Table 3 – List of coordinates according to (SAE, 1976).

Coordinate	Description
x	Motion on the longitudinal plane of symmetry, positive in the forward direction
y	Lateral motion, positive to the right side of the vehicle
z	Vertical motion, positive downward with respect to the vehicle
p	Roll velocity about x
q	Pitch velocity about y
r	Yaw velocity about z

The study of longitudinal dynamics is the analysis of the vehicle's motion in the x-axis and can be divided into vehicle and powertrain dynamics (RAJAMANI, 2006). The first part considers the forces that act on the chassis and tires while the vehicle is in forward motion, while the second describes the behavior of the engine and drivetrain due to power demand and driver's input.

Considering the steady-state operation of a vehicle with weight F_G in a road with grade γ , three resistant forces are developed: the aerodynamic drag F_D , which acts at the CP (Center of Pressure), inducing load transfer to the rear wheels, rolling friction $F_{R,I}$ and $F_{R,II}$, and grade force $F_G \sin(\gamma)$ (HEIßING; ERSOY, 2011; LEAL; ROSA; NICOLAZZI, 2012). The power delivered by the engine is converted into tractive forces $F_{T,I}$ and $F_{T,II}$ at the

front and rear axles, respectively. The diagram in Figure 9 shows where the forces are applied.

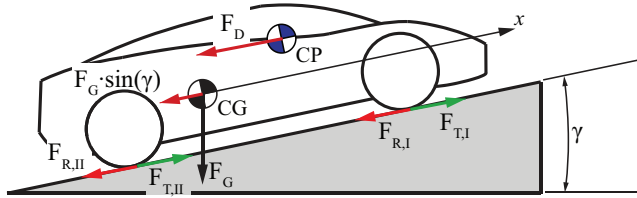


Figure 9 – Force diagram for a vehicle in generic ride conditions. The CP is the center of aerodynamic pressure.

From the Newton's Second Law, the equation that describes the movement of the vehicle yields to

$$(F_{T,I} + F_{T,II}) - [F_G \sin(\gamma) + (F_{R,I} + F_{R,II}) + F_D] = m_v^* \frac{d^2}{dt^2}(x) \quad (2.1)$$

where m_v^* is the term of inertia, which accounts the inertia of all rotational components. Starting with the resistive forces, the model for grade resistance derives from a simple trigonometric relation, already shown in Figure 9 and given as follows

$$F_S = F_G \sin(\gamma) \quad (2.2)$$

According to (HEIßING; ERSOY, 2011), on a dry road and straight line driving, the tire rolling resistance can be calculated using (2.3), where f_R is the rolling-resistance coefficient.

$$F_R = f_R F_G \sin(\gamma) \quad (2.3)$$

Nevertheless, the mechanism of contact between the tire and road surface depends on many characteristics of the road and tires, such that the

coefficient f_R in general isn't constant. Jazar (2008a) presents a model that considers the influence of the velocity \dot{x} on f_R , which is given in Eq. (2.4).

$$f_R = f_0 + f_1 \dot{x}^2 \quad (2.4)$$

The values of f_0 and f_1 have to be determined experimentally for an individual tire. According to Jazar (2008a), typical values of these constants are $f_0 = 0.010$ and $f_1 = 7 \times 10^{-6} s^2/m^2$.

In Table 4 are listed some reference values for f_0 according to the road condition. Further models considering the inflation pressure and vertical force on the tire are presented in (MOZHAROVSKII et al., 2007; JAZAR, 2008a; EJSMONT et al., 2016).

Table 4 – Values of f_0 for different road conditions. Adapted from (JAZAR, 2008a; GILLESPIE, 1992).

Pavement Condition	f_0
Sand	0.15 ~ 0.3
Gravel	0.045 ~ 0.16
Stone paving	0.033 (very good) ~ 0.085 (poor condition)
Tarmac	0.01 (very good) ~ 0.23 (poor condition)
Concrete	0.008 (very good) ~ 0.02 (poor condition)

The magnitude of the aerodynamic drag is determined using

$$F_D = \left(\frac{1}{2} \rho_{air} \dot{x}|_{rel,air}^2 \right) C_D A_f \quad (2.5)$$

where ρ_{air} is the density of the air, A_f is the projected frontal area of the vehicle and C_D the drag coefficient. Notice that the velocity $\dot{x}|_{rel,air}$ is not relative to a fixed coordinate system in the ground, but to the air flow.

In (HUCHO, 1998), several approaches to model and improve the drag in passenger vehicles are presented, including attachment of trailers and convoy driving. CFD (Computer Fluid Dynamics) simulations and experiments in wind tunnels are the most common methods to estimate the value of C_D , and for modern passenger vehicles its value varies from 0.30 to 0.37.

Besides these three effects, two more should be considered: the efficiency of the drivetrain and the inertia of the vehicle (LEAL; ROSA; NICOLAZZI, 2012). The losses in a gearbox depend on the load and lubrication system, among other factors, but its efficiency is expected to be within the ranges shown in Table 5.

Table 5 – Efficiency range for different types of transmission. Adapted from (NAUNHEIMER et al., 2011).

Type of Transmission	Efficiency η [%]
Passenger car, conventional gearbox	92 ~ 97
Automatic transmission with various gear ratios	90 ~ 95
Mechanical CVT	87 ~ 93

Defining the ratio of input and output power of the drivetrain as

$$\eta_{driv} = \frac{P_{in}}{P_{out}} \quad (2.6)$$

and considering the relation between power and angular velocity, the torque at the output shaft of the drivetrain is defined as follows

$$T_{out} = T_{in} i \eta_{driv} \quad (2.7)$$

where i is the total gear ratio and T_{in} is the input torque. Therefore, part of the driver torque can be deducted, based on the transmission efficiency, in order to achieve similar results of dynamic response. Further considerations about the friction in the drivetrain will be discussed in Section 2.2.

Finally, the effects of inertia are manifested only during acceleration events. In these cases, besides the changes of linear velocity in x , the rotational parts, e.g. shafts and gears, also have their rotational velocity modified. Leal, Rosa e Nicolazzi (2012) propose a coefficient to compensate the rotational inertia, given as follows

$$\delta_M = \frac{[4 J_w + i_d^2 (J_d + J_g + i_g^2 J_e)]}{m_v R_w^2} \quad (2.8)$$

where J_w, J_d, J_g, J_e are the inertia of the tires and wheels, differential, gearbox and engine, respectively, R_w is the dynamic radius of the tire and i_d, i_g are respectively the gear ratios of the differential and gearbox. The impact of the inertia on the vehicle longitudinal dynamics is further discussed in Section 2.2.

The tractive force is already defined by Equation (2.7), but is important to define its limits. There are two main aspects that limit the traction: the power delivered by the engine and the adhesion at the tireprint.

On the engine's side, according to (JAZAR, 2008a), the power delivered by the engine, for a constant throttle position, is well approximated by a third-order polynomial of the engine's angular velocity $\dot{\theta}_e$, as described in Equation 2.9, where the coefficients a, b and c are constants, adjusted experimentally.

$$P_{eng} = a \dot{\theta}_e^3 + b \dot{\theta}_e^2 + c \dot{\theta}_e \quad (2.9)$$

Again, considering the relation between power and angular velocity, the torque at the wheel is given as follows

$$T_w = [a (\dot{\theta}_e i)^2 + b (\dot{\theta}_e i) + c] i \quad (2.10)$$

where i is the total gear ratio. Since the gear ratio is an independent parameter, the Equation (2.10) provides a family of curves. An envelope is a curve tangent to all the members of the family, thus the limit of torque for a given range of velocities. According to (JAZAR, 2008a), the torque envelope for a vehicle with an internal combustion engine is determined as follows

$$T_{env} = \frac{R_w}{27 a^2 \dot{x}} \left[C_{env}^3 + 3 b C_{env}^2 + 9 c a C_{env} \right] \quad (2.11)$$

where

$$C_{env} = \left(-b - \sqrt{b^2 - 3 a c} \right) \quad (2.12)$$

Therefore, regardless of the used gear ratio, the limit of torque provided by the powertrain is defined by the envelope. On the other hand, the transmission of force to the ground is limited by the friction between tire and road. For a vehicle with front wheel drive, according to (LEAL; ROSA; NICOLAZZI, 2012), the maximum transmissible torque is given as follows

$$T_{layout}^{max} = R_w \mu_t F_G \cos(\gamma) \left[\frac{(1 - l_x) + f_R (h_{CG}/L)}{1 + \mu_t (h_{CG}/L)} \right] \quad (2.13)$$

where h_{CG} is the height of the center of gravity with respect to the ground, L the wheelbase, μ_t the friction coefficient between the tire and the road, and l_x the front weight distribution, given as follows

$$l_x = \frac{F_{z,rear}}{F_G} \quad (2.14)$$

where $F_{z,rear}$ is the reaction force at the rear axle, measured statically.

Considering the torque curve from the first example of Chapter 2 in (GILLESPIE, 1992), the additional parameters of Table 6 and the road as an horizontal plane, the behavior of the modeled forces can be summarized in a single plot, shown in Figure 10.

Table 6 – Additional properties used to calculate the resistant forces and traction limits (GILLESPIE, 1992; JAZAR, 2008a).

Property	Value	Property	Value
C_D	0.4 [-]	ρ_{air} [kg/m ³]	1.225 [-]
$f_{R,0}$	0.015 [-]	$f_{R,1}$ [s ² /m ²]	7×10^{-6} [-]
μ_t	0.9 [-]	h_{CG} [m]	0.53 [-]
M	1406 [kg]	l_x	0.63 [-]

As expected, the curves of torque delivered by the powertrain are tangent to the curve defined by the envelope and the maximum velocity is achieved with the fifth gear, close to the limit defined by the envelope. Also, for velocities above 12 km/h, the torque provided by the powertrain in the first gear exceeds the limit imposed by the layout, which indicates the occurrence of

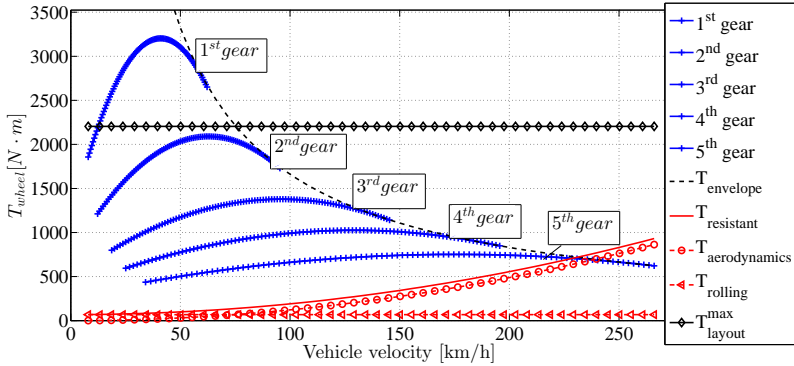


Figure 10 – Torque delivered by the powertrain and maximum achievable traction torques according to the envelope and vehicle layout.

longitudinal tire slip. Lastly, for plane roads ($\gamma = 0$), the aerodynamic forces prevail only for velocities above 75 km/h, approximately, thus the rolling resistance has major relevance in urban driving conditions.

The diagram of Figure 10 is a summary of the results obtained with the quasi-static analysis of the longitudinal motion of a vehicle. Although this approach covers important aspects of performance, the assumptions considered to develop the model do not allow it to provide reliable information on the behavior of the drivetrain, which is important to evaluate the fuel consumption.

The most restricting considerations are the fully coupled clutch and small tire slip ratio, such that the velocity of the vehicle can be determined based on the velocity of the engine and gear ratio, only. Besides the frequent violation of these hypothesis in urban traffic conditions, they lead the system to unfeasible conditions, such as $\dot{\theta}_e = 0$ when the vehicle is stopped, or overestimation of the available torque at the tireprint, since the friction between the tires and road is not predicted.

From the above considerations, it is observed that the quasi-static model represents poorly the drivetrain dynamics and its application is limited to certain conditions. In order to set an strategy to reduce the fuel consumption, it is necessary to develop an enhanced model, which couples both dynamics

of the chassis and driveline.

2.2 3-DOF MODEL OF POWERTRAIN AND VEHICLE LONGITUDINAL DYNAMICS

In this section, it is proposed a mathematical model to overcome the limitations of the quasi-static model. The adopted methodology is the Euler-Lagrange equations of second kind, an energetic approach which divides the system according to the energy reservoirs.

2.2.1 Equations of Motion for Longitudinal Dynamics

The quasi-static model considers the powertrain and vehicle chassis as a single DoF system. However, the conditions assumed for the development of the model are often violated, specially due to the slip at the clutch and interface between tire and road.

Considering the contact at both interfaces, the dynamics of the engine, drivetrain and chassis become decoupled, leading to a system with three minimum coordinates. In Figure 11, it is shown a schematic of an automotive transmission and the three kinematic energy reservoirs that will be considered in the model, highlighted in different colors. The translational inertia is represented by $(M + J_{w,ND})$, which takes into account the mass of the chassis and equivalent inertia of all non-driver wheels. In this case, the fidelity of the model decreases for the cases with high slip ratio at the driven wheels.

The ICE can be considered as a single DoF system, regardless of its number of cylinders, since the components move synchronously with the crankshaft. Also, they contribute to the total inertia of the system, which becomes a nonlinear function of the crankshaft angle.

Considering the structural representation of the crank-slide mechanism and its inertial and geometric properties shown in Figure 12, the kinetic energy

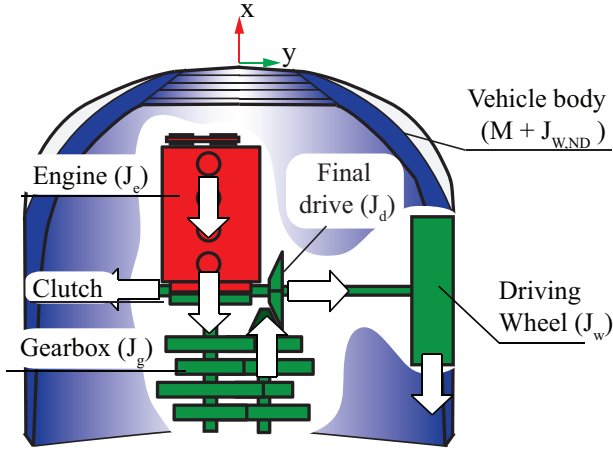


Figure 11 – Layout of the powertrain considered as reference for the development of the model. The white arrows indicate the direction of power flow.

of an ICE with n_{cyl} cylinders is given as follows

$$T_{engine}^* = \frac{1}{2} \dot{\theta}_c^2 \left(J_c + \sum_{i=1}^{n_{cyl}} \tau(\theta_i) \right) \quad (2.15)$$

where the function $\Psi(\theta_i)$ is described in Eq. 2.16

$$\begin{aligned} \tau = & J_R \left[\frac{(L_c \cos(\theta_i))^2}{L_R^2 - (L_c \sin(\theta_i) - h)^2} \right] + m_R \left[\frac{L_c^2}{L_R^2} \cos^2(\theta_i) (L_{R,G} - \right. \\ & \left. L_R)^2 + L_c^2 \left[\sin(\theta_i) + \frac{L_{R,G} \cos(\theta_i) (L_R \sin(\theta_i) - h)}{L_R \sqrt{L_R^2 - (L_c \sin(\theta_i) - h)^2}} \right]^2 \right] + \quad (2.16) \\ & m_P L_c^2 \left[\sin(\theta_i) + \frac{\cos(\theta_i) (L_R \sin(\theta_i) - h)}{\sqrt{L_R^2 - (L_c \sin(\theta_i) - h)^2}} \right] \end{aligned}$$

and θ_i is the crankshaft angle shifted in $\theta_{s,i}$ for the cylinder i , defined as

$$\theta_i = \theta_c + \theta_{s,i} \quad (2.17)$$

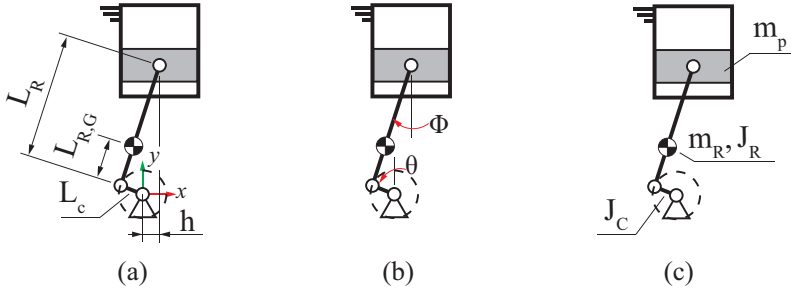


Figure 12 – Schematic of the crank-slide mechanism. (a) Main dimensions; (b) Reference angles; (c) Inertial properties.

For the sake of brevity, the complete development of the equations using an energetic approach can be found in the Appendix B, which was based on the kinematic analysis presented in (MA; PERKINS, 2003).

The Euler-Lagrange equations of second kind are obtained using

$$\frac{d}{dt} \frac{\partial \mathcal{L}}{\partial \dot{q}_j} - \frac{\partial \mathcal{L}}{\partial q_j} = \mathbf{F}_j - \mathbf{D}_j \quad (2.18)$$

where q_j , \mathbf{F}_j and \mathbf{D}_j are the generalized coordinate, force and dissipative energy functions related to the degree of freedom j . The function \mathcal{L} is the Lagrangian defined as

$$\mathcal{L} = T_{tot}^* - V_{tot} \quad (2.19)$$

where V_{tot} and T_{tot}^* are the total potential and kinetic energy of the system, respectively. Applying (2.15) to (2.18), the equation of motion for the engine yields to

$$\ddot{\theta}_c \left[J_c + \sum_{i=1}^{N_{cyl}} \tau(\theta_i) \right] + \frac{1}{2} \dot{\theta}_c^2 \sum_{i=1}^{N_{cyl}} \left[\frac{\partial \tau(\theta_i)}{\partial \theta_c} \right] = \mathbf{F}_e - \mathbf{D}_e \quad (2.20)$$

where θ_c is the engine's crankshaft angle. As discussed in Appendix B, the nonlinear term on the left side of (2.20) induces an oscillation of the velocity if a constant torque is applied. Although the frequency and magnitude of the oscillations depend on the engine layout, the increase of the crankshaft's inertia attenuates the variations on the velocity, as shown in Figure 13. The results were obtained with the model of a 4-cylinder engine used in Appendix B, with only an initial velocity as boundary condition. The maximum multiplication of the crankshaft's inertia was set to 40, based on the example used to obtain the data of Figure 10.

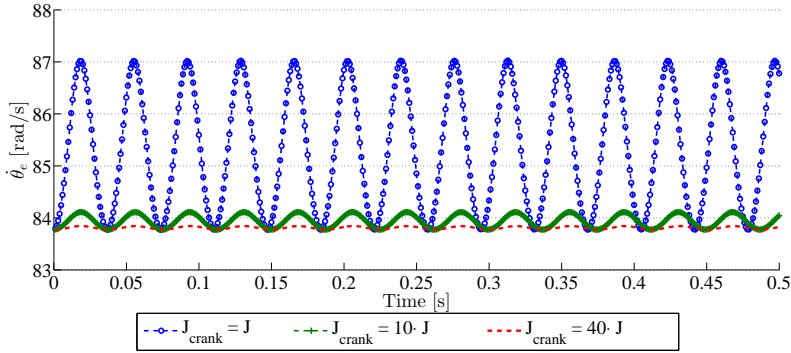


Figure 13 – Crankshaft's velocity result for different values of inertia for the flywheel using a multibody dynamic model in AdamsTMView. The variable J indicates the original value of the crankshaft inertia.

The additional crankshaft's inertia is equivalent, in practice, to the contributions of the drivetrain and vehicle body. Since most of the time the oscillations are attenuated by further inertia of the vehicle and the time step required the nonlinearities at high engine speed would be considerably small, increasing the computation time, a linear model with a mean value for the inertia of the engine is a better fit for the purposes of this work. Therefore, the Equation (2.20) can be simplified to

$$\ddot{\theta}_e J_{e,eq} = \mathbf{F}_e - \mathbf{D}_e \quad (2.21)$$

where $J_{e,eq}$ is the equivalent linearized inertia of the engine. The right side of (2.21) can be written as

$$\mathbf{F}_e - \mathbf{D}_e = (T_{e,b} - T_{clt}) - 0 \quad (2.22)$$

where T_{clt} is the torque consumed by friction at the clutch and $T_{e,b}$ is the mean brake torque of the engine, which is measured on a test bench equipped with a dynamometer. Since the measurements on test bench detect the net torque at the crankshaft, the effect of internal power losses in the ICE are already accounted in the measured value and the dissipative term can be set to zero, as stressed in Equation (2.22).

It is important to emphasize that the consideration above does not imply the absence of energy dissipation in the system. However, it does limit the validity of the model to the cases which the net torque at the crankshaft is known. Further considerations on the friction and internal losses of engines can be found in (STOTSKY, 2009) and (WONG; TUNG, 2016). The model of the torque delivered by the engine, as well as one for fuel consumption, is detailed in Chapter 3.

Connected to the ICE through a clutch, the drivetrain corresponds to the second reservoir of kinetic energy. There are various types and layouts for transmission systems, however, most of the urban passengers cars adopt solutions similar to the schematic shown in Figure 14. The inertia of the gears are identified in the form $J_{j,k}^o$, where o identifies the object (gearbox or differential), j the pair of gears and k the axle.

If the linear motion of the dog rings (dog clutch) is neglected, the gearbox also presents only one degree of freedom. Adopting the same methodology applied for the engine, the kinetic energy of the gearbox is given as follows

$$T_{gearbox}^* = \frac{1}{2} \left(\frac{\dot{\theta}_d}{i_s} \right)^2 \left[J_c i_s^2 + \sum_{j=1}^{N_{gears}} J_{j,2}^g + \sum_{j=1}^{N_{gears}} J_{j,1}^g i_j^2 \right] \quad (2.23)$$

where i_s corresponds to the selected gear ratio and J_c is the inertia of the

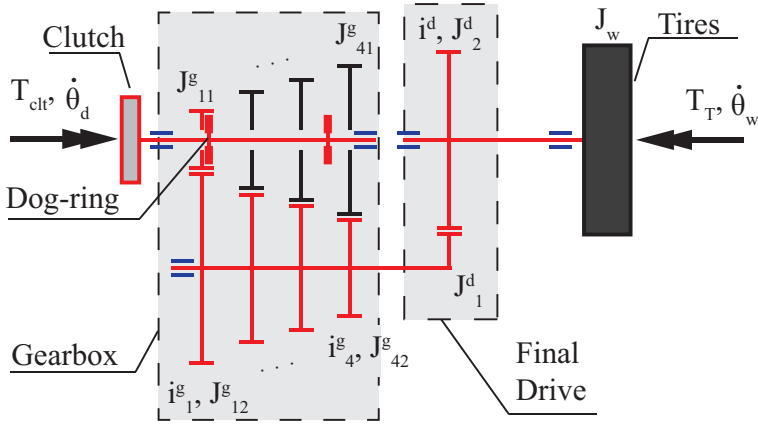


Figure 14 – Structural representation of an automotive transmission. The components highlighted in red are the ones which transmit power when the first gear is selected

clutch disc. For the final drive, also with respect to the angular velocity $\dot{\theta}_d$, the kinetic energy is described as

$$T_{drive}^* = \frac{1}{2} \left(\frac{\dot{\theta}_d}{i_s} \right)^2 \left(J_1^d + \frac{J_2^d}{i_d^2} \right) \quad (2.24)$$

where i_d is the gear ratio of the differential. The last components are the driving wheels, which have their kinetic energy defined as

$$T_{wheels}^* = \frac{1}{2} \left(\frac{\dot{\theta}_d}{i_s i_d} \right)^2 (2 J_w) \quad (2.25)$$

where J_w is the inertia of the wheels. Therefore, the total kinetic energy of the system is the sum of Equations (2.23), (2.24) and (2.25), which corresponds to the lagrangian operator, described in Equation (2.19). Applying the Euler-Lagrange approach, described in Equation (2.18), the equation that describes

the dynamics of the drivetrain yields to

$$\ddot{\theta}_d \frac{1}{i_s^2} \left[J_c i_s^2 + \left(\sum_{j=1}^{N_{gears}} J_{j,2}^g + \sum_{j=1}^{N_{gears}} J_{j,1}^g i_j^2 \right) + J_1^d + \frac{1}{i_d^2} \left(J_2^d + 2 J_w \right) \right] = \mathbf{F}_d - \mathbf{D}_d \quad (2.26)$$

The torques acting on the system derive from the friction at the clutch, as considered for the engine, and tires interface, which pushes the vehicle in the longitudinal direction. The dissipation of energy is equivalent to the torque consumed by the gearbox and differential due to friction between mechanical components, varying according to the load and angular velocity. Hence, the Equation (2.26) can be written as

$$\ddot{\theta}_d \frac{1}{i_s^2} \left[J_c i_s^2 + \left(\sum_{j=1}^{N_{gears}} J_{j,2}^g + \sum_{j=1}^{N_{gears}} J_{j,1}^g i_j^2 \right) + J_1^d + \frac{1}{i_d^2} \left(J_2^d + 2 * J_w \right) \right] = \left(T_{clt} - \frac{F_t R_w}{i_d i_s} \right) - T_d(\dot{\theta}_d) \quad (2.27)$$

The equation that describes the torque transmitted by the clutch as a function of the axial force, assuming the condition of uniform wear and the system completely locked up, is given as follows

$$T_{clt} = \frac{1}{4} F_{ax} \mu_{clt} (D_o - D_i) n_f \quad (2.28)$$

where F_{ax} is the axial force, μ_{clt} is the coefficient of friction at the interface, D_o is the outer diameter and D_i is the inner diameter of the clutch, and n_f is the number of pairs of faces in contact, as shown in Figure 15

In order to adequate the model to transient conditions, the behavior of the coefficient of friction was modified, based on the work developed by Pica et al. (2016). The authors present the friction coefficient as a function of the slip velocity and temperature, which was adjusted using a least-square

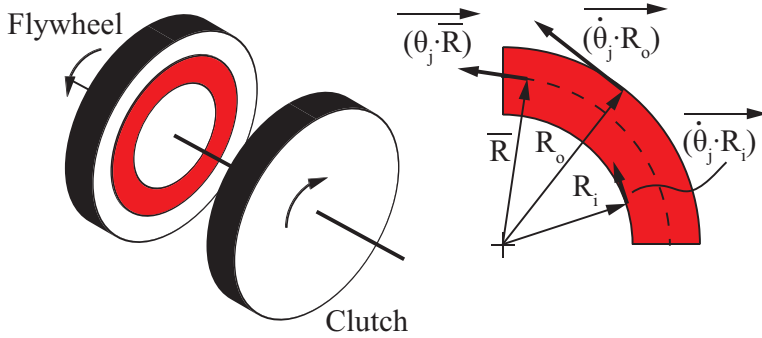


Figure 15 – Tangential velocities at the contact surface between clutch and flywheel. R_i and R_o are the inner and outer radius of the contact surface.

identification method, comparing to experimental data. According to their work, the torque transmitted by the clutch is modeled as

$$T_{fc} = n_f R_\mu F_{ax} \quad (2.29)$$

where R_μ is the equivalent friction radius which is a function of the coefficient of friction and clutch diameters, which is calculated using Equation 2.30.

$$R_\mu(\theta_{rel}, \Omega) = \frac{1}{R_o - R_i} \int_{R_i}^{R_o} \mu_{clt}(r, \theta_{rel}, \Omega) r dr \quad (2.30)$$

The coefficient of friction is a function of the tangential relative velocity $r \dot{\theta}_{rel}$ and temperature Ω at the interface, defined as

$$\mu_{clt}(\dot{\theta}_{rel}, \Omega) = \mu_s + (\mu_d(\Omega) - \mu_s) [\tanh(c_\mu r \dot{\theta}_{rel})]^{\frac{1}{3}} \quad (2.31)$$

With the purpose to simplify the function obtained in Equation (2.30), and consequently its implementation on the dynamic model, some modifications are adopted in Equation 2.31. The exponent of the hyperbolic tangent is set to 1 and the value of μ_s is considered zero, such that the function becomes anti-symmetric with respect to the Y-axis. This anti-symmetry is an

important characteristic, since it guarantees that the torque consumed by the clutch behaves similarly for positive and negative slip velocities. Moreover, it simplifies the implementation of the model, since the hysteresis is not predicted and, therefore, it is not necessary to switch any constants with respect to the magnitude of the friction coefficient.

Also, the tangential velocity in the argument of the hyperbolic function is substituted by the mean tangential velocity, which can be obtained using

$$\bar{v}_{tan} = \bar{R}_{clt} \dot{\theta}_{rel} = \frac{(R_o + R_i)}{2} \dot{\theta}_{rel} \quad (2.32)$$

such that the simplified equivalent radius yields to

$$R_{\mu,simp} = \frac{(D_o + D_i)}{4} \mu_{d,clt} \tanh(c_{\mu,clt} \bar{R}_{clt} \dot{\theta}_{rel}) \quad (2.33)$$

The simplified model is similar to one used for the complete lock-up, differing only on the expression for the coefficient of friction. Comparing the results of the simplified equation to the ones obtained with the model developed in (PICA et al., 2016), for the same clutch geometry and values of $c_{\mu,clt}$, n_f , $\mu_{d,clt}$ and axial force, the magnitude of the equivalent radius is drastically reduced, as shown in Figure 16.

Evaluating the simplified and complete models, it was observed a deviation in magnitude, which could be reduced using a scale factor S_f , obtained with the mean difference between the results. Therefore, the obtained model for the torque transmitted by the clutch yields to Equation 2.34. The results of the equivalent radius obtained with the simplified and complete model, divided by the outer radius of the clutch, are shown in Figure 16.

$$T_{clt} = S_f n_f R_{\mu,simp} F_{ax} \quad (2.34)$$

The driving force F_t , second component of the force term in Equation (2.27), is generated by the friction at the tire interface, which depends on characteristics of the tire and pavement, as well as on suspension and steering

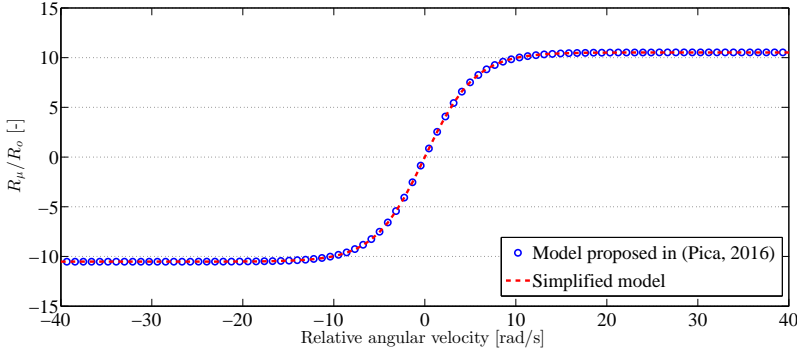


Figure 16 – Comparison between the models of equivalent radius. The adjusted model corresponds to the simplified equation multiplied by the scale factor.

angles. Moreover, the friction is an invariant of the system, meaning that the allowable friction force in the horizontal (road) plane is unique within certain conditions and, therefore, the lateral and longitudinal forces at the tire are coupled.

For the present work, only the forward motion of the vehicle is analyzed. Therefore, the influence of the suspension and steering systems is neglected, such that the models of longitudinal force can be simplified to the case of pure longitudinal slip.

The *Magic Formula*, presented in (PACEJKA, 2006), is a semi-empirical model of tires that takes into account several properties of the tire. For a vehicle in straight forward motion, the longitudinal generated by the tire is modeled as

$$F_t = D_x \sin\{C_x \arctan[B_x \kappa_x - E_x (B_x \kappa_x - \arctan(B_x \kappa_x))]\} + S_{V_x} \quad (2.35)$$

where the coefficients D_x , C_x , B_x , E_x , S_{V_x} and κ_x are constant and defined based on experimental results. However, measuring the properties of tires is an expensive task and there is not much available information on commercial tires. On the other hand, the coefficient of friction behaves, according to the

Magic formula and with respect to the slip ratio, similarly to the curves shown in Figure 17.

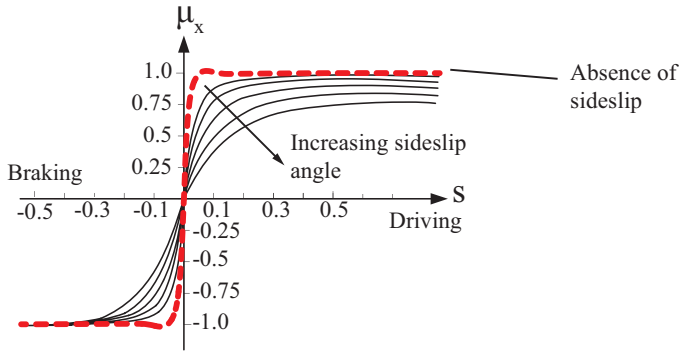


Figure 17 – Behavior of the friction coefficient, according to the *Magic Formula*, as a function of the side-slip angle and longitudinal slip velocity. Adapted from (JAZAR, 2008b).

For small side-slip angles, the behavior of the curves can be approximated using a function similar to Equation (2.30), which leads to curves with similar shape to the ones shown in Figure 17. Hence, the proposed model for longitudinal force at the tires is defined as

$$F_t = F_z \mu_t(v_s) \tag{2.36}$$

where N is the dynamic reaction of the driving axle, perpendicular to the ground, and $\mu_t(v_s)$ is the coefficient of friction at the tire’s interface, written as a function of the slip velocity v_s and given as follows

$$\mu_t(s) = \mu_{d,t} \tanh(c_{\mu,t} v_s) \tag{2.37}$$

The variable $\mu_{d,t}$ is the dynamic friction coefficient between tire and road surface. The constant $c_{\mu,t}$ is used to adjust the slope of the curve in the transient region, and it should be set carefully, in order to avoid excessive slip ratios during steady-state operation. For the sake of brevity, the determination

of the normal reaction F_z will not be explored in this text and it can be found in (GILLESPIE, 1992; LEAL; ROSA; NICOLAZZI, 2012)

The last term of Equation (2.27) to be discussed is the dissipation of torque. As presented during the introduction, the drivetrain consumes about 5% of the power delivered by the engine and it can be assumed as constant for manual transmissions (NAUNHEIMER et al., 2011).

However, looking into the drivetrain, the power sinks are various and many of them are sensitive to the lubricant temperature, torque load and angular speed. In (FERNANDES et al., 2015a; NAUNHEIMER et al., 2011), the power dissipated in transmission systems are classified as load dependent and independent, and according to the mechanical components.

In order to calculate the total power losses, some approaches were found in the literature. Fernandes et al. (2015a) describe the power losses of each component of the system with respect to their operation conditions and characteristics. For a generic transmission system, the power losses can be defined as

$$P_{Loss}(T, \dot{\theta}) = (P_{g,i} + P_{g,d}) + (P_{b,i} + P_{b,d}) + P_{s,i} + P_{a,i} \quad (2.38)$$

where the subscripts g , b , s and a indicate the losses due to gears, bearing, seals and auxiliary, respectively. The letters d and i indicate if the term is dependent or independent of the load.

The terms of Equation (2.38) are detailed in (FERNANDES et al., 2015a; FERNANDES et al., 2015b) and the model is calibrated for a wind turbine system. Although complete, the model developed by the authors requires detailed information about the bearings and constructive aspects of the gears, shrinking the range of cases where the model can be applied due to lack of available information.

In (NAUNHEIMER et al., 2011), the power losses are indicated by the efficiency of the drivetrain, alike to the approach taken in the quasi-static model. Since the magnitude of the losses depend on the load and velocity, the

authors present a map of transmission efficiency based on this parameters, as shown in Figure 18.

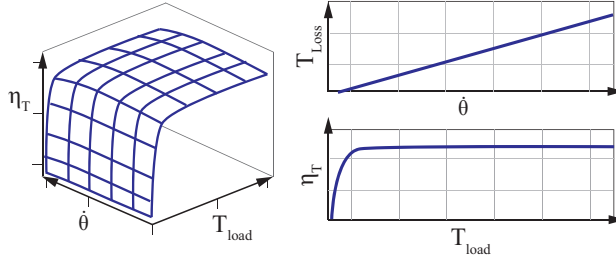


Figure 18 – Common shape of an efficiency map for a automotive transmission. The plots in the right show the behavior of the resistance torque and efficiency for constant load and speed, respectively. Adapted from (NAUNHEIMER et al., 2011).

The drawback of the model proposed Equation (2.7), even with a variable efficiency, is the deviation of the model for low load conditions. For example, when the input torque is zero, the power dissipation also becomes zero, regardless of the angular velocity, which implies the absence of a dissipating torque. Therefore, it is proposed an adjusted equation for the torque losses, given as follows

$$T_d = (1 - \eta_T^*) T_{clt} + B_{d,L} \dot{\theta}_d \tag{2.39}$$

where η_T^* is the adjusted efficiency and $B_{d,L}$ is the viscous damping factor of the drivetrain. Both variables should be determined such that the global efficiency lies within the limits found in the literature. Hence, even when the clutch is decoupled, the friction of the drivetrain is accounted on the vehicle dynamics, improving the response of the model for minor loads conditions.

The last reservoir of kinetic energy is defined by the translating mass and the driven wheels, which rotate according to the velocity of the vehicle.

Hence, the total kinetic energy of the reservoir is determined as

$$T_t^* = \frac{1}{2} \dot{x}^2 \left(m_v + 2 \frac{J_w}{R_w^2} \right) \quad (2.40)$$

where M is the mass of the vehicle. Applying the Equation of Euler-Lagrange, (2.18), the equation of motion for the translational mass yields to

$$\ddot{x} \left(m_v + 2 \frac{J_w}{R_w^2} \right) = \mathbf{F}_t - \mathbf{D}_t \quad (2.41)$$

The right side of Equation (2.41) is given by the difference of the traction force to the resistant forces, already described for the quasi-static model. Therefore, the equation for the translating movement yields to

$$\ddot{x} \left(m_v + 2 \frac{J_w}{R_w^2} \right) = F_t - (F_s + F_R + F_D) \quad (2.42)$$

where F_s , F_R and F_D are described in (2.2), (2.3) and (2.5), respectively.

Finally, the equations of motion can be arranged in a single nonlinear system of differential equations, defined as

$$\begin{cases} J_e \ddot{\theta}_e = T_{e,b} - T_{clt} \\ J_d(i_s) \ddot{\theta}_d = \left(T_{clt} - \frac{F_t R_w}{i_d i_s} \right) - T_d(\dot{\theta}_d) \\ \left(M + 2 \frac{J_w}{R_w^2} \right) \ddot{x} = F_t - (F_s + F_R + F_D) \end{cases} \quad (2.43)$$

2.2.2 Verification Analyses

In order to verify the developed equations, a similar model with rigid bodies was proposed using AdamsTMView, represented in Figure 19. Differently from the approach taken in the last section, this software allows the user to model the parts and assembly the system, similar to a *Computer Aid Design* (CAD) tool, and the equations are withdrawn from the solid model.

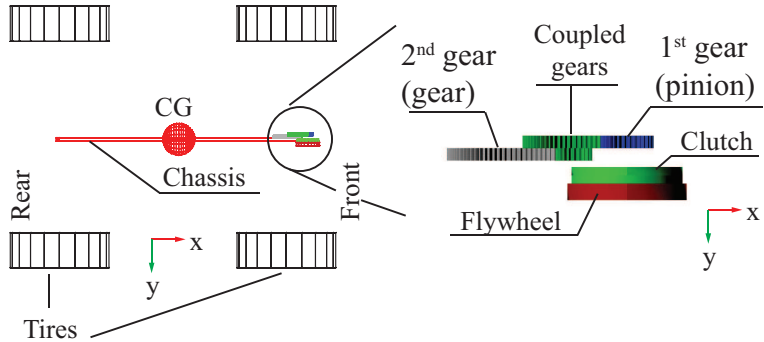


Figure 19 – Top view of the complete vehicle model developed in Adams™View. On the right, a detailed schematic of the transmission layout used in the model.

Furthermore, it has different numerical solvers than Matlab™ and it is widely accepted in the industry.

As shown in Figure 19, the gearbox was simplified to a single gear ratio, since the procedure to shift gears is not relevant at this point. Both gearbox and differential were considered as cylindrical spur gears and the dissipation torque acts directly at the clutch disc, with magnitude given by Equation (2.39).

The rolling resistance and aerodynamic drag act at the CG of the system, and were modeled according to Equations (2.5) and (2.3), respectively. The contact at the clutch and tire interfaces were defined using impact formulation and standard settings for surface stiffness and damping ratio. The friction model was set to Coulomb's, with slide effects only. Further properties of the model are listed in Table 7.

The system of equations (2.43) was implemented using Simulink, supported by a Matlab™ script, which assigns values to the parameters and set the simulation conditions. The values of geometric and inertial parameters were withdraw from the model in Adams™View, shown in Table 7, and the coefficients for the friction and torque dissipation models, listed in Table 8, were adjusted according to the results obtained with the reference model.

Table 7 – Set up parameters for the model in Adams™View.

Parameter	Value	Parameter	Value
J_e [kg m ²]	0,133	J_c [kg m ²]	0.018
R_i [mm]	67	R_o [mm]	95
$\mu_{s,clt}$ [-]	0.54	$\mu_{d,clt}$ [-]	0.54
i_g [-]	4.29	J_g [kg m ²]	296.7×10^{-6}
η_g [-]	0.92	$B_{d,L}$ [N m s]	2.12×10^{-3}
i_d [-]	4.56	J_d [kg m ²]	417.5×10^{-6}
R_w [mm]	307.5	J_w [kg m ²]	3.61×10^{-5}
$\mu_{static,t}$ [-]	0.9	$\mu_{d,t}$ [-]	0.9
M [kg]	1096.5	h_{CG} [mm]	530.3
L [mm]	2510	l_x [-]	0.402
$f_{R,0}$ [-]	0.015	$f_{R,1}$ [s ² m ⁻²]	7×10^{-6}
C_x [-]	0.34	ρ_{air} [kg m ⁻³]	1.225
A_f [m ²]	2.16	g [m s ⁻²]	9.806

The models were simulated for the same initial conditions, defined as:

- Initial velocity of the flywheel $\dot{\theta}_e = 300 \text{ min}^{-1}$ (31, 42 rad s⁻¹);
- Initial velocity of the drivetrain $\dot{\theta}_c = 0 \text{ rad s}^{-1}$;
- Initial velocity of the vehicle $\dot{x} = 0 \text{ m s}^{-1}$.

Table 8 – Assigned values for the properties of the friction models.

Parameter	Value	Parameter	Value
$\mu_{d,clt}$ [-]	0,27	$c_{\mu,clt}$ [-]	0,95
S_f [-]	0,83	n_f [-]	2
$\mu_{d,t}$ [-]	0,90	$c_{\mu,t}$ [-]	100

The input torque on the flywheel and axial force acting on the clutch were considered step functions at $t = 1$ s, with magnitude of 45 N m and 5 kN, respectively. The used solvers and their respective configurations are listed in Table 9.

Additionally to the presented conditions, the models were tested for 0° and 4° of grade, in order to verify all the resistance loads. For 10 s of

Table 9 – Parameters adopted for the simulations in Simulink and AdamsTMView.

Simulink Solver Configurations	
Solver	ODE45 (Dormand-Prince)
Maximum allowed time-step	1×10^{-4} s
Type	Variable-step
Adams TM View Solver Configurations	
Simulation type	Dynamic
Solver	WSTIFF
Formulation	SI2
Maximum allowed time-step	1×10^{-4} s

simulation time and absence of slope, the results of engine, clutch and vehicle velocities are shown in Figure 20.

Besides the the velocities of the kinetic energy reservoirs, the longitudinal load transfer was verified, due to its close relation to the model of driving force. In Figure 21 the results for the first 5 seconds of simulation are shown and, comparing the curves, the developed model presents a smoother behavior than the reference, which is good both in terms of numerical solution of equations and correlation to the physical phenomenon. Also, the difference of peak is of 2.5% and it is reduced to 0.5% during the steady acceleration.

From the plots in the previous Figures, it is concluded that both models converge to the same behavior, indicating that the system defined by (2.43) is mathematically consistent. Moreover, the adopted simplifications do not deviate significantly the behavior of the system, which is interesting both from the computational and physical interpretation sides. The magnitude of the relative deviation between the velocities is shown in Figure 22, in terms of frequency and over simulation time.

The major differences happen up to $t = 1$ s, before the contact between flywheel and clutch disk starts and when the vehicle is not in motion. The deviation is justified by minor differences between the initial conditions of the cases. The equations in AdamsTMView consider the spacial motion of the bodies and, since in the initial condition the tires are at the imminence of

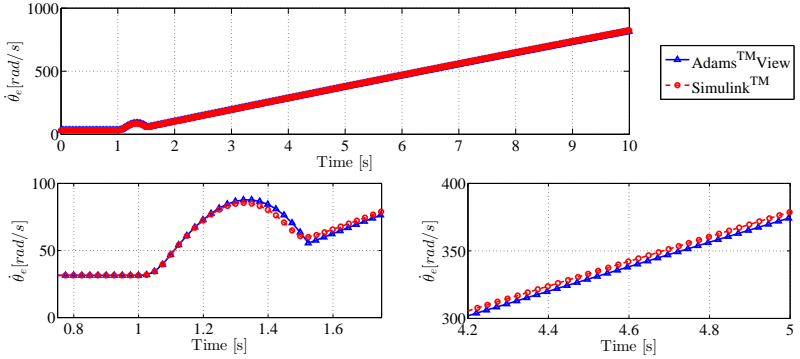
lift, the vehicle presents small displacements until it achieves the equilibrium, leading to the presented results. After that, the differences achieve a maximum of 0.82% for the engine angular velocity at $t = 10$ s.

Adding a grade of 4° , the results obtained with the proposed model still are close to the reference. The deviation between models is represented in Figure 23 and achieves a maximum of 1,33% for the engine angular velocity at $t = 10$ s.

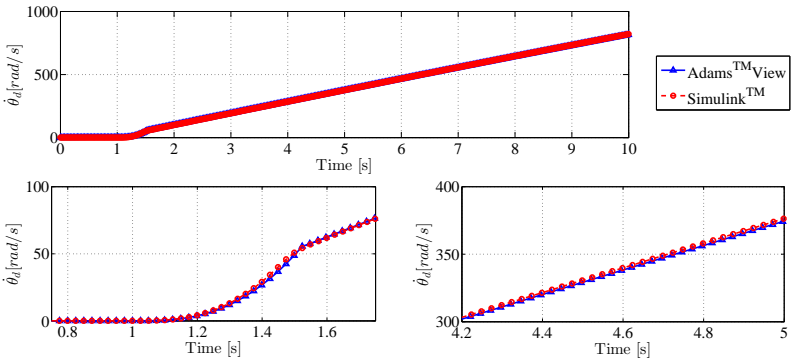
2.3 SUMMARY AND CONCLUSIONS

In this chapter, it was developed a mathematical model of the longitudinal and powertrain dynamics of a vehicle. Differently from the quasi-static approach, the model presents 3 DoF, being capable to represent separately the behavior of the engine, drivetrain and longitudinal motion. This characteristic is relevant to estimate the fuel consumption in urban traffic conditions, which presents start and stop events with high frequency.

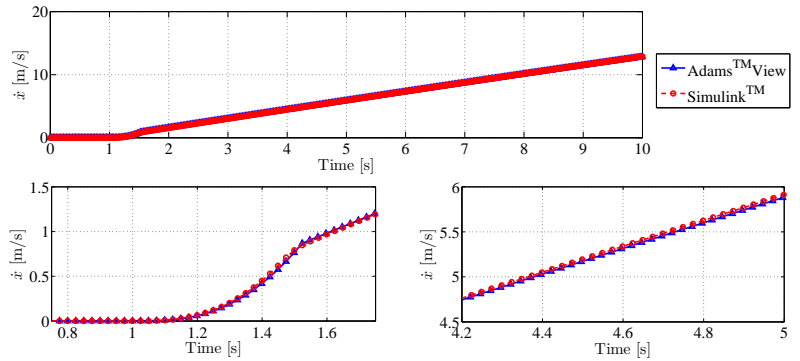
As results of this development, the obtained model has been proved physically coherent and presented similar behavior when compared to a similar model in a commercial software. The next chapter is dedicated to the development of models to represent the torque delivered by the engine and fuel consumption, as well as the algorithm of the drive assistant, which is the objective of this work.



(a) Results of engine angular velocity θ_e .



(b) Results of velocity $\dot{\theta}_d$, obtained for the drivetrain.



(c) Results of vehicle velocity \dot{x} .

Figure 20 – Results of velocity for the main reservoirs of kinetic energy, obtained with the reference model and developed system.

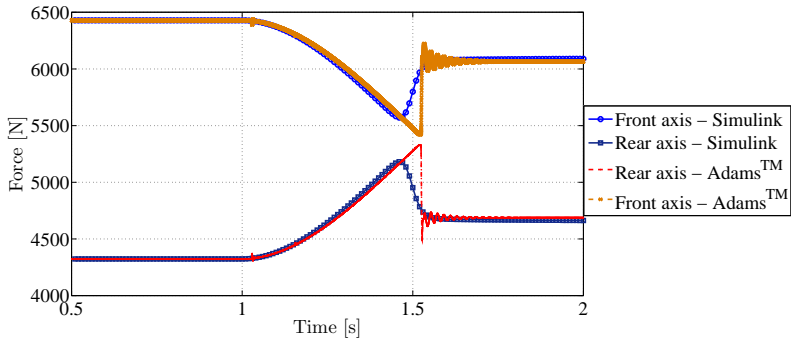


Figure 21 – Comparison between the results of longitudinal load transfer obtained with both models

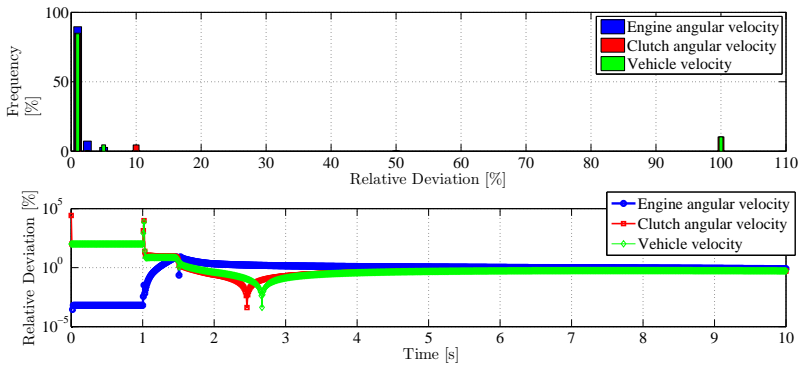


Figure 22 – Frequency of relative deviation between results and deviation over simulation time, for the three reservoirs of kinetic energy, in the simulation with plain road

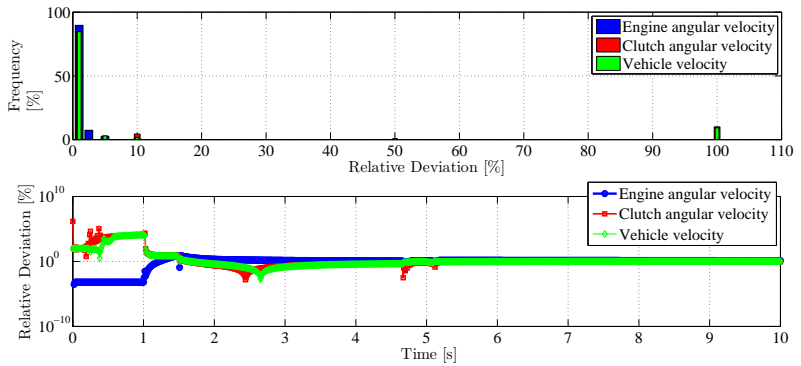


Figure 23 – Frequency of relative deviation between results and deviation over simulation time, for the three reservoirs of kinetic energy

3 DEVELOPMENT OF THE DRIVER ASSISTANT

3.1 LITERATURE REVIEW

In the introductory chapter, a few methods to increase the fuel efficiency of vehicles were discussed. However, according to Saerens, Diehl e Bulck (2010), two important strategies should also be considered: improving the road infrastructure and traffic management, and changing the driving behavior.

The traffic and driving behavior are closely related, and both information are relevant to design eco-driving systems. In (ZHENG et al., 2015), the authors propose a method of energy management for hybrid vehicles, which takes into account available traffic information, obtained periodically from a Intelligent Transportation System (ITS) or a Global Positioning System (GPS). Using an optimal control strategy, the simulations performed by the authors indicated improvements in fuel efficiency up to 11.6%.

Luin, Petelin e Mansour (2017) also performed analyses of the impact of the road on overall fuel efficiency, by adapting a VSP model (Vehicle Specific Power) to calculate the energy consumption for the engine on idle speed. The VSP approach calculates the energy required by the vehicle during changes of velocity and elevation, as well as to overcome the resistances due to rolling friction and aerodynamic drag. However, it does not take explicitly the influence of the powertrain dynamics into account. As an outcome of their study, the authors observed on the results that elevation changes influence considerably on the power demanded by the vehicle and, therefore, the road profile also should be considered as a parameter to increase the fuel efficiency of a vehicle fleet.

On the driver behavior side, Matsumoto, Park e Kawashima (2014) performed a comparative study between Japanese and German eco-driving techniques and their influence on fuel consumption. While in Japan it is recom-

mended a soft start, with gentle acceleration, in Germany the recommendation is to accelerate quickly in order to achieve the engine's fuel efficient range as fast as possible. The experiments performed in the research pointed out that the Japanese approach provides lower coast state ratio than the German strategy, leading to higher overall fuel consumption. When the vehicle is coasting, the driver tends to adopt low throttle input, condition which leads to low fuel consumption for a wide range of velocities, as shown in Figure 24.

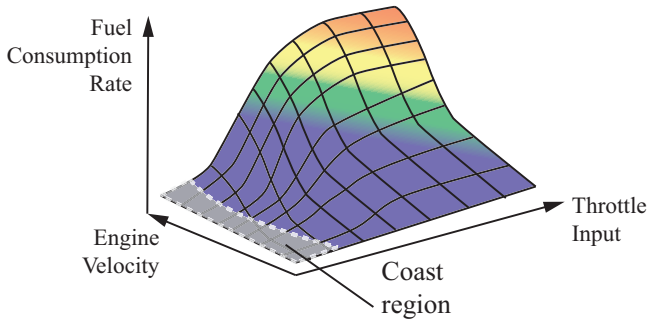


Figure 24 – Shape of a typical fuel consumption map as function of the engine speed and throttle position. Adapted from (MATSUMOTO; PARK; KAWASHIMA, 2014).

Similarly, Son et al. (2016) compared the behavior of drivers in United Kingdom to Korean drivers, in order to analyze the relation between fuel consumption and driving style. In their experiments, the authors observed that the fuel efficiency was affected by the driver's choice of speed and level of attentiveness, among further behavioral aspects. Moreover, the dominant variables that interfere on the fuel efficiency in the UK are different from the ones in South Korea, which indicates that cultural differences in driving style should be considered during the development of eco-driving systems.

The growth on the level of integration between driver and vehicle through multiple interfaces has accelerated the development of vehicle driving assistant systems. In (BIRRELL; FOWKES; JENNINGS, 2014) it is performed a study to evaluate the effect of a smart-driving application on driving performance. The application provides recommendations of headway distance,

gear change, acceleration and braking, in order to increase the safety and fuel efficiency during the operation of the vehicle. The experiments performed by Birrell, Fowkes e Jennings (2014) indicated an increase of 4.1% of fuel efficiency with the adoption of the application, associated with changes on the behavior of the drivers, such as reduction of the mean engine speed.

Similar systems are reported in (KLUNDER et al., 2009), where the expected implementation and effectiveness rates of the analyzed method are provided. For a comparative matter, the report indicates an expected improvement of fuel efficiency of 20% for with the adoption of eco-driving assistance combined with economic driving education. Automatic engine shutdown and gear shift indicator are indicated as solutions to reduce the emission of CO_2 up to 10%.

Also, Voort, Dougherty e Maarseveen (2001) say that by preparing the drivers to change their driving habits, it is possible for them to keep completing the same journeys within similar time ranges and with significant less fuel. The study carried out by the authors focuses on presenting a prototype of driver advisor system, tested in a driving simulator. The rule-based advisor back-calculates the minimum fuel consumption for the performed maneuvers, based on a the vehicle's specific fuel consumption map, and provides a feedback to the driver. The results of the experiments pointed out that the drivers were capable of reducing the fuel consumption up to 16% with the driving assistant, against 9% obtained without support. Furthermore, according to the authors, there is an optimal driver behavior, which minimizes the fuel consumption of a vehicle for a given journey.

Eckert (2017) presents a computational and experimental analyses, which evaluates the influence of gear shift strategies on vehicles' longitudinal dynamics. In the first part of his study, the author determined experimentally the maps of torque and fuel consumption for a vehicle and developed a mathematical model of its longitudinal dynamics. Then, alike the previous references, the best gear shift strategy is defined through an optimization problem, solved with a genetic algorithm. The simulation model was submitted to the Brazilian driving cycle NBR6601 and, compared to the strategy of gear shift proposed

by the manufacturer, the optimized approach achieved 15% of fuel economy. With respect to the experimental analyses, they were carried on a chassis dynamometer and the deviations varied from 3.6% to 5.5%.

The developments reviewed in this section focus on the driver's influence over the longitudinal performance of a vehicle. Differently from the ones presented in the introductory chapter, the proposed solutions to reduce the fuel consumption either demand improvements on the infrastructure (e.g. route selection and road quality) or modification of the driver behavior.

The infrastructural aspects are highly dependent on local factors, such as landscape, climate and road administration, therefore, defining a generic strategy to reduce fuel consumption based on them is very limited. The driver, however, is capable to control the vehicle's motion based on spatial sensitivity and by accessing a few parameters: throttle level and brakes, gear ratio and steering degree.

Since the behavior of a driver depends on multiple human characteristics, including cultural aspects, acting on the education of new drivers, although necessary, is a long term solution. Moreover, it is dependent on the adherence of the method that would be taught in driving schools and its compatibility to the adopted vehicle. Hence, a driver assistant with throttle and gear shift controllers could be used to modify the driving parameters towards the direction of the best operating range of the ICE, improving the fuel efficiency of the vehicle.

3.1.1 Automotive Controllers and Driver Assistance Systems

Driver Assistance Systems are support tools which take over the control of some driving parameters in order to improve the driver's safety and comfort (AMMON; SCHIEHLEN, 2009). Among the developed systems, maneuvering/parking support, lane keeping assistance, stability control and collision avoidance are a few examples of the most known features of modern vehicles. In the literature three relevant control methods were found as mainly used for the design of driver assistants on fuel economy: fuzzy logic, optimal control

and model predictive control.

Chou et al. (2012) present a eco-driver assistant implemented as a 7-rule fuzzy controller. The system estimates the vehicle loads by collecting information of sensors from OBD (On-Board Diagnosis) and CAN bus, and calculates the fuel economy using an heuristic model. A similar methodology is applied in (BALDANIA; SAWANT; PATKI, 2014), however the authors focus on fuel saving through improvements on the activation of the air conditioning system. The implemented system has 150 rule combinations an 4 different outputs, which interfere on the compressor and fan speed, expansion valve and air-conditioner mode.

In both cases, the adoption of fuzzy controllers increased the energetic efficiency of the vehicle. Nevertheless, the authors did not compared their developments with an optimum strategy, which leads to the minimum fuel consumption. Moreover, as concluded in (BALDANIA; SAWANT; PATKI, 2014), the performance of the fuzzy controller is highly dependent on how the rules are structured, which demands enough knowledge of the system behavior in beforehand.

Alternatively to the Fuzzy Logic, optimal control methods allow the fuel-economy driving aids to achieve their maximum potential. Three general approaches are used to address optimal control problems: dynamic programming, indirect and direct methods; where the third is the most widespread and accepted method, due to its capacity to handle inequality constraints and structural changes. However, the indirect methods lead to Euler-Lagrange equations and include the Pontryagin's Maximum Principle, which gives a physical insight over the solution, which is interesting from the analysis point of view (SAERENS; DIEHL; BULCK, 2010).

In (CHENG; NOUVELIÈRE; ORFILA, 2013), dynamic programming was implemented to define the optimum velocity profile with respect to fuel consumption of a vehicle and considering the driver's comfort. Lin, Gorges e Liu (2014) present a similar development, yet for a pure electric vehicle and using an objective function that considers only the energy consumption and driver's preferences. In both cases, a considerable amount of energy could be

saved, however, the obtained solutions are specific for the journeys simulated by the authors. Furthermore, performing dynamic programming online is computationally costly, therefore, the hardware requirements would increase substantially.

Xu et al. (2017) present the development of an optimal controller using an approximation of the Pontryagin's Maximum Principle, simplifying the algorithm proposed on the original method. Among many aspects of the carried analyses, the authors have considered the variation of the road slope, which is known to present high influence on fuel consumption and is not frequently found in the literature.

The work presented by Shao e Sun (2017) is a proposal of an adaptive and optimized cruise control to improve fuel efficiency. The authors adopted a quasi-static model of vehicle dynamics and the gear shift was scheduled according to the velocity and acceleration of the vehicle. The proposed controller was obtained using a nonlinear programming solver applied to an objective function, which has terms related to fuel consumption and ride comfort. Also, the authors modify the optimization process in order to make it robust, such that variations in the traffic would not affect the controller severely. An important aspect of the optimization procedure is the normalization of the terms in the objective function, such that they can be properly weighted and the effect of ill-scaled gradients is reduced. The results shown improvements up to 23.5% of fuel economy.

Analogously to the previous work, Kamal et al. (2010) develop an eco-driving system using model predictive control. The authors also take into account the distance between the host and preceding vehicle, simulating a usual traffic condition. The control algorithm updates iteratively the states of the model and, based on a given cost function, calculates the best control inputs and implements them on the system, as shown in the flow chart of Figure 25. The simulation of the proposed algorithm, compared to further models found in the literature, has been shown significant potential of fuel saving.

Jing et al. (2016) developed a speed controller oriented for fuel economy, where the optimal solution is calculated under model predictive control.

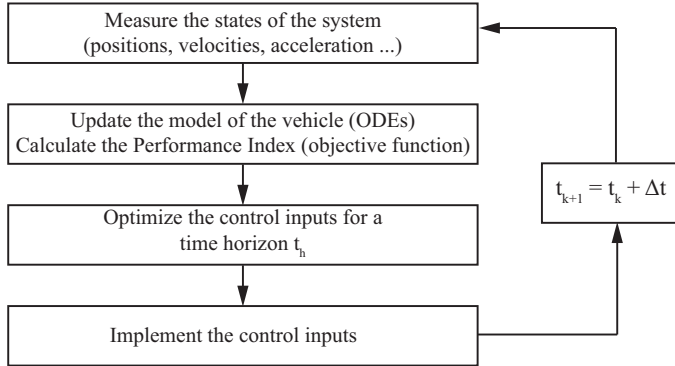


Figure 25 – Generic flow chart of the MPC algorithm. Adapted from (KAMAL et al., 2010).

In order to apply the method for real time applications, the algorithm divides the problem into simplified smaller ones, such that optimal solutions can be achieved faster. Further than developed in (KAMAL et al., 2010), the proposed algorithm also calculates the best gear sequence, which is obtained with a finite state machine and has its optimality proven by the Pontryagin's Maximum Principle. However, the algorithm became more complex than the previous ones and it was tested only through simulations.

At last, Li et al. (2017) also presents a cruise controller based on model prediction, enhanced with data of road elevation. In order to calculate the optimum control sequence, the problem was discretized using a pseudospectral technique to a nonlinear programming solver. The authors present an important discussion regarding the hard constraints that the range of gear ratios, rotation and torque impose to the optimization problem. The boundaries are softened by adding penalizations to the objective function, avoiding numerical singularities. Furthermore, the stability of the controller is also discussed, since there is no mathematical guarantee of stability for model prediction control.

The works reviewed in this section have similar objectives, which were achieved through different methods and considering different aspects of vehicle longitudinal dynamics. In most of them, the control strategies used

exterior signals to the engine, such as longitudinal acceleration and forward vehicle distance, in order to perform calculations of optimal control inputs. Also, the proposed assistants take over the control of the longitudinal dynamics most of the time, which increases the both driver's comfort and complexity of the control algorithm.

Based on the characteristics of the presented review, a drive assistant for improving fuel efficiency is proposed in the following section.

3.2 DRIVER ASSISTANT FOR FUEL CONSUMPTION IMPROVEMENT

The main purpose of the suggested Driver Assistant (DA) is to reduce the fuel consumption of a vehicle by adjusting some of the driver's actions: throttling and gear shifting. In order to achieve it, the following design requirements were defined, taking the literature analysis as reference:

- The safety of the occupants has higher priority than reducing fuel consumption. Therefore, adjustments of the throttle position should be limited, such that the vehicle will not accelerate during braking events;
- The input signals of the DA should be limited, as much as possible, to ones commonly used to control the engine, e.g. position of the throttle and velocity of the engine. This limitation avoids the addition of new components to the vehicle and facilitates the implementation of the system in commercial vehicles;
- The structure of the controller should not be vehicle-specific, such that it can be transferred to different powertrain systems, with minor setup modifications, and still being capable to perform fuel consumption optimization.

The development of the algorithm of the DA starts with the definition of the functions that describe the fuel consumption and mean torque delivered by the engine. These functions will provide the necessary inputs to the dynamic

model and to evaluate the directions to move the operation point towards the conditions of maximum efficiency. Then, the equations and algorithm that describe the behavior of the assistant are defined, based on the dynamics of the system and signals available in the model. At last, the algorithm is tested for simple velocity profiles, in order to verify its consistency with respect to the formulation and design requirements.

3.2.1 Torque and Fuel Consumption Maps

Embedded control systems usually operate under tight processing constraints, therefore, detailed multiphysics models cannot be used to perform calculations, and instead, simplified models are adopted (GUZZELLA; ONDER, 2010; ISERMANN; MÜNCHHOF, 2011). These models either derive from the physics of the phenomena, e.g. Mean-Value Models, or present pure mathematical characteristics, as static maps. In practice, the first approach is adopted for complex processes, such as prediction of pollutant emissions, while the second is applied to most of the engine characteristics, as timing of spark ignition and injection nozzles, due to its low processing costs and easy implementation.

The static maps inserted in the Engine Control Unit (ECU) are surrogate models that rely on a summary of experimental data used to calibrate the engine operation, which derive the values of interest using available signals (GUZZELLA; ONDER, 2010). Among the mathematical structures found in the literature, methods using look-up tables and Artificial Neural Networks (ANN) arose most frequently, justified by their capability to represent nonlinear systems with flexibility and low computational cost.

In practice, look-up table maps are the most used tool, due to its simplicity of implementation (ISERMANN; MÜNCHHOF, 2011). Its structure consists of a grid of inputs, where each node has an associated height, as represented in Figure 26. The interpolation of intermediate nodes is a two-step process: locating the nodes on the grid that are the nearest to the operating condition, and performing a bilinear area interpolation, given in Equation 3.1 (ISERMANN; MÜNCHHOF, 2011)

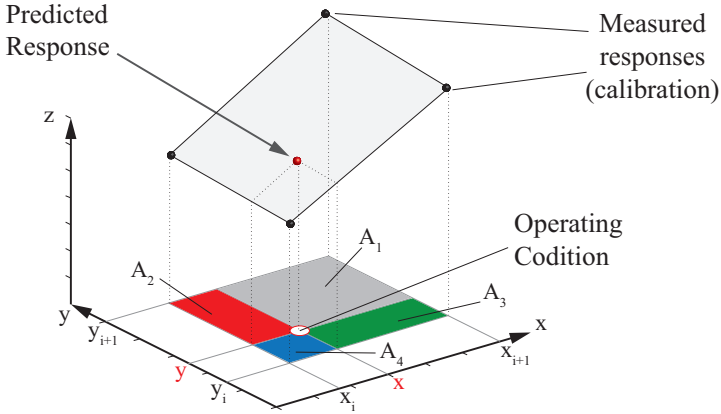


Figure 26 – Representation the method used to interpolate intermediary conditions using Look-up Tables. Adapted from (ISERMANN; MÜNCHHOF, 2011).

$$Z(x, y) = \left(Z(x_{i+1}, y_{i+1}) A_1 + Z(x_i, y_{i+1}) A_2 + Z(x_{i+1}, y_i) A_3 + Z(x_i, y_i) A_4 \right) \left(\sum_{j=1}^4 A_j \right)^{-1} \quad (3.1)$$

where A_j correspond to the areas shown in Figure 26. The quality of the approximation depends on the level of refinement of the grid and it is assumed that the entire operating range is within it. Also, although computationally simple, the amount of required data do build a look-up table model grows exponentially with the number of dimensions and, therefore, its use is, in practice, limited to one or two dimensional maps.

Artificial Neural Network models (ANN), on the other hand, are capable of representing nonlinear systems with multiple inputs and outputs, while the computational cost has minor increase. Furthermore, ANN do not demand a step of node search, as required for the look-up tables, and can be used as functions $Z = F(x_1, x_2, \dots, x_n)$, which is a better fit to the purposes of this work.

In (HAYKIN, 1998), an ANN is defined as a massively parallel distributed processor, which contains simpler units called "neurons" and is capable of storing knowledge, as well as making it available for use. The preparation of a ANN model requires, at first, the selection of the architecture and then, the execution of a training procedure (KOZIEL; CIAURRI; LEIFSSON, 2011).

A wide variety of architectures is available in the literature, however, this work focus on a particular structure named Multi-Layer Feed-forward Network (MLN), represented in Figure 27. This architecture allows the network to withdraw higher order information from the system of interest and is recommended for modeling of static processes (ISERMANN; MÜNCHHOF, 2011). The number of neurons and layers will be defined heuristically, since there is no specific method to determine these parameters.

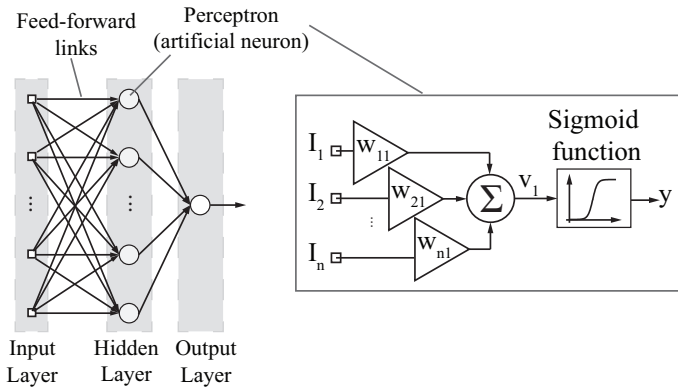


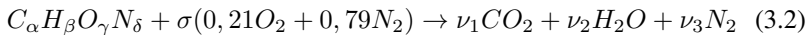
Figure 27 – Representation of a multi-layer perceptron, with n inputs and a single output. Adapted from (ISERMANN; MÜNCHHOF, 2011).

Inputs and neurons, in the hidden and output layer, are connected by synaptic links, which multiply the signal by a synaptic weight w_{ij} . After the links, the signals are summed at the node and it is applied a nonlinear operation, named activation function, which limits the output of the neurons. In (ISERMANN; MÜNCHHOF, 2011; HAYKIN, 1998), a few options of functions are listed, however, for the sake of simplicity, the sigmoid function was adopted for this work.

After defining the structure of the ANN, a training procedure, also called "learning", is performed. This process consists of submitting the network to a simulated environment where the model will be used, while optimizing its synaptic weights, such that the error of the model is minimized (HAYKIN, 1998; ISERMANN; MÜNCHHOF, 2011). Therefore, the training requires two sets of data: one which is repeatedly presented to the ANN while its weights are being modified, and other to verify how the model behaves when unknown data, within the sampled space used for the first set, is presented. For the sake of brevity, the algorithm and mathematical development of the training procedure was kept out of the text, nevertheless, it is detailed in (HAYKIN, 1998).

By definition, the development of surrogate models do not require any previous knowledge of the system to be modeled. However, understanding the laws of physic related to the process that will be represented by the model provides an insight of which input and output signals, as well as properties and operation conditions, are the most relevant, such that the training data can be sorted and reduced. Furthermore, the probability of achieving satisfactory results with a sorted set of data increases, since only relevant data will be presented to the ANN during the training phase.

Concerning the models required for this work, both torque and fuel consumption are correlated associated to the combustion phenomena. The oxidation reaction of a generic hydrocarbon fuel, considering stoichiometric conditions and standard dry air composition, is represented in Equation 3.2.



where the coefficients σ , ν_1 , ν_2 and ν_3 depend on the chemical composition of the fuel (values of α , β , γ and δ). From Equation 3.2, the air/fuel ratio can be defined as

$$AF = \sigma \frac{(0,21 M_{O_2} + 0,79 M_{N_2})}{M_{fuel}} \quad (3.3)$$

where M_i is the molar mass of the substance i . Hence, the relation between air and fuel mass flow ratios (\dot{m}_{air} , \dot{m}_f) is determined as follows

$$\dot{m}_f = \frac{\dot{m}_{air}}{AF} \quad (3.4)$$

During the operation of an ICE, the value of AF is hardly constant due to multiple reasons. Therefore, it is adopted a feedback control system which, based on target values of air/fuel ratio and measurements of the intake mass flow ratio and oxygen concentration in the exhaust gases, adjusts the fuel mass flow ratio. The measurements at the intake derive from a Manifold AirFlow (MAF) or Manifold Absolute Pressure (MAP), while the oxygen concentration is measured using a lambda sensor at the exhaust pipe, as shown in Figure 28.

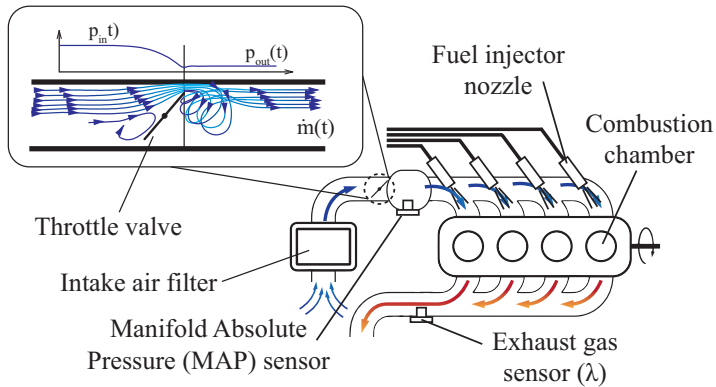


Figure 28 – Schematic of an ICE indicating the main sensors for controlling the AF ratio. Adapted from (GUZZELLA; ONDER, 2010).

Considering the engine as a volumetric pump and assuming compressible fluid behavior, complete conversion of potential to kinetic energy up to the narrowest point and fully turbulent flow after the throttle (GUZZELLA; ONDER, 2010), the mass flow is modeled as follows

$$\dot{m}_{air}(t) = c_d A_t(t) \frac{p_{in}(t)}{\sqrt{R_g \Omega_{in}}} \Psi \left(\frac{p_{in}(t)}{p_{out}(t)} \right) \quad (3.5)$$

where Ψ is the flow function and it can be approximated using

$$\Psi \left(\frac{p_{in}(t)}{p_{out}(t)} \right) = \left\{ \begin{array}{ll} \frac{1}{\sqrt{2}}, & \text{for } p_{out} < \frac{1}{2} p_{in} \\ \sqrt{\frac{2 p_{out}}{p_{in}} \left(1 - \frac{p_{out}}{p_{in}} \right)} & \text{for } p_{out} \geq \frac{1}{2} p_{in} \end{array} \right\} \quad (3.6)$$

where c_d , $A_t(t)$, Ω_{in} and R_g are the coefficient of discharge, throttle opening area, temperature of the intake flow and ideal gas constant, respectively. The manifold dynamics, for compressible conditions, is modeled as follows (GUZZELLA; ONDER, 2010)

$$\frac{d}{dt} p_m(t) = \frac{R_g \Omega_M}{V_m} \left(A_t(t) \frac{p_{in}}{\sqrt{R_g \Omega_m}} \frac{1}{\sqrt{2}} - \frac{p_m(t)}{R_g \Omega_m} \frac{\eta_V V_d \dot{\theta}_e}{N 2\pi} \right) \quad (3.7)$$

where Ω_M is the mean temperature in the manifold, N the number of revolutions per cycle, V_d the displaced volume, η_V the volumetric efficiency and the engine velocity $\dot{\theta}_e$ is considered roughly constant over a few cycles.

With exception of the throttle angle and engine velocity, the remaining variables depend either on environmental conditions, e.g. inlet pressure, or on the design and control of the engine, e.g. volumetric efficiency. Given the objectives of this work and for the sake of brevity, it was decided that the driver assistant cannot interfere on the control of the AF ratio. Hence, the fuel consumption, with respect to the engine operating conditions, becomes a function of the throttle opening area, defined by the driver, and the engine speed, result of the engine dynamics, as shown in Equations 3.3, 3.5, and 3.7.

Similarly, the mean available torque at the crankshaft can be estimated using

$$T_c = \frac{e(\dot{\theta}_e, AF, \Omega_e, \dots) H_l}{N 2\pi} \frac{1}{1 + \sigma} \frac{V_d \eta_V}{R \Omega_m(t)} p_m(t) - \frac{V_d}{N 2\pi} p_{me0} \quad (3.8)$$

where e is the thermodynamic efficiency of the engine, H_l the lower heating value of the fuel and p_{me0} is the term of pressure related to pumping and friction losses.

The thermodynamic efficiency depends on several variables, including the AF ratio, ignition timing and engine velocity, which makes it highly dependent on the engine model and control. Similarly, the internal losses vary with the load and engine velocity, as well as with the operation time, since the lubricant properties and engine geometry are affected by the temperature (GUZZELLA; ONDER, 2010; HEYWOOD, 1988). The dynamics of the manifold pressure $p_m(t)$, on the other hand, are described as a function of the throttle position and engine velocity, as discussed before.

Due to the available data for the development of this work, the input variables of Equation 3.8 will be narrowed down to the throttle opening and engine velocity. It is important to emphasize that the validity of the ANN model is limited to the conditions of the tests used for data acquisition and its degree of fidelity is bounded by the measured variables. Therefore, the data used for this work accounts implicitly the terms of thermal and mechanical efficiencies, as well as the characteristics of the fuel and behavior of the ECU.

Once defined the structure, input and output variables of the maps that represent the performance of the engine, it is possible to define the algorithm for the driver assistant.

3.2.2 Algorithm of the Driver Assistant

The proposed algorithm is based on the structure observed in (KAMAL et al., 2010) and it is shown in Figure 29.

The first calculation step converts the inputs into terms of an objective function, which is used to minimize the fuel consumption. The torque demand is defined as follows

$$T_{Ref}(X_G, \dot{\theta}_e) = \frac{X_G T_{w,max}}{\exp((\theta_e^*)^{s_v})} \quad (3.9)$$

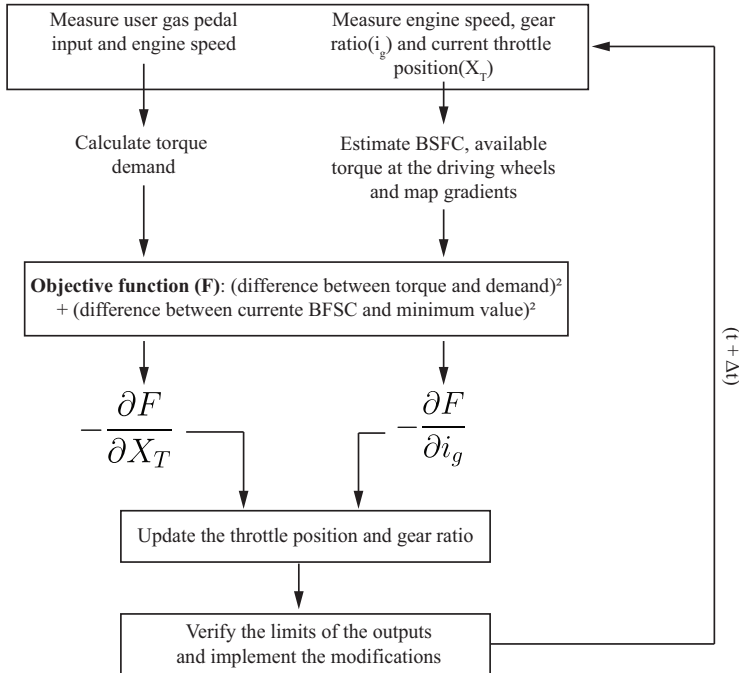


Figure 29 – Structure of the proposed driver assistant algorithm, based on the method proposed in (KAMAL et al., 2010)

where X_G is the throttle pedal input, $T_{w,max}$ the maximum achievable torque at the wheel and s_v is a constant to adjust the behavior of the function. The variable $\dot{\theta}_e^*$ corresponds to the engine velocity normalized to the interval $[0, 1]$, considering the idle and maximum speed.

This function allows the driver assistant to favor the demand of torque at low engine speeds, requiring high gear ratios to increase the acceleration. On the other hand, when the engine achieves a certain velocity, the demand for torque decreases and, consequently, lower gear ratios can be used, allowing the vehicle to achieve cruise velocities. In Figure 30 it is shown the results of the evaluation of the function, for $X_G \in [0, 1]$ and $\dot{\theta}_e \in [900, 4500]min^{-1}$ and $s_v = 5$.

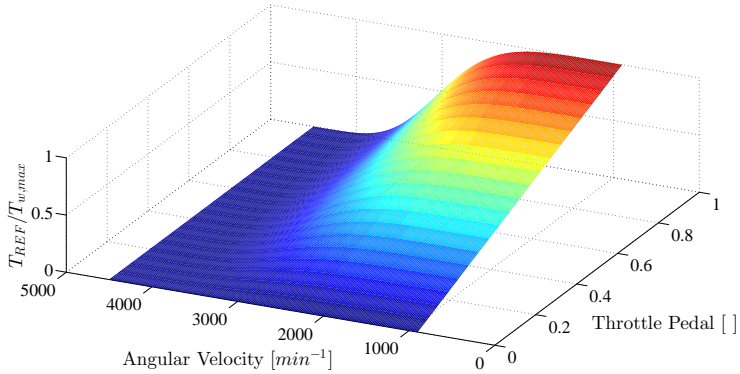


Figure 30 – Evaluation of the torque demand function for $X_G \in [0, 1]$ and $\dot{\theta}_e \in [900, 4500] \text{min}^{-1}$ and $s_v = 5$

Simultaneously, it is estimated the torque available at the wheel and Break Specific Fuel Consumption (BSFC), here identified by the variable Φ , as well as the partial derivatives of the maps of torque and BSFC, with respect to the throttle opening.

The objective function proposed for the driver assistant has two components: the squared difference between the torque demand an estimated value, and the squared difference between the estimated BSFC and minimum achievable value. It is mathematically described in Equation 3.10.

$$F\left(X_T, \dot{\theta}_e, i_g\right) = \left[\frac{T_{Ref} - T_e(X_T, \dot{\theta}_e) i_g i_d}{T_{w,max}} \right]^2 + \left[\frac{\Phi(X_T, \dot{\theta}_e) - \Phi_{min}}{\Phi_{max} - \Phi_{min}} \right]^2 \quad (3.10)$$

The approach adopted to minimize the objective function is based on a gradient method for direction search in optimization algorithms. The steepest descent method defines the direction of optimization as the negative of the gradient vector of the cost function, since the gradient has the same direction as the one of maximum increase of the cost function. Although this method uses only first order information and does not consider the previous directions

to accelerate the convergence (ARORA, 2017), it is very simple and robust, which is usually required for control applications.

Since the velocity of the engine is a variable of level (GUZZELLA; ONDER, 2010), therefore, an output of the system dynamics, the objective function can be seen as a function of two input variables: X_T and i_g . Thus, the gradient vector yields to

$$\nabla F(X_T, i_g) = \begin{bmatrix} 2 \left(F_1 \frac{\partial \Phi}{\partial X_T} + F_2 \frac{\partial T_e}{\partial X_T} \right) \\ 2 F_3 \end{bmatrix} \quad (3.11)$$

where

$$\begin{aligned} F_1 &= \frac{\Phi(X_T, \dot{\theta}_e) - \Phi_{min}}{(\Phi_{max} - \Phi_{min})^2} \\ F_2 &= \frac{\left(T_{Ref} - T_e(X_T, \dot{\theta}_e) i_g i_d \right) (-i_g i_d)}{T_{w,max}^2} \\ F_3 &= \frac{2 \left(T_{Ref} - T_e(X_T, \dot{\theta}_e) i_g i_d \right) \left(-i_d T_e(X_T, \dot{\theta}_e) \right)}{T_{w,max}^2} \end{aligned} \quad (3.12)$$

Then, the the throttle position and gear ratio are updated using

$$\begin{aligned} X_T(t + \Delta t) &= X_T(t) - 2 \left(K_{t,\Phi} F_1 \frac{\partial \Phi}{\partial X_T} + K_{t,T} F_2 \frac{\partial T_e}{\partial X_T} \right) \\ i_g(t + \Delta t) &= i_g(t) - 2 K_i F_3 \end{aligned} \quad (3.13)$$

where the coefficients $K_{t,\Phi}$, $K_{t,T}$ and K_i can be adjusted according to the magnitude of the associated terms and desired update step. The role of the gains in the proposed system is analogous to the gains of a common PID (Proportional-Integral-Derivative) Controller. The actions of the DA are weighted according to the value of the gains, such that either performance or fuel economy can be

set as the preference of the driver. For the sake of brevity, the adjustment of the gains in this work will be explored using a DoE-based (Design of Experiments) approach.

The last step of the algorithm consists of verifying the magnitude of the updated values, such that the responses are limited to feasible ranges. In the case of the gear ratio, the value is discretized according to the intervals of the gearbox and it is limited by the maximum and minimum gear ratios. For safety reasons, the throttle angle has an additional constraining, which corresponds to $\pm 10\%$ of gas pedal input, provided by the driver. Hence, if the driver has no intention to accelerate the vehicle ($X_G = 0$), the driver assistant will not increase the throttle angle, as well as during accelerations, the torque at the wheel cannot be considerably reduced, affecting the maneuverability.

3.2.3 Preliminary Analysis

The objective of the analyses in this section is to verify the behavior of the dynamic system with the developed driver assistant algorithm under simple and well known conditions, such that inconsistencies can be detected and solved. Additionally, the mathematical consistency of the strategy used to develop the algorithm can be verified, by observing which regions of the maps were achieved more often during the simulations.

The dynamic system adopted for the tests is similar to the one used in Chapter 2, implemented on Simulink and verified using Adams TMView. The main modification was an expansion of the gearbox from one to five gears, based on the vehicle FIATTMPunto 2008, with a 1.4L engine, also used for further simulations in this work. The updated values of the vehicle properties are listed in Table 10.

The target data used for training the surrogate models of fuel consumption rate and mean torque were intentionally designed as paraboloid functions of the throttle opening and engine velocity, given in Equations 3.14 and 3.15. Therefore, the points of minimum fuel consumption and maximum torque can be set to different operating conditions, which is important to verify the

Table 10 – Characteristics of the simulated vehicle, adapted from (ECKERT, 2017).

Component	Variable	Value	Unity
Equivalent Inertia of the ICE	J_e	0.138	kg m ²
Equivalent inertia of the gearbox			
1st gear	J_g^1	0.0017	kg m ²
2nd gear	J_g^2	0.0024	kg m ²
3rd gear	J_g^3	0.0037	kg m ²
4th gear	J_g^4	0.0058	kg m ²
5th gear	J_g^5	0.0073	kg m ²
Gear Ratio			
1st gear	i_g^1	4.273	[-]
2nd gear	i_g^2	2.238	[-]
3rd gear	i_g^3	1.444	[-]
4th gear	i_g^4	1.029	[-]
5th gear	i_g^5	0.838	[-]
Inertia of the final drive	J_d	1.52×10^{-4}	kg m ²
Final drive ratio	i_d	4.4	[-]
Inertia of the wheel and tire	J_w	0.72	kg m ²
Frontal area of the vehicle	A_f	2.16	kg m ²
Drag coefficient	C_d	0.34	[-]
Wheelbase	L	2.510	m ²
Height of the CG	h_{cg}	0.53	m
Rear weight distribution	l_x	0.40	[-]
Number of clutch faces	n_f	2	[-]
Internal clutch radius	R_i	67	mm
Outer clutch radius	R_o	95	mm
Clutch dynamic friction coefficient	$\mu_{d,clt}$	0.27	[-]
Tireprint dynamic friction coefficient	$\mu_{d,t}$	0.90	[-]

capability of the algorithm to handle different maps.

$$T_{e,*}(\dot{\theta}_e, X_T) = \left[- \left(\frac{\dot{\theta}_e}{\dot{\theta}_{e,max}} - \frac{\dot{\theta}_{e,@T_{max}}}{\dot{\theta}_{e,max}} \right)^2 - (X_T - X_{T,@T_{max}})^2 \right] T_{max} \quad (3.14)$$

$$FC_*(\dot{\theta}_e, X_T) = \left[\left(\frac{\dot{\theta}_e}{\dot{\theta}_{e,max}} - \frac{\dot{\theta}_{e,@FC_{min}}}{\dot{\theta}_{e,max}} \right)^2 + (X_T - X_{T,@FC_{min}})^2 \right] FC_{max} + FC_{min} \quad (3.15)$$

Using the equations above, two sets of maps were obtained for two different points of minimum fuel consumption: one considering the conditions of minimum fuel consumption at $X_T = 0.1$ and $\dot{\theta}_e = 2200 \text{ min}^{-1}$ and the other at $X_T = 0.8$ and $\dot{\theta}_e = 3000 \text{ min}^{-1}$. In both cases, the condition of maximum torque was kept the same, $X_T = 0.95$ and $\dot{\theta}_e = 3200 \text{ min}^{-1}$, and the ranges of angular velocity and throttle position were $[900, 4500] \text{ min}^{-1}$ and $[0, 1]$, respectively.

The map of BSFC was derived from the previous calculations, using

$$\Phi_*(\dot{\theta}_e, X_T) = \frac{FC_*(\dot{\theta}_e, X_T)}{T_{e,*}(\dot{\theta}_e, X_T) \dot{\theta}_e} \quad (3.16)$$

In order to perform the training procedure, 100 points were randomly sampled from the formulation above for each set of maps, where 75 were used for actually training and 25 for verification of the model. The configurations of the neural networks were defined experimentally and the final results are listed in Table 11.

Once added the maps to the model, the inputs of the system becomes the throttle angle and gear ratio. Hence, it is necessary to model the behavior of the driver, which is capable to accelerate, brake, shift gears and operate the clutch, based on information available in the cockpit. According to (PETERS; NILSSON, 2007), driving can be seen as a control task, where the input signals are perceived through the senses and the control actions are based on conscious or unconscious decisions. Given the numerous tasks performed simultaneously by a person while driving a vehicle, and considering the aspects of learning through experience and perception of the external world, it is hard to find a

Table 11 – Final configuration of the ANN and results of the training and verification procedures

Properties	$FC_{min} @ X_T = 0,1 \text{ and } \dot{\theta}_e = 2200 \text{ min}^{-1}$		
	Fuel Cons.	Mean Torque	BSFC
Number of neurons	5	5	5
Learning rate	0.01	0.01	0.01
Number of iterations	5×10^5	5×10^5	5×10^5
R^2 - Training	0.999900	0.999452	0.999925
R^2 - Verification	0.999751	0.999422	0.999238
$FC_{min} @ X_T = 0,8 \text{ and } \dot{\theta}_e = 3000 \text{ min}^{-1}$			
Number of neurons	5	5	5
Learning rate	0.01	0.01	0.01
Number of iterations	5×10^5	5×10^5	5×10^5
R^2 - Training	0.999912	0.999452	0.999763
R^2 - Verification	0.999802	0.999422	0.996862

closed concept of a full model of a driver in the literature (CARSTEN, 2007; PETERS; NILSSON, 2007).

However, in the simulations to be performed, only the longitudinal dynamics are considered, such that the behavior of the driver can be simplified. Also, it is not the purpose of this work to evaluate the influence of the driver's behavior on the system, but to compare the performance of the driver assistant with respect to a "standard driver", which has a predictable reaction in front of known disturbances of velocity.

Hence, as proposed by (WEIR; CHAO, 2007), a continuous Proportional-Integral Controller (PI) is adopted to control the accelerator and brake pedals. Since braking dynamics are not addressed in this work, the braking force is assumed to be proportional to the drivers input and saturated, which would correspond to the maximum braking force.

With respect to the clutch, it is considered that the driver only acts on the clutch pedal to avoid engine velocities below the idle speed. Hence, it is adopted an exponential function with saturation at the maximum axial force, as shown in the block diagram of Figure 31. The standard gearshift strategy is the one suggested in (FIAT, 2008).

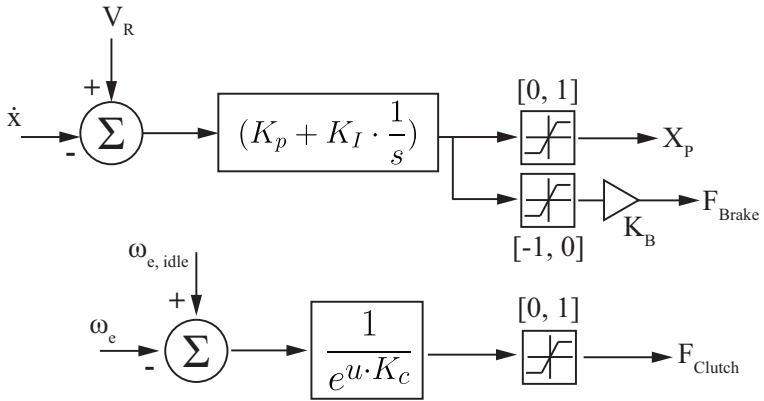


Figure 31 – Block diagram of the driver model for controlling the accelerator pedal, brake and clutch forces.

Integrating the controller of the throttle pedal, clutch axial force and the driver assistant algorithm to the original system of equations, the block diagram becomes similar to the one shown in Figure 32.

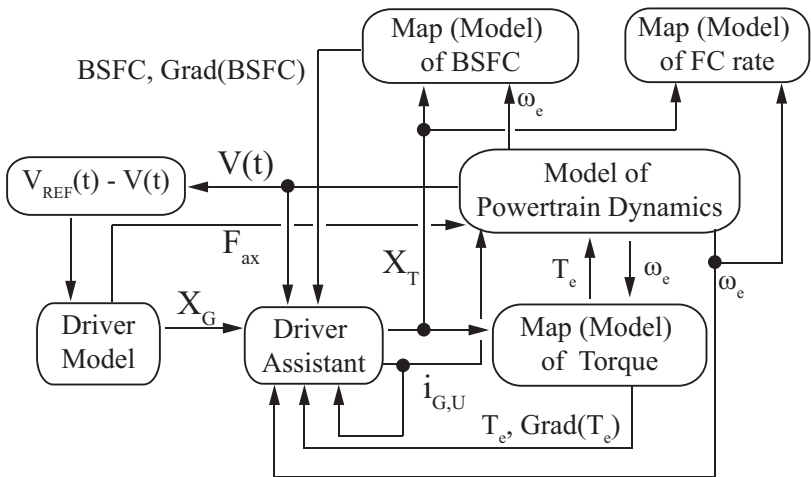


Figure 32 – Block diagram of the complete model, including the driver assistant and model of the driver behavior.

The gains of the driver model were adjusted iteratively, with the objective to reduce the difference between the reference and achieved velocity throughout the simulation time. The metric adopted to evaluate the deviation of velocity is given as follows

$$(1 - R) = \sqrt{\frac{\left[\sum_{i=1}^N (V_R(t) - \bar{V}_R) (\dot{x}(t) - \bar{\dot{x}}) \right]^2}{\sum_{i=1}^N (V_R(t) - \bar{V}_R)^2 \sum_{i=1}^N (\dot{x}(t) - \bar{\dot{x}})^2}} \quad (3.17)$$

where the $(1 - R)$ is the complement of the correlation factor R and the upper bar indicates the mean value of the data series. This metric is applicable to any kind of data set (NAVIDI, 2014 apud ECKERT, 2017) and was adopted to keep the results comparable to the references in future simulations.

Also, the coefficients $K_{t,\Phi}$, $K_{t,T}$ and K_i of the driver assistant were set to 0, such that it does not interfere on the behavior of the driver, and the gearshift strategy was set as standard. The velocity profile used for the simulations was based on the study carried out by Matsumoto, Park e Kawashima (2014), simulating a start and stop events, as shown in Figure 33, and the first set of maps was adopted. The solver and its configurations to simulate the system are listed in Table 12.

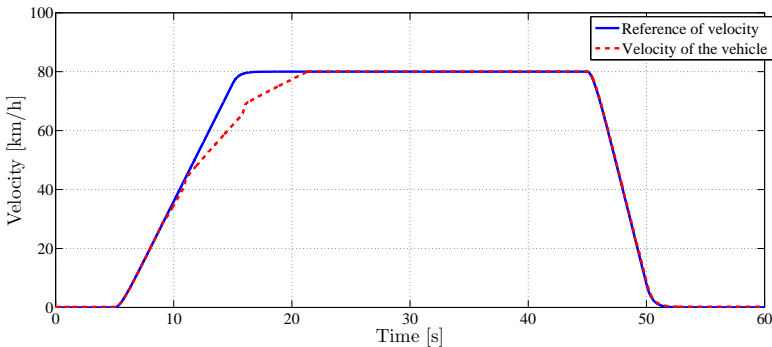


Figure 33 – Velocity profile used to adjust the gains of the driver model and the response of the vehicle for the best obtained configuration.

Table 12 – Parameters adopted for the simulations in Simulink.

Simulink Solver Configurations	
Solver	ode23t(mod. stiff/Trapezoidal)
Maximum allowed time-step	1×10^{-2} s
Type	Variable-step

The evolution of the model over the iterations is shown in Figure 34 and the best result achieved $(1 - R) = 4.77 \cdot 10^{-3}$. The same procedure was repeated for the second set of maps, however, no significant differences (above 1%) were observed.

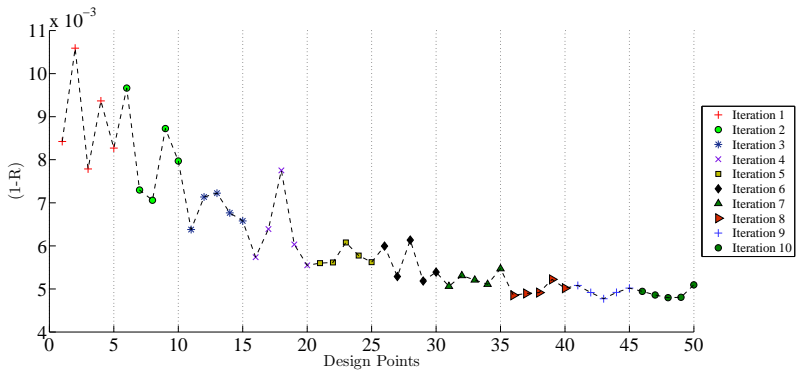


Figure 34 – Values of $(1-R)$ obtained for each iteration of the procedure used to adjust the driver model (PI Controller)

Nevertheless, the best configuration of the PI led to high frequency oscillations of the throttle pedal input, as shown in Figure 35. Although validating the controller with respect to real human response is not of interest for this work, it is common sense that such response cannot be performed by a regular driver. Therefore, the gains were attenuated and a first order filter with time constant of 1s was adopted after the PI, such that the throttle input could be closer to the response of an average driver. This adaptation led to an increase of 2.5% of the $(1-R)$ criterion and the final response of the driver is also shown in Figure 35.

For the purpose to verify the behavior of the driver assistant, the gains

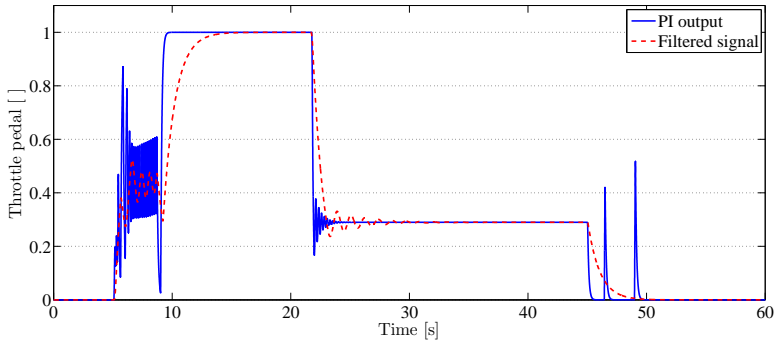


Figure 35 – Throttle pedal input using the PI controller with minimum (1-R) and filtered signal.

$K_{t,\Phi}$, $K_{t,T}$ and K_i were defined only according to the magnitude of the partial derivatives. Also, the same procedure was repeated for different velocities (40, 60, 80 and 100 km/h) in order to observe the behavior of the system under different load conditions.

The velocity profiles achieved with both maps were identical, as shown in Figure 36. Such result is expected, since the driver and the map of torque were the same for all cases, as well as the gearshift strategy yield to similar results, as shown in Figure 37.

Concerning the gearshift, the vehicle started with the lowest gear ratio in all cases, which is a reflect of the DA algorithm. For low torque demands, which happens when the vehicle is stationary, the algorithm searches for the lowest torque multiplication factor, regardless of future events. When the vehicle starts the movement ($t = 5$ s), the gear ratio is rapidly increased and the powertrain delivers torque with magnitude close to the reference value.

The signal of the throttle position presented differences when the maps were modified and more significantly for the cases with velocities above 40 km/h, as shown in Figure 38. This deviation is a result of the shape and position of the point of minimum of the BSFC maps, which in the first case was set to low throttle opening (0.1) and in the second to a higher value (0.8). Therefore,

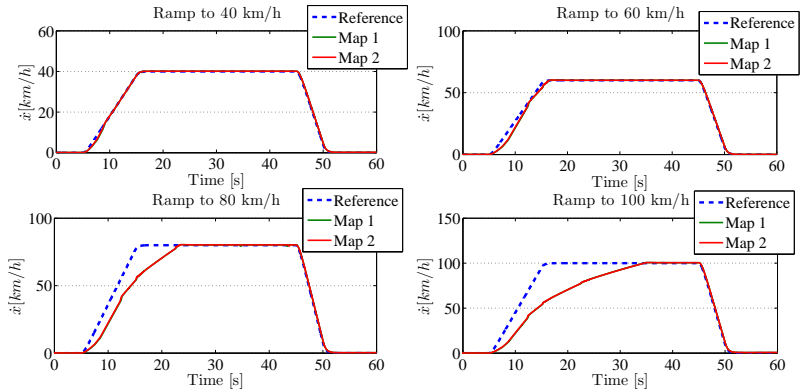


Figure 36 – Comparison between the reference velocity profile and results achieved with the DA, for different levels of velocity.

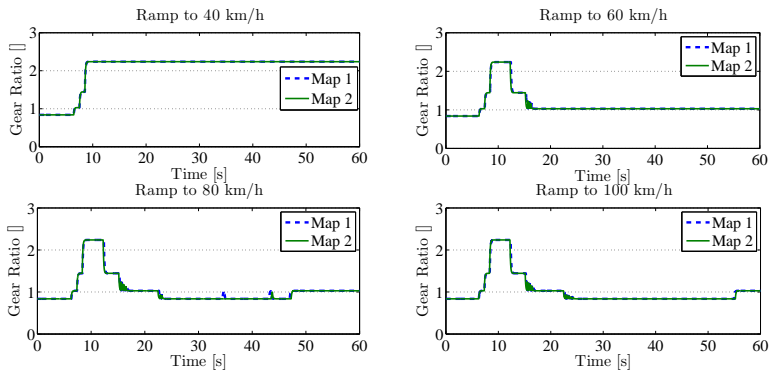


Figure 37 – Gear ratio over simulation time for different velocities and both validation maps.

for the simulations with the Map 1, in order to reduce the fuel consumption, the throttle position was kept as low as possible, while in the simulations with the second set of maps, the throttle angle was increased by the DA algorithm.

In order to confirm the analysis of the throttle angle, the saturation of $\pm 10\%$ of the user throttle pedal input was amplified to $\pm 50\%$ and the simulations of the ramp to 80 km/h were performed again. As expected, the algorithm of the assistant reduced the throttle position more severely for the

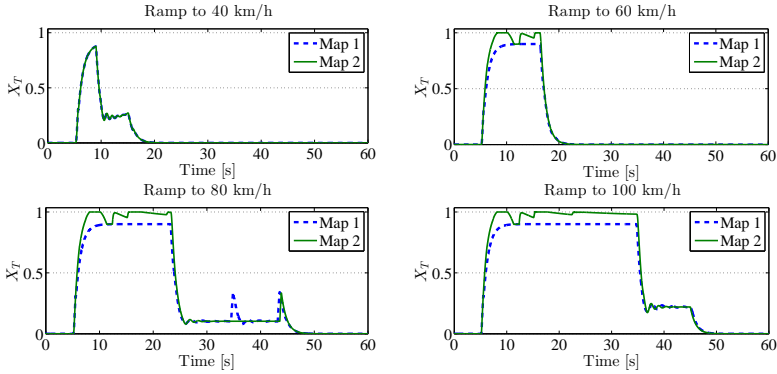


Figure 38 – Throttle opening for both maps and different velocity profiles.

case with the first set of maps, in order to push the operation point towards the region of minimum BSFC, as shown in Figure 39. In the simulation with the second map, there were no significant changes, due to the proximity of the operation points to the region of minimum BSFC.

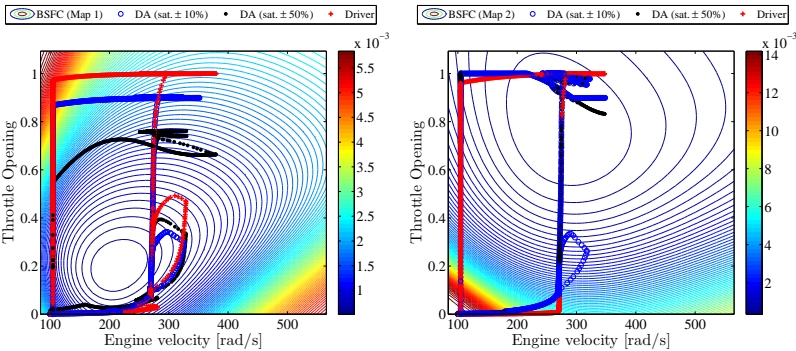


Figure 39 – Regions of the BSFC Maps achieved during the simulation of a ramp to 80 km/h.

Nevertheless, as discussed during the development of the algorithm, the purpose of constraining the actions of the driver assistant is to avoid interfering on the maneuverability. In Figure 40 the velocity profiles obtained with both constraints are shown and it can be seen that increasing the range of the DA

correction led to a small delay during the acceleration, as well as to minor changes in the gearshift strategy. Given the degree of simplicity of these simulations, the constraining of the throttle correction will be further analyzed during the simulations performed in the case of study, presented in the next chapter.

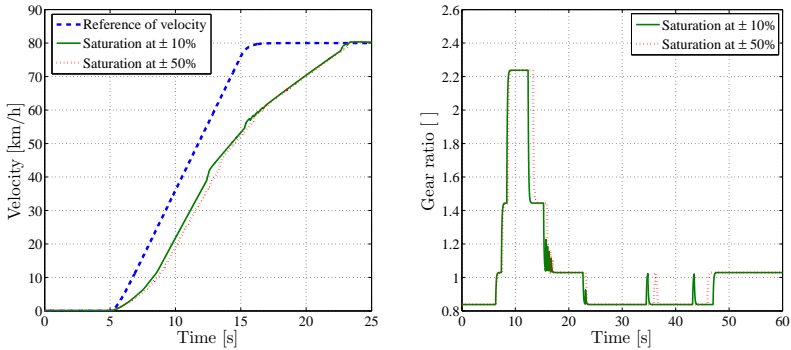


Figure 40 – Comparison of the results of velocity and gear ratio obtained with 10% and 50% of tolerance for the DA correction.

The results presented up to this point indicate that the algorithm of the DA shifts the operation conditions imposed by the driver towards the region of low BSFC. Furthermore, it did not caused any instability nor affected severely the handling of the vehicle, for the considered values of gains and velocity profiles. Nevertheless, as noticed during the analysis of the used gear ratios, the algorithm was not capable to reach the highest gear ratio at the beginning of the movement, behavior which might be uncomfortable for the driver. This and further aspects of the DA system will be analyzed in the next chapter, where the performance of the proposed method is compared to a strategy found in the literature to minimize the fuel consumption of a specific vehicle.

3.3 IMPLEMENTATION ON REAL SYSTEMS

The technical aspects regarding the implementation of the driver assistant in a vehicle will not be discussed in this text. However, some insights over

the physical realization of the proposed system are anticipated, since this topic is important for the completeness of this research.

Concerning the instrumentation and signal processing, the measurements related to the engine are already performed for the actuation of fuel injectors and on spark plugs. The measurement of velocity is also performed and displayed to the driver on the information panel and, therefore, the identification of the selected gear would be added, in case any further system does not demand this signal, and a position sensor for measuring the level of the throttle pedal.

The processing demand and necessary hardware to perform the calculation will depend on the desired level of automation. A fully automatized system will require the proposed algorithm to fit the real-time constraints imposed by the Engine Control Unit (ECU) and, therefore, some simplifications might be needed, specially the section dedicated to calculate the gradients of the maps. Resuming the discussion about the surrogate models, Look Up Tables could be used to store the gradient information and substitute the use of ANN, reducing the calculation demand.

A simpler alternative would be the implementation of advising signs on the panel, similarly to the fuel economy indicator shown in Figure 41. In this case, the driver is responsible to act on the system, according to the displayed signal, in order to reduce the fuel consumption.

On the implementation side, this approach is simpler than the previous suggestion, mainly because the calculations can be performed outside the ECU and do not have tight time constraints to deliver the results. Also, on the driver-safety side, the driver would not expect the vehicle to perform any undesired action, however, a careful study concerning the driver's attention should be carried, since these additional alerts on the instrumentation panel might not deviate the attention of the driver.



Figure 41 – Indicator of fuel economy in the instrumentation panel of a passenger vehicle. Adapted from (SANDOVAL, 2008)

3.4 SUMMARY AND CONCLUSIONS

Reducing fuel consumption of a vehicle depends, among many variables, on the driving style. Therefore, adapting the driver inputs to the powertrain is a convenient form to improve the efficiency of the system without interfering on the design of components.

In this section it was presented the development of a driver assistant algorithm, which has shown potential to improve the fuel efficiency of a vehicle. The literature research provided an overview of a few methods to control applied to longitudinal dynamics that could be used to improve the fuel economy for urban traffic conditions. Among the methods, the ones derived from optimization methods and model-based prediction were adopted to define the algorithm for this work due to possibility to withdraw physical meaning and to the proximity of the formulation to the purposes of the algorithm.

The mathematical equations defined for the Driver Assistant were integrated to the model developed in Chapter 2 and tested under simple conditions. The algorithm presented both stability and capacity to adapt its actions to different engine maps, such that the engine operation point could be moved to regions of higher efficiency than the ones resulted from the drivers input.

4 PERFORMANCE ASSESSMENT OF THE DRIVER ASSISTANT

In the previous chapter a first assessment of the system's behavior after the implementation of the Driver Assistant algorithm and using surrogate models to calculate the engine outputs. Although the analyses were conclusive, the velocity profile adopted for the simulations does not represent most of the urban traffic conditions and the fuel consumption was not quantified for those cases.

In this chapter, the behavior of proposed system is further analyzed, considering a velocity profile capable to represent urban traffic conditions and engine maps developed with data from an actual vehicle. Furthermore, the performance of the DA is compared to the a standard gearshift strategy, proposed by the vehicle manufacturer, and the fuel-economy strategy, proposed by Eckert (2017).

4.1 METHODOLOGY

The velocity profile selected for the simulations is determined by the standard ABNT NBR 6601, used for measuring the total ICE emissions in a chassis dynamometer test bench. The standard is applicable to light duty vehicles and the proposed velocity profile simulates an average of the driving conditions in urban roads (ABNT, 2016). This reference cycle was selected due to the its range of velocities, presence of multiple start and stop events, as shown in Figure 42, and to compare the obtained results to the ones presented in (ECKERT, 2017).

The properties of the simulated vehicle are the same listed in Table 10. Additionally, the set of data used to develop the surrogate models were adopted from (ECKERT et al., 2016; ECKERT, 2017), corresponding to 100 sampled points in the design space formed by the throttle position and engine

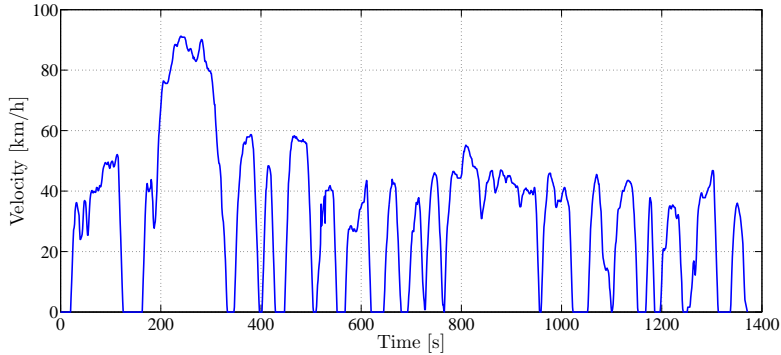


Figure 42 – Velocity profile for measuring vehicle emissions according to the standard NBR6601 (ABNT, 2016).

velocity. The conditions adopted for the training procedure are listed in Table 13, as well as the obtained R^2 for both training and validation. The calculated torque, fuel consumption and BSFC surfaces for the range of operation of the engine are shown in Figure 43.

Table 13 – Results of the training and verification procedures to develop the engine maps of a FIAT TMPunto.

Properties	Maps		
	Fuel Cons.	Mean Torque	BSFC
Number of neurons	5	5	5
Learning rate	0.005	0.005	0.005
Number of iterations	5×10^5	5×10^5	5×10^5
R^2 - Training	0.997800	0.999980	0.999999
R^2 - Verification	0.995893	0.996069	0.995228

The model of the driver was adopted the same adopted for the preliminary analyses. Resuming the consideration of the driver's behavior, the model adopted for this work does not fully represent the human behavior, however, it is capable repeat its responses to similar stimuli, which is necessary to compare different gearshift strategies.

The solver and its setup were defined the same as listed in Table 12.

All the simulations were performed with the same configuration of the solver and the results were verified in a second round of simulations, with reduced time-step.

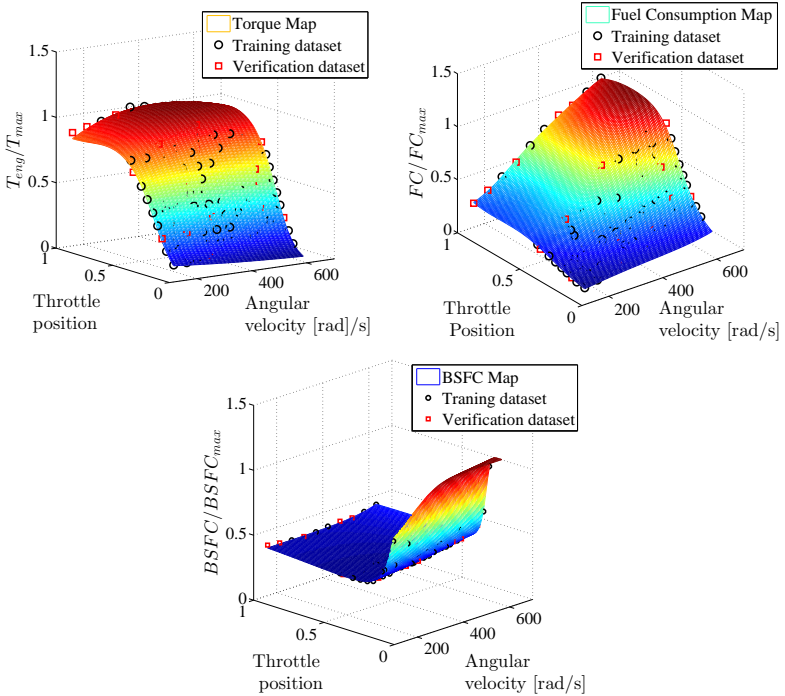


Figure 43 – Maps generated using the trained ANN models.

Then, the approach to verify the system of equations and evaluate the performance of the proposed DA consists of the following steps:

1. Simulations of the system considering the standard gearshift strategy, proposed by the manufacturer, and the modified method proposed in (ECKERT, 2017), identified as "Eckert's", in order to compare the results of mileage and correlation between the reference and achieved velocities;
2. Simulation of the system considering the interference of the DA system

and exploration of its setup in order to improve performance;

3. Presentation of the obtained results and comparison with the ones presented in (ECKERT, 2017).

4.2 RESULTS AND DISCUSSION

4.2.1 Simulations with reference strategies

The summary of the results obtained with the simulations considering the standard and modified gearshift strategies is presented in Table 14. The highest deviations were observed in the correlation between the reference and vehicle velocities and, therefore, also in the overall traveled distance.

Table 14 – Comparison between the results obtained experimentally by Eckert (2017) and the ones calculated using the proposed model.

Reference Values (ECKERT, 2017)				
Simulation case	Distance [km]	Consumed fuel [ℓ]	(1-R)	Mileage [km/ ℓ]
Standard	11.625	0.986	0.008	11.785
Eckert's	11.470	0.846	0.009	13.549
Simulation Results				
Standard	11.997	1.035	0.0007	11.587
Eckert's	11.993	0.874	0.0008	13.724

The results presented in (ECKERT, 2017) were obtained experimentally, where a human driver operated the vehicle. Since the response of the driver is slower than the PI controller, which was adjusted to reduce the deviation between reference value and response, the model achieves better correlation results and the overall distance becomes similar to the one proposed in the standard (11.996 km).

The procedure to shift gears is also a reason for the differences in the velocity results. For this work, the driver is capable to shift gears without acting on the clutch and the procedure is completed almost instantly, as shown in Figure 44. In order to avoid numeric singularities, a first-order filter was

used to attenuate both gear ratio and gearbox inertia signals, as indicated in Figure 44.

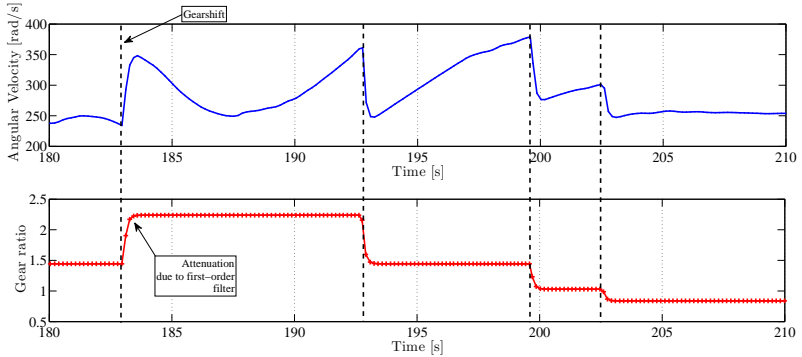


Figure 44 – Engine velocity oscillations due to shifting gears for a time frame of the NBR6601 simulation with the standard gearshift strategy.

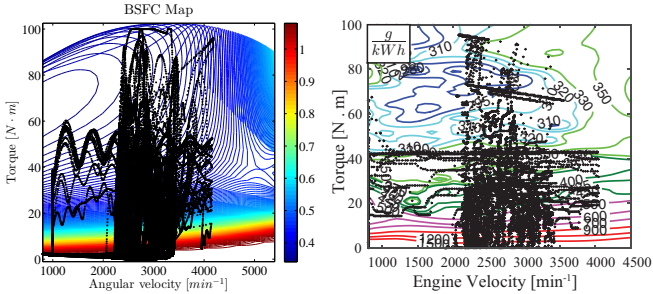
Finally, the last sources of deviations in the model are the differences between the maps, which can be seen in Figure 45. Although the data was withdrawn from the reference in the literature, the ANN models still are approximations of the maps and, therefore, some differences are expected.

Despite the differences between the engine models, the estimations of mileage differed only in 1.7% for the standard strategy and -1.3% for the gearshift proposed in (ECKERT, 2017), according to Table 14. Furthermore, as shown in Figure 45, the simulated vehicle achieved similar regions of the maps, if compared to the reference, which indicates that the behavior of the system is well approximated by the model and consistent with the literature.

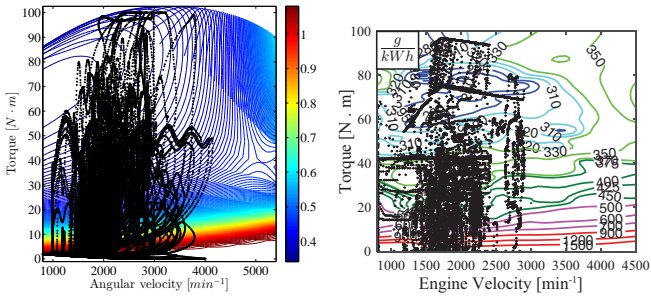
Since the verification of the model is concluded, the following procedure consists of simulating the vehicle, considering the interference of the DA algorithm.

4.2.2 Simulations considering the DA

The first simulations of considering the DA consist of exploring a space of feasible values for the constants $K_{t,\Phi}$, $K_{t,T}$ and K_i . Differently from the



(a) Operating points for the simulations with the standard gearshift strategy



(b) Operating points for the simulations with Eckert's gearshift strategy.

Figure 45 – Maps of BSFC with operating points obtained with the proposed model (left) and by the literature reference (right, adapted from (ECKERT, 2017)).

simulations of Chapter 3, the reference of velocity is kept the same, while the gains are modified. Since it is not the purpose of this work to find the best configuration of the controller, no optimization algorithm was used in this phase.

The values of the gains for the experiments were determined using the Latin Hypercube Sampling (LHS) technique, which is widely applied in Design of Experiments (DoE), it can cope with many-variable problems and it ensures that all portions of each design variable are represented (KERAMAT; KIELBASA, 1997).

In order to illustrate the method of sampling, consider a bi-dimensional

design space, as shown in Figure 46. If N_s samples are desired, each dimension is equally divided within the boundaries of the design, such that the coordinates can be described as integers in the interval $I_s = [0, N_s - 1]$. A design generated by the LHS consists of a group of points with integer coordinates within the interval I_s and that are no two points with a common coordinate (GROSSO; JAMALI; LOCATELLI, 2009).

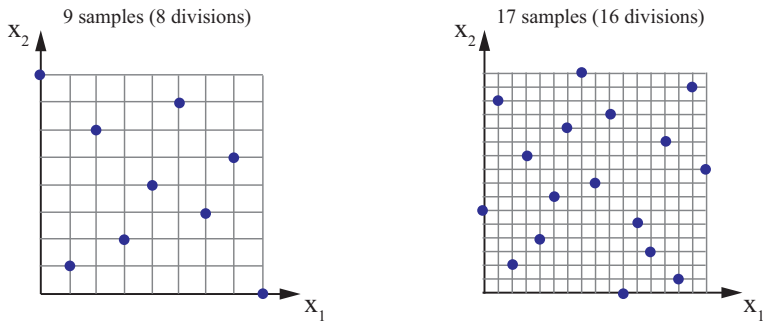


Figure 46 – Example of two populations sampled from a bidimensional space with LHS with different number of samples

For the proposed analysis, 300 points were sampled from the space formed by the gains $K_{t,\Phi}$, $K_{t,T}$ and K_i , considering the boundaries presented in Table 15. The boundaries of the values were defined based on the experience gathered with previous simulations and the sampled points are shown in Figure 47

Table 15 – Boundary values for the gains during the design exploration

Parameter	Lower boundary	Upper boundary
K_i	0.1	100
$K_{t,T}$	0.01	1
$K_{t,\Phi}$	0.01	1

In order to reduce the computational effort, the simulation time was reduced to 330 s. Hence, the vehicle is submitted only to two start-and-stop events, where the second achieves highway velocity. Furthermore, a stop-

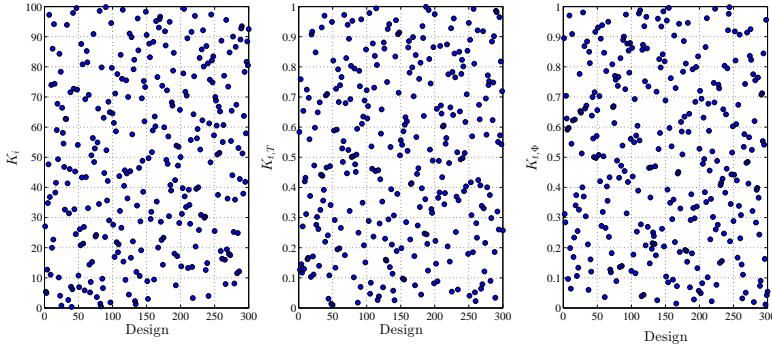


Figure 47 – Results of LHS for the gains $K_{t,\Phi}$, $K_{t,T}$ and K_i of the Driver Assistant.

condition based on the run time was added, such that simulations with unfeasible configurations of the controller could be terminated earlier. Further configurations of the solver and model were kept the same as the previous simulations.

The results of average fuel consumption and correlation between velocities for the feasible designs are shown in Figure 48. The distribution of the points indicates the existence of a trade-off between fuel efficiency and longitudinal performance, which is a common sense.

In order to withdraw the correlations between the results and the values of the the gains, the plot of Figure 48 is expanded to the scatter plots in Figures 49, 50 and 51. The results in 49 indicate a strong correlation between the adjustment of K_i and the behavior of the system, where intermediate values led to the results with best performance-to-fuel consumption ratio. However, the plots in 50 and 51 do not point any visible correlation between the value of the gains and simulation results.

The difference of sensitiveness between the gains can be explained by the restrictions adopted for the correction of the throttle position. While the gear ratio is limited only by the extreme values, the throttle position has to be within $\pm 10\%$ of the throttle imposed by the driver and, therefore, its

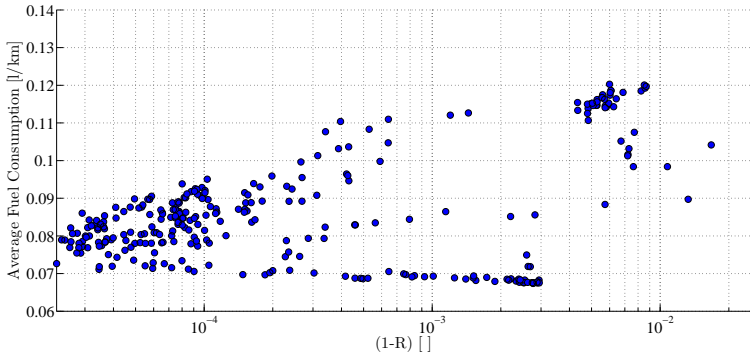


Figure 48 – Results of average fuel consumption and correlation between the reference and achieved velocities

adjustments, which are dependent of $K_{t,T}$ and $K_{t,\Phi}$, do not interfere in the results as much as the update of the gear ratio.

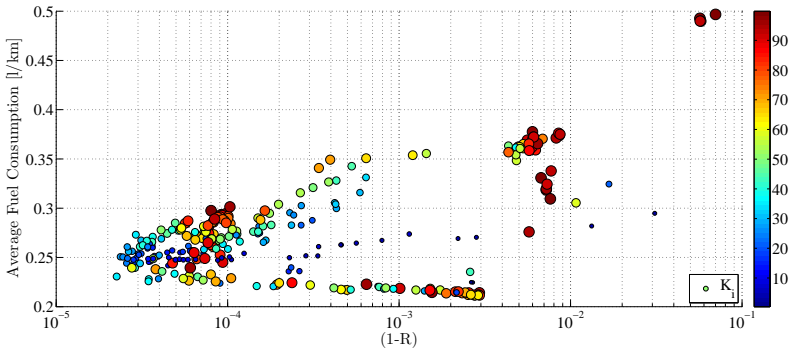


Figure 49 – Size and color of the bubbles according to the value of K_i

In Table 16, three extreme results obtained with the experiments are listed: the lowest fuel consumption, the highest velocity correlation and the best performance-to-fuel consumption ratio, obtained with

$$D_{best} = \min \left\{ \sqrt{FC *^2 + (1 - R) *^2} \right\} \quad (4.1)$$

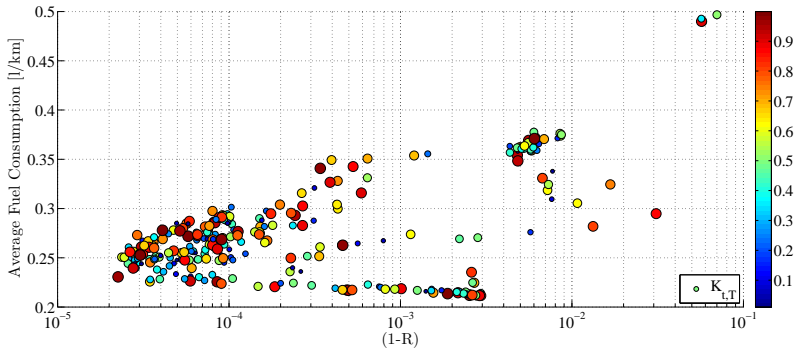


Figure 50 – Size and color of the bubbles according to the value of $K_{t,T}$

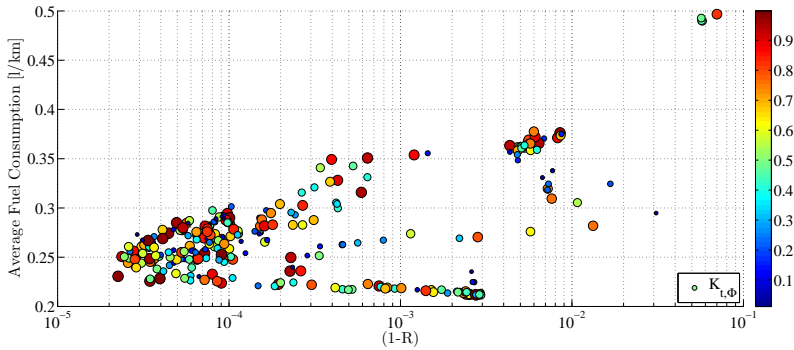


Figure 51 – Size and color of the bubbles according to the value of $K_{t,\Phi}$

where * indicates that the values are normalized between [0, 1], considering the maximum and minimum values obtained with the experiments for each parameter.

Given the objective of reducing the disturbances on the maneuverability, only the case of best ratio between fuel consumption and the metric (1-R) is considered for the following analyses. The summary of the main results for the simulation considering the complete cycle and the selected configuration of the DA, as well as the ones obtained with the reference strategies, are shown in Table 17.

Table 16 – Summary of the main results obtained with the experiments

Parameter	Minimum Fuel Consumption	Minimum (1-R)	Best Ratio
K_i	63.71	35.66	66.13
$K_{t,T}$	0.5508	0.9575	0.9525
$K_{t,\Phi}$	0.5538	0.9735	0.4887
Average Mileage [km/ℓ]	14.84	13.76	14.56
(1-R)	2.771×10^{-3}	2.254×10^{-5}	4.967×10^{-4}

Table 17 – Summary of the simulated models

Strategy	Distance [km]	Fuel Cons. [ℓ]	(1-R)	Mileage [km/ℓ]
FIAT	11.993	1.035	0.0007	11.587
Eckert's	11.993	0.874	0.0008	13.724
DA	11.969	0.876	0.0003	13.663

As detailed in Table 17, the obtained results are similar to the ones obtained with the strategy proposed in (ECKERT, 2017). Describing the results as time series, it is possible to identify the differences between the models. For the sake of legibility, the results are displayed for three sections of the urban cycle: one with a single start-and-stop event and intermediate velocity, the second where the vehicle achieves highway velocities and the last contains multiple start-and-stop events and the vehicle achieves typical urban traffic velocities.

The first results to be compared are the gear ratio and velocity of the vehicle over the simulation time, shown in Figures 52, 53 and 54. As already observed in previous simulations, the DA maintains the gear ratio at low values as much as possible, according to the torque demand imposed by the driver. In terms of velocity, the highest deviation occurs in the second section (Figure 53), close to $t = 200$ s, when the vehicle is accelerating towards the maximum speed.

The gearshift profile reflects on the throttle and angular velocity of the engine, as shown in Figures 55, 56, 57. In the three cases the DA pushed the throttle position to higher values than the standard case, while avoiding high

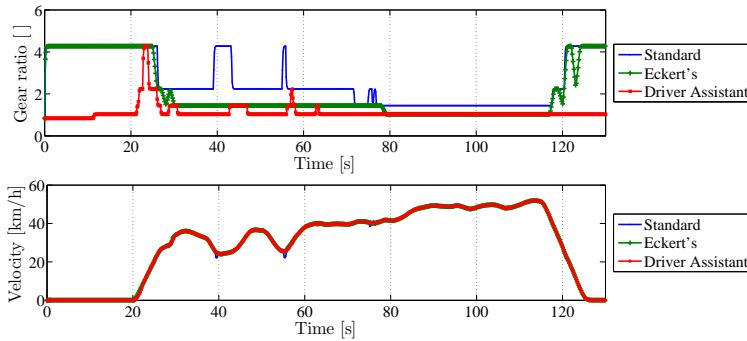


Figure 52 – Gear ratio and velocity results for the first section of the urban cycle

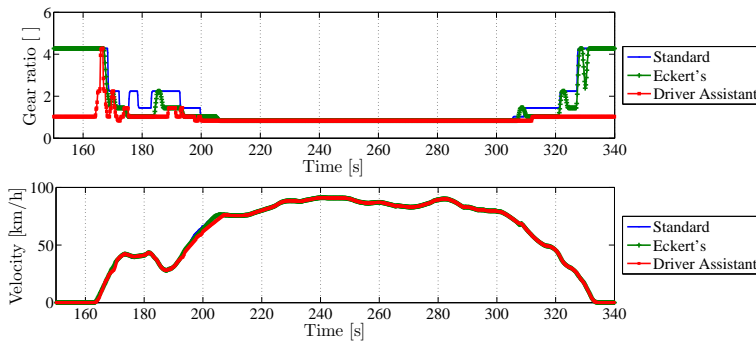


Figure 53 – Gear ratio and velocity results for the section of highest velocity of the cycle

values of angular velocity, results which were similar to the ones obtained with the strategy proposed in (ECKERT, 2017).

Between $t = 450$ s and $t = 500$ s, the throttle valve presents intense oscillations, which could invalidate the use of static maps to model the behavior of the engine. However, evaluating the section, showed in Figure 58, it is observed that the period of oscillation is approximately 2 s, which is close to the time response of the intake system. Since the results of the simulations were

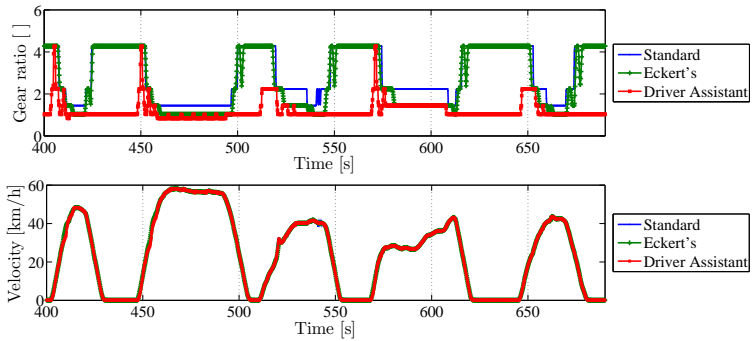


Figure 54 – Gear ratio and velocity results for the section of multiple start and stop events during the cycle

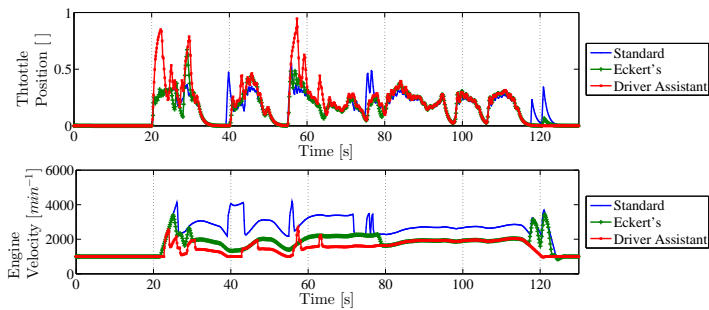


Figure 55 – Throttle angle and engine velocity results for the first section of the urban cycle

coherent and similar to the data obtained in (ECKERT, 2017), no corrections were adopted, nevertheless, this topic should be addressed in future works, given its close relation to the fidelity of the representation of the ICE.

Hence, the proposed algorithm prioritizes the modification of the throttle opening to adjust the available torque at the wheel, since increasing the velocity of the engine leads to higher fuel consumption. It is also important to notice that at high vehicle speed, the angular velocity of the engine and throttle position converged to similar values, as shown in Figure 56. Since the

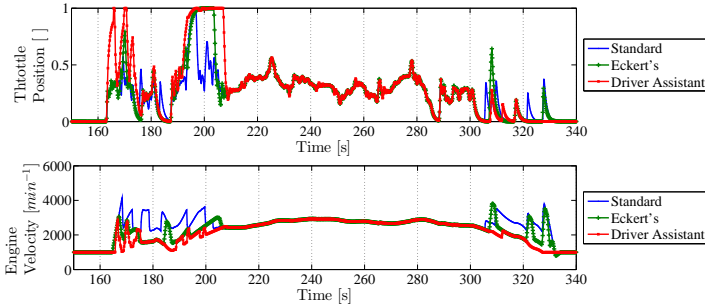


Figure 56 – Throttle angle and engine velocity results for the section of highest velocity

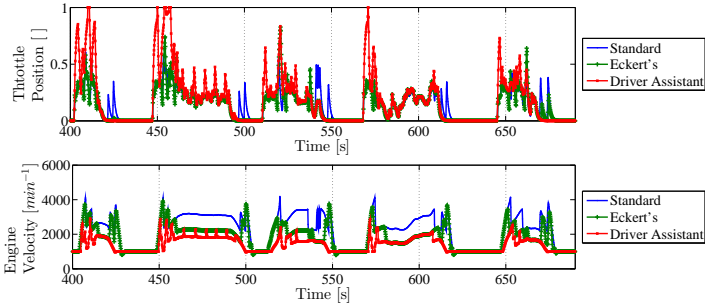


Figure 57 – Throttle angle and engine velocity results during multiple start-and-stop events

lowest gear ratio is usually designed for high fuel efficiency at cruise velocities, the similarity of the results also indicates that the corrections of the DA are coherent with the objective of reducing the fuel consumption.

The analyses about the fuel consumption are supported by the curves in Figures 59, 60, 61. In the first section, the fuel consumption rate with the standard strategy is higher than the alternative methods during most of the time, leading to an accumulated fuel consumption approximately 30% higher than the one obtained with the proposed DA at $t = 130s$, as shown in Figure 59.

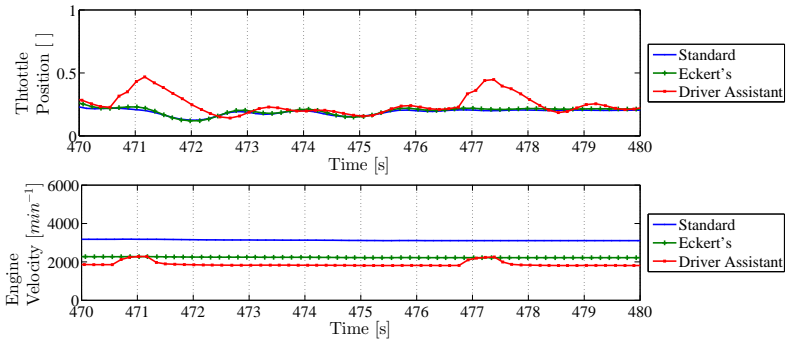


Figure 58 – Zoom of a section in sector 3, which presented intense oscillations of the throttle valve.

During the second section, the three methods behave nearly the same. Therefore, the difference between the curves of accumulated fuel consumption in Figure 60 remains approximately constant during the selected time range, changing from 0.0315ℓ to 0.0221ℓ . In the last section, similarly to the first, the fuel consumption rate induced by the standard strategy is higher than in the other cases, increasing the difference of the consumed amount, as shown in Figure 61.

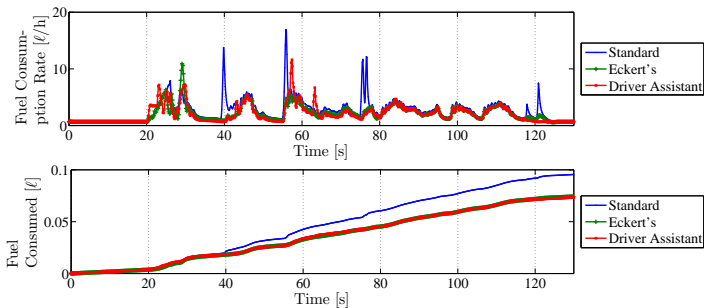


Figure 59 – Fuel consumption results for the first section

Calculating the BSFC for the engine velocities and throttle positions achieved in each case, the maps shown in Figure 62 are obtained. Observing

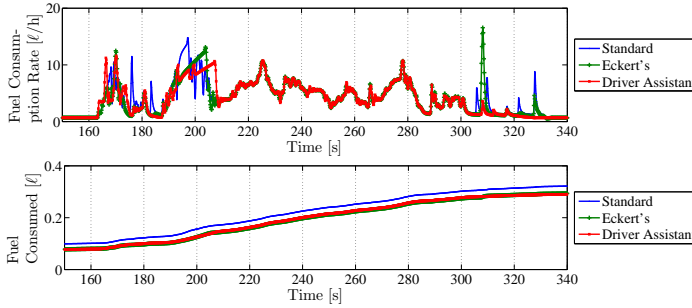


Figure 60 – Fuel consumption during the section of highest velocity

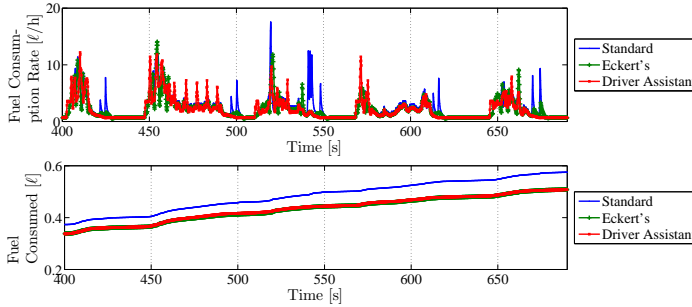


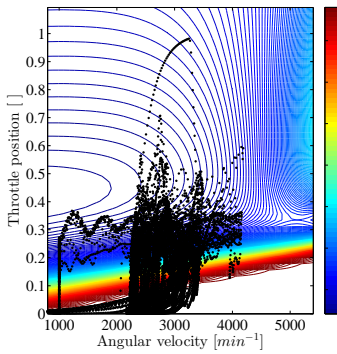
Figure 61 – Fuel consumption in the section with multiple stops

the concentration of the points, the proposed method does push the operation conditions towards the region of minimum BSFC, which was one of the objectives of the driver assistant and already observed in the simulations of Chapter 3.

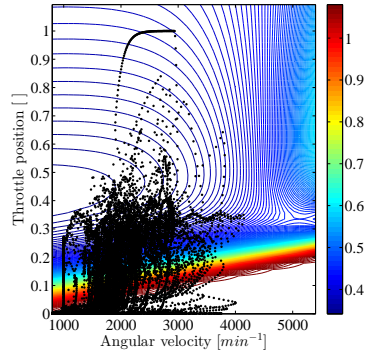
Normalizing the axes in Figure 62 to the interval $[0, 1]$, the distance between the operating points and the condition of lowest BSFC can be calculated using 4.2.

$$D = \sqrt{(X_{T,n} - X_{T,min})^2 + (\dot{\theta}_{e,n} - \dot{\theta}_{e,min})^2} \quad (4.2)$$

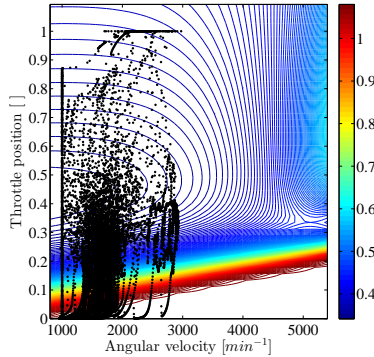
where $X_{T,n}$, $\dot{\theta}_{e,n}$ are the points achieved during the simulation and $X_{T,min}$,



(a) Map of BSFC with operating points obtained with the standard strategy.



(b) Map of BSFC with operating points obtained with Eckert's strategy.



(c) Map of BSFC with operating points obtained with the driver assistant.

Figure 62 – BSFC Maps for different operation strategies.

$\dot{\theta}_{e,min}$ are the conditions of lowest BSFC. Analyzing the number of occurrences of the distance values for each simulation, the histogram in Figure 63 is obtained, where the weighted arithmetic mean of the distance for the simulations with standard, modified and DA strategies are 0.601, 0.486 and 0.423, respectively.

If compared to the standard gearshift strategy, based on the distribution of the bars and mean values, the DA allows the powertrain to operate closer

to the point of minimum BSFC. Analyzing the accumulated results, while in the simulation with the standard gearshift method 34,5% of the points have distance up to 0.5 to optimal point, the modified strategy yield to 74.6% and the proposed method to 88.9% of the points within the same range.

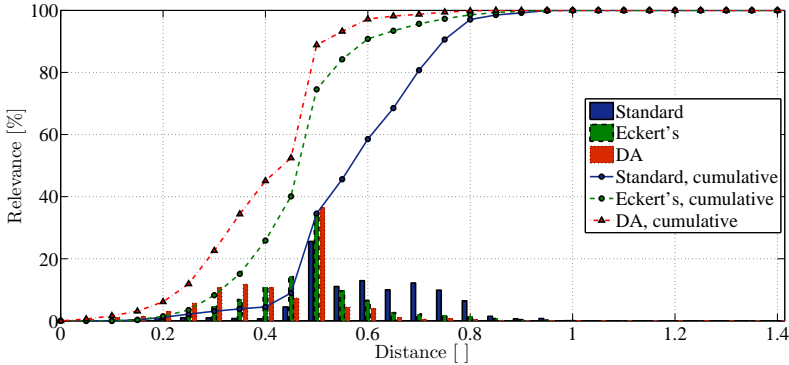


Figure 63 – Histogram indicating the level of occurrence for possible distances between points of operation and the point of minimum BSFC

4.3 SUMMARY AND CONCLUSIONS

In this chapter, the proposed model of vehicle longitudinal dynamics was verified by comparison to the results available in the literature. The urban cycle and vehicle considered in (ECKERT, 2017) were used to set the reference of velocity for the driver and to set up the parameters of the model. Furthermore, the strategies of gearshifting proposed by the manufacturer and by the reference were simulated with the proposed model, leading to deviations below 2% for the fuel consumption results and coherent values of deviation between velocity profiles, due to the nature of the experiments performed by Eckert (2017).

Additionally, the algorithm of the DA was implemented in the model and the adjustment of its constants briefly explored, indicating that the performance of the system has a higher correlation with the corrections of the gear ratio than the throttle opening. Also, the analyses of the powertrain's behavior

with different methods to reduce the fuel consumption were condensed in three distinct sections of the urban cycle, such that specific characteristics of each method could be detected. The analyses indicated that the DA shifted the gear ratio and throttle angle to similar values obtained with the strategy proposed in (ECKERT, 2017) and, therefore, it is a potential tool to increase the fuel economy.

Finally, a comparison between the proximity of the conditions of powertrain operation to the point of minimum BSFC for each method was carried. It was observed that the algorithm proposed in this work pushes the region of operation towards the point of interest, confirming the results obtained in the previous chapter and demonstrating the physical insight of the controller actions, as commented during the design phase.

5 CONCLUSIONS

This research presented a study on powertrain and vehicle longitudinal dynamics, with emphasis on strategies to reduce the fuel consumption. New environmental regulations and many economic reasons motivate similar developments in the industry, in order to help the engineering teams to meet the best compromise between efficiency, drivability and customer requirements.

For the development of a fuel saving strategy, it is important to describe the vehicle as a dynamic system and understand the basic principles of its longitudinal motion. A mathematical model with three DoF was presented, where aspects concerning the nonlinearities of friction phenomena and simplifications of mathematical models were detailed. Due to the different nature of the systems, an energetic approach, Euler-Lagrange Equations of 2^{nd} kind, was adopted, reducing the effort to obtain the equations of movement that models the behavior of the system.

The model was verified using a reference model in MSC AdamsTMView and the results of the first time derivative of each minimum coordinate were compared, as shown in Figure 20. The comparison indicated that the models behave similarly and, therefore, the proposed system of equations well approximates the behavior of an actual vehicle. Furthermore, a significant contribution of this work is that, differently from the quasi-static model, the adopted approach allows the analysis of start and stop events, since the engine can be decoupled by the clutch, and it considers the longitudinal slip at the tires, which also influences the fuel consumption, which has not been considered in many of the reviewed works.

Once the mathematical model of the vehicle was established, the algorithm of the fuel saving strategy could be defined. Preceding the mathematical development, a survey of the literature state of the art was presented, where methods and tools used for driver assistant systems, specifically for fuel saving procedures, were identified. The review was followed by the methods of

mapping the engine performance using surrogate models and, for this work, Artificial Neural Networks were used to model both engine mean torque and fuel consumption. Although more complex than the usual tools, ANNs are more flexible and can be adjusted with smaller data sets, reducing the costs of simulation and data fitting. Moreover, regardless of the size of the domain, i.e. number of dimensions, it is possible to withdraw information of gradient of the maps, which was fundamental for the algorithm developed during this research and a differential of the proposed strategy, and also a major contribution of this work.

The proposed algorithm was inspired on the Model Predictive Control approach, which considers the dynamics of the system to calculate the control actions. The signal flow was adapted from the structure proposed in (KAMAL et al., 2010), leading to the algorithm shown in Figure 29, which was implemented in parallel to the previous system of equations related to vehicle dynamics. Some requisites related to the implementation of the DA on an actual vehicle were considered, such as the availability of measurement signals and safety of the driver, leading to design constraints.

In order to perform the simulations, the behavior of the driver was assumed similar to a PI controller, adjusted using a gearshift called "standard", proposed by the vehicle's manufacturer, and customized maps of torque and fuel consumption were defined, such that the influence of the shape of the maps could be investigated. Using velocity ramps similar to ones defined in (MATSUMOTO; PARK; KAWASHIMA, 2014), preliminary analyses concerning the behavior of the system were carried out, and, through visual comparison, the proposed algorithm was capable to push the engine operating points closer to the point of minimum BSFC.

At last, the system is evaluated on a case of study, where the performance of the fuel-saving algorithm is compared to the results obtained with the standard and an optimized gearshift strategies, available in the literature. The simulated velocity profile is defined in the standard NBR6601 and the vehicle adopted for the simulations was a FIAT TMPunto 2008, 1.4L. The coefficients of the model and maps were calibrated by comparing the experimental simu-

lated to the experimental results obtained in (ECKERT, 2017) and differences below 2% were observed in the calculation of fuel consumption.

The simulations performed with the DA, as shown in Table 17, indicated that the proposed method has great potential for fuel saving, as the optimized strategy proposed by Eckert (2017). Furthermore, from the results in Figure 62 and histogram of Figure 63 it is observed that with the proposed algorithm, the obtained region of operation was the closest to the optimum BSFC, which was the main objective of developed auxiliary system. Hence, the objective of decreasing fuel consumption without severe interference on the drivability was achieved and the performance of the proposed algorithm is comparable to the references in the literature.

5.1 FUTURE DEVELOPMENTS

The implementation of the algorithm proposed on an actual vehicle is the first and most intuitive development that could derive from this work. As already discussed in Chapter 4, two possible approaches are fully automatic DA, which requires deeper understanding on hardware limitations and interface with vehicle controllers, or messages suggesting actions to the driver displayed on the instrumentation panel, requiring better understanding of driver cognitive capabilities and driving safety requirements.

On the simulation front, it is possible to expand the dynamic model to hybrid powertrain systems with multiple energy sources and converters. Since the alternative-fueled vehicles showed significant reduction of pollutant emissions and fuel consumption, aligning the proposed strategy to the flexibility of multiple power sources might lead to interesting results. Also on the side of vehicle dynamics, a model of braking dynamics could be added to the system of equations, such that the viability of energy recovery systems could be analyzed.

In addition, the objective function can also be modified for different purposes, such as maximizing the available power at the driving wheels or minimizing the wear of specific components, such as batteries or clutch. Modi-

fyng the algorithm based on multiple objective optimization problems would also be an interesting development that can derive from this work, as well as increasing the number of input variables of the engine maps, such as temperature of the cooling fluid and manifold pressure, which is possible due to the flexibility of the chosen surrogate modeling technique. Furthermore, defining a verification procedure to check if there is any condition that violates the validity of the model, e.g. rapid throttle oscillations or overheating of the engine, would be very interesting contribution to the research.

Also, defining a method to adjust the gains of the proposed algorithm, since only heuristic methods were used in this research. An analytic approach may provide some physical insight over the adjustment of the variables and facilitate the setup of the driver assistant.

Finally, it is also possible to extend the proposed strategy for stationary power generating systems and evaluate the feasibility to implement transmission systems in order improve the fuel efficiency and increase the flexibility of operation.

BIBLIOGRAPHY

AMMON, D.; SCHIEHLEN, W. Advanced road vehicles: Control technologies, driver assistance. In: _____. *Dynamical Analysis of Vehicle Systems: Theoretical Foundations and Advanced Applications*. Vienna: Springer Vienna, 2009. p. 283–304. ISBN 978-3-211-76666-8. Disponível em: <https://doi.org/10.1007/978-3-211-76666-8_7>.

ARORA, J. S. Chapter 10 - numerical methods for unconstrained optimum design. In: ARORA, J. S. (Ed.). *Introduction to Optimum Design (Fourth edition)*. Fourth edition. Boston: Academic Press, 2017. p. 423 – 453. ISBN 978-0-12-800806-5. Disponível em: <<https://www.sciencedirect.com/science/article/pii/B978012800806500010X>>.

ASSOCIAÇÃO BRASILEIRA DE NORMAS TÉCNICAS. *NBR 6601: Veículos rodoviários automotores leves — determinação de hidrocarbonetos, monóxido de carbono, óxidos de nitrogênio, dióxido de carbono e material particulado no gás de escape*. Rio de Janeiro, 2016. 49 p.

BALDANIA, M. D.; SAWANT, D. A.; PATKI, A. B. Fuel saving of an automobile using fuzzy logic based embedded controller. In: *2014 IEEE International Conference on Advanced Communications, Control and Computing Technologies*. [S.l.: s.n.], 2014. p. 136–140.

BIRRELL, S. A.; FOWKES, M.; JENNINGS, P. A. Effect of using an in-vehicle smart driving aid on real-world driver performance. *IEEE Transactions on Intelligent Transportation Systems*, v. 15, n. 4, p. 1801–1810, Aug 2014. ISSN 1524-9050.

CARSTEN, O. From driver models to modelling the driver: What do we really need to know about the driver? In: _____. *Modelling Driver Behaviour in Automotive Environments: Critical Issues in Driver Interactions with Intelligent Transport Systems*. London: Springer London, 2007. p. 105–120. ISBN 978-1-84628-618-6. Disponível em: <https://doi.org/10.1007/978-1-84628-618-6_6>.

CHENG, Q.; NOUVELIÈRE, L.; ORFILA, O. A new eco-driving assistance system for a light vehicle: Energy management and speed optimization. In: *2013 IEEE Intelligent Vehicles Symposium (IV)*. [S.l.: s.n.], 2013. p. 1434–1439. ISSN 1931-0587.

- CHOU, W.-Y. et al. Intelligent eco-driving suggestion system based on vehicle loading model. In: *2012 12th International Conference on ITS Telecommunications*. [S.l.: s.n.], 2012. p. 558–562.
- DEMPSEY, A. B.; CURRAN, S. J.; WAGNER, R. M. A perspective on the range of gasoline compression ignition combustion strategies for high engine efficiency and low nox and soot emissions: Effects of in-cylinder fuel stratification. *International Journal of Engine Research*, v. 17, n. 8, p. 897–917, 2016. Disponível em: <<http://dx.doi.org/10.1177/1468087415621805>>.
- ECKERT, J. J. *Desenvolvimento de Bancada Dinamométrica para Validação da Influência de Estratégias de Troca de Marchas na Dinâmica Veicular Longitudinal*. Tese (Doutorado), Campinas, SP, 2017.
- ECKERT, J. J. et al. Vehicle gear shifting strategy optimization with respect to performance and fuel consumption. *Mechanics Based Design of Structures and Machines*, v. 44, n. 1-2, p. 123–136, 2016. Disponível em: <<http://dx.doi.org/10.1080/15397734.2015.1094669>>.
- EJSMONT, J. et al. Influence of load and inflation pressure on the tyre rolling resistance. *International Journal of Automotive Technology*, v. 17, n. 2, p. 237–244, Apr 2016. ISSN 1976-3832. Disponível em: <<http://dx.doi.org/10.1007/s12239-016-0023-z>>.
- EUROPEAN COMMISSION. *Reducing CO2 emissions from passenger cars*. [S.l.], 2016. Disponível em: <http://ec.europa.eu/clima/policies/transport/vehicles/cars_en>. Acesso em: 12 jan. 2017.
- EUROPEAN ENVIRONMENT AGENCY. *Evolution of CO2 emissions from new passenger cars by fuel*. European Environment Agency, 2015. Disponível em: <<https://www.eea.europa.eu/data-and-maps/daviz/data-visualization-27#tab-based-on-data>>. Acesso em: 03 jul. 2017.
- FERNANDES, C. M. et al. Gearbox power loss. part i: Losses in rolling bearings. *Tribology International*, v. 88, n. Supplement C, p. 298 – 308, 2015. ISSN 0301-679X. Disponível em: <<http://www.sciencedirect.com/science/article/pii/S0301679X14004198>>.
- FERNANDES, C. M. et al. Gearbox power loss. part ii: Friction losses in gears. *Tribology International*, v. 88, n. Supplement C, p. 309 – 316, 2015. ISSN 0301-679X. Disponível em: <<http://www.sciencedirect.com/science/article/pii/S0301679X14004320>>.
- FIAT AUTOMÓVEIS S.A. *FIAT Punto 2008*: Manual de uso e manutenção. Brasil, 2008. 226 p.

GILLESPIE, T. D. *Fundamentals of vehicle dynamics*. Warrendale, PA: Society of Automotive Engineers, 1992. ISBN 978-1560911999.

GROSSO, A.; JAMALI, A.; LOCATELLI, M. Finding maximin latin hypercube designs by iterated local search heuristics. *European Journal of Operational Research*, v. 197, n. 2, p. 541 – 547, 2009. ISSN 0377-2217. Disponível em: <<http://www.sciencedirect.com/science/article/pii/S0377221708006644>>.

GUZZELLA, L.; ONDER, C. H. Mean-value models. In: _____. *Introduction to Modeling and Control of Internal Combustion Engine Systems*. Berlin, Heidelberg: Springer Berlin Heidelberg, 2010. p. 21–146. ISBN 978-3-642-10775-7. Disponível em: <https://doi.org/10.1007/978-3-642-10775-7_2>.

HAYKIN, S. *Neural Networks: A Comprehensive Foundation*. 2nd. ed. Upper Saddle River, NJ, USA: Prentice Hall PTR, 1998. ISBN 0132733501.

HEIBING, B.; ERSOY, M. *Chassis Handbook*. 1. ed. Wiesbaden: Vieweg+Teubner Verlag, 2011. (ATZ/MTZ-Fachbuch). Fundamentals, Driving Dynamics, Components, Mechatronics, Perspectives. ISBN 978-3-8348-0994-0.

HEYWOOD, J. B. *Internal Combustion Engine Fundamentals*. [S.l.]: McGraw-Hill, 1988. ISBN 0-07-028637-X.

HOOPER, P. R.; AL-SHEMMERI, T.; GOODWIN, M. J. Advanced modern low-emission two-stroke cycle engines. *Proceedings of the Institution of Mechanical Engineers, Part D: Journal of Automobile Engineering*, v. 225, n. 11, p. 1531–1543, 2011. Disponível em: <<http://dx.doi.org/10.1177/0954407011408649>>.

HUCHO, W.-H. Chapter 4 - aerodynamic drag of passenger cars. In: HUCHO, W.-H. (Ed.). *Aerodynamics of Road Vehicles*. 4th. ed. Warrendale, PA: SAE International, 1998. p. 131 – 238. ISBN 0-7680-0029-7.

INMETRO. *Tabelas de Consumo/Eficiência Energética - Veículos Automotores Leves*. [S.l.], 2017. Disponível em: <http://www.inmetro.gov.br/consumidor/pbe/veiculos_leves_2017.pdf>. Acesso em: 08 jul. 2017.

ISERMANN, R.; MÜNCHHOF, M. Neural networks and lookup tables for identification. In: _____. *Identification of Dynamic Systems: An Introduction with Applications*. Berlin, Heidelberg: Springer Berlin Heidelberg, 2011. p. 501–537. ISBN 978-3-540-78879-9. Disponível em: <https://doi.org/10.1007/978-3-540-78879-9_20>.

JAZAR, R. N. Driveline dynamics. In: _____. *Vehicle Dynamics: Theory and Application*. Boston, MA: Springer US, 2008. p. 165–216. ISBN 978-0-387-74244-1. Disponível em: <https://doi.org/10.1007/978-0-387-74244-1_4>.

JAZAR, R. N. Tire dynamics. In: _____. *Vehicle Dynamics: Theory and Application*. Boston, MA: Springer US, 2008. p. 95–163. ISBN 978-0-387-74244-1. Disponível em: <https://doi.org/10.1007/978-0-387-74244-1_3>.

JING, J. et al. Design of a fuel economy oriented vehicle longitudinal speed controller with optimal gear sequence. In: *2016 IEEE 55th Conference on Decision and Control (CDC)*. [S.l.: s.n.], 2016. p. 1595–1601.

KAMAL, M. A. S. et al. On board eco-driving system for varying road-traffic environments using model predictive control. In: *2010 IEEE International Conference on Control Applications*. [S.l.: s.n.], 2010. p. 1636–1641. ISSN 1085-1992.

KERAMAT, M.; KIELBASA, R. Latin hypercube sampling monte carlo estimation of average quality index for integrated circuits. In: _____. *Analog Design Issues in Digital VLSI Circuits and Systems: A Special Issue of Analog Integrated Circuits and Signal Processing, An International Journal Volume 14, Nos. 1/2 (1997)*. Boston, MA: Springer US, 1997. p. 131–142. ISBN 978-1-4615-6101-9. Disponível em: <https://doi.org/10.1007/978-1-4615-6101-9_11>.

KLUNDER, G. A. et al. *Impact of Information and Communication Technologies on Energy Efficiency in Road Transport - Final Report*. Delft, Netherlands, 2009.

KOBAYASHI, S.; PLOTKIN, S.; RIBEIRO, S. K. Energy efficiency technologies for road vehicles. *Energy Efficiency*, v. 2, n. 2, p. 125–137, May 2009. ISSN 1570-6478. Disponível em: <<http://dx.doi.org/10.1007/s12053-008-9037-3>>.

KOZIEL, S.; CIAURRI, D. E.; LEIFSSON, L. Surrogate-based methods. In: _____. *Computational Optimization, Methods and Algorithms*. Berlin, Heidelberg: Springer Berlin Heidelberg, 2011. p. 33–59. ISBN 978-3-642-20859-1. Disponível em: <https://doi.org/10.1007/978-3-642-20859-1_3>.

LEAL, L. d. C. M.; ROSA, E. da; NICOLAZZI, L. C. *Uma introdução à modelagem quase-estática de automóveis*. Florianópolis, Brasil: Publicação interna do GRANTE/UFSC, 2012.

LEE, H.; KIM, H. Improvement in fuel economy for a parallel hybrid electric vehicle by continuously variable transmission ratio control.

- Proceedings of the Institution of Mechanical Engineers, Part D: Journal of Automobile Engineering*, v. 219, n. 1, p. 43–51, 2005. Disponível em: <<http://dx.doi.org/10.1243/095440705X6514>>.
- LI, S. E. et al. Performance enhanced predictive control for adaptive cruise control system considering road elevation information. *IEEE Transactions on Intelligent Vehicles*, v. 2, n. 3, p. 150–160, Sept 2017. ISSN 2379-8858.
- LIN, X.; GÖRGES, D.; LIU, S. Eco-driving assistance system for electric vehicles based on speed profile optimization. In: *2014 IEEE Conference on Control Applications (CCA)*. [S.l.: s.n.], 2014. p. 629–634. ISSN 1085-1992.
- LUIN, B.; PETELIN, S.; MANSOUR, F. A. Modeling the impact of road network configuration on vehicle energy consumption. *Energy*, v. 137, n. Supplement C, p. 260 – 271, 2017. ISSN 0360-5442. Disponível em: <<http://www.sciencedirect.com/science/article/pii/S0360544217311386>>.
- MA, Z.-D.; PERKINS, N. C. An efficient multibody dynamics model for internal combustion engine systems. *Multibody System Dynamics*, v. 10, n. 4, p. 363–391, 2003. ISSN 1573-272X. Disponível em: <<http://dx.doi.org/10.1023/A:1026276619456>>.
- MATSUMOTO, S.; PARK, T.; KAWASHIMA, H. A comparative study on fuel consumption reduction effects of eco-driving instructions strategies. *International Journal of Intelligent Transportation Systems Research*, v. 12, n. 1, p. 1–8, Jan 2014. ISSN 1868-8659. Disponível em: <<https://doi.org/10.1007/s13177-013-0066-8>>.
- MATTARELLI, E.; CANTORE, G.; RINALDINI, C. A. Advances in the design of two-stroke, high speed, compression ignition engines, advances in internal combustion engines and fuel technologies. 2013. Disponível em: <<http://www.intechopen.com/books/advances-in-internal-combustion-engines-and-fuel-technologies/advances-in-the-design-of-two-stroke-high-speed-compression-ignition-engines>>.
- MERKER, G. P. et al. Engine combustion. In: _____. *Simulating Combustion: Simulation of combustion and pollutant formation for engine-development*. Berlin, Heidelberg: Springer Berlin Heidelberg, 2006. p. 60–97. ISBN 978-3-540-30626-9. Disponível em: <http://dx.doi.org/10.1007/3-540-30626-9_4>.
- MILES, S. R.; GHANDHI, J. B. Investigation of reactivity-controlled compression ignition combustion in a two-stroke engine. *Proceedings of the Institution of Mechanical Engineers, Part D: Journal of Automobile Engineering*, v. 230, n. 13, p. 1835–1848, 2016. Disponível em: <<http://dx.doi.org/10.1177/095440701562455>>.

- MOZHAROVSKII, V. V. et al. Determination of resistance to rolling of tires in dependence on operating conditions. part 1. method of multifactorial experiment. *Journal of Friction and Wear*, v. 28, n. 2, p. 154–161, Apr 2007. ISSN 1934-9386. Disponível em: <<http://dx.doi.org/10.3103/S1068366607020055>>.
- NAUNHEIMER, H. et al. Mediating the power flow. In: _____. *Automotive Transmissions: Fundamentals, Selection, Design and Application*. Berlin, Heidelberg: Springer Berlin Heidelberg, 2011. p. 73–99. ISBN 978-3-642-16214-5. Disponível em: <https://doi.org/10.1007/978-3-642-16214-5_3>.
- NAVIDI, P. W. *Statistics for Engineers and Scientists*. [S.l.]: McGraw-Hill Education, 2014. ISBN 9780073401331.
- PACEJKA, H. B. Chapter 4 - semi-empirical tyre models. In: PACEJKA, H. B. (Ed.). *Tyre and Vehicle Dynamics (Second Edition)*. Second edition. Oxford: Butterworth-Heinemann, 2006. p. 156 – 215. ISBN 978-0-7506-6918-4. Disponível em: <<http://www.sciencedirect.com/science/article/pii/B9780750669184500046>>.
- PATEL, D. Cvt cyber bulletin board study. In: *SAE Technical Paper*. SAE International, 2006. Disponível em: <<http://dx.doi.org/10.4271/2006-01-1311>>.
- PETERS, B.; NILSSON, L. Modelling the driver in control. In: _____. *Modelling Driver Behaviour in Automotive Environments: Critical Issues in Driver Interactions with Intelligent Transport Systems*. London: Springer London, 2007. p. 85–104. ISBN 978-1-84628-618-6. Disponível em: <https://doi.org/10.1007/978-1-84628-618-6_5>.
- PICA, G. et al. Dry dual clutch torque model with temperature and slip speed effects. *Intelligent Industrial Systems*, v. 2, n. 2, p. 133–147, Jun 2016. ISSN 2199-854X. Disponível em: <<https://doi.org/10.1007/s40903-016-0049-6>>.
- RAJAMANI, R. Longitudinal vehicle dynamics. In: _____. *Vehicle Dynamics and Control*. Boston, MA: Springer US, 2006. p. 95–122. ISBN 978-0-387-28823-9. Disponível em: <http://dx.doi.org/10.1007/0-387-28823-6_4>.
- RÉSHETOV, L. *Mecanismos auto-alineadores: Manual del constructor*. Mir, 1988. ISBN 9785030006253. Disponível em: <<https://books.google.com.br/books?id=LKYrAgAACAAJ>>.
- RICARDO, M.-B.; APOSTOLOS, P.; YANG, M. Overview of boosting options for future downsized engines. *Science China Technological Sciences*,

v. 54, n. 2, p. 318–331, Feb 2011. ISSN 1862-281X. Disponível em: <<http://dx.doi.org/10.1007/s11431-010-4272-1>>.

RODEMANN, T. et al. Many-objective optimization of a hybrid car controller. In: _____. *Applications of Evolutionary Computation: 18th European Conference, EvoApplications 2015, Copenhagen, Denmark, April 8-10, 2015, Proceedings*. Cham: Springer International Publishing, 2015. p. 593–603. ISBN 978-3-319-16549-3. Disponível em: <http://dx.doi.org/10.1007/978-3-319-16549-3_48>.

RODEMANN, T.; NISHIKAWA, K. Can evolutionary algorithms beat dynamic programming for hybrid car control? In: _____. *Applications of Evolutionary Computation: 19th European Conference, EvoApplications 2016, Porto, Portugal, March 30 – April 1, 2016, Proceedings, Part I*. Cham: Springer International Publishing, 2016. p. 789–802. ISBN 978-3-319-31204-0. Disponível em: <http://dx.doi.org/10.1007/978-3-319-31204-0_50>.

RYU, W. et al. Performance analysis of a cvt clutch system for a hybrid electric vehicle. *International Journal of Automotive Technology*, v. 10, n. 1, p. 115–121, 2009. ISSN 1976-3832. Disponível em: <<http://dx.doi.org/10.1007/s12239-009-0014-4>>.

SAE, J. I. R. *Vehicle Dynamics Terminology*. Warrendale, PA, 1976.

SAE, J. I. R. *Hybrid Vehicle (HEV) and Electric Vehicle Terminology*. Warrendale, PA, 2007.

SAERENS, B.; DIEHL, M.; BULCK, E. Van den. Optimal control using pontryagin's maximum principle and dynamic programming. In: _____. *Automotive Model Predictive Control: Models, Methods and Applications*. London: Springer London, 2010. p. 119–138. ISBN 978-1-84996-071-7. Disponível em: <https://doi.org/10.1007/978-1-84996-071-7_8>.

SANDOVAL, G. *G1 andou no novo Fiat Mille Economy*. 2008. Disponível em: <<http://g1.globo.com/Noticias/Carros/0,,MUL740235-9658,00-G+ANDOU+NO+NOVO+FIAT+MILLE+ECONOMY.html>>.

SCHULTZE, A.; LIENKAMP, M. Potential of an improved energy efficiency in the chassis. *Automotive and Engine Technology*, v. 1, n. 1, p. 15–25, Dec 2016. ISSN 2365-5135. Disponível em: <<http://dx.doi.org/10.1007/s41104-016-0009-x>>.

SERRARENS, A.; VELDPAUS, F. *Powertrain control of a flywheel assisted driveline with CVT*. Eindhoven: Technische Universiteit Eindhoven, 1999.

SHAO, Y.; SUN, Z. Robust eco-cooperative adaptive cruise control with gear shifting. In: *2017 American Control Conference (ACC)*. [S.l.: s.n.], 2017. p. 4958–4963.

SHARMA, T. K.; RAO, G. A. P.; MURTHY, K. M. Homogeneous charge compression ignition (hcci) engines: A review. *Archives of Computational Methods in Engineering*, v. 23, n. 4, p. 623–657, Dec 2016. ISSN 1886-1784. Disponível em: <<http://dx.doi.org/10.1007/s11831-015-9153-0>>.

SON, J. et al. Comparative study between korea and uk: relationship between driving style and real-world fuel consumption. *International Journal of Automotive Technology*, v. 17, n. 1, p. 175–181, Feb 2016. ISSN 1976-3832. Disponível em: <<https://doi.org/10.1007/s12239-016-0017-x>>.

STOTSKY, A. A. Engine friction estimation at start. In: _____. *Automotive Engines: Control, Estimation, Statistical Detection*. Berlin, Heidelberg: Springer Berlin Heidelberg, 2009. p. 85–98. ISBN 978-3-642-00164-2. Disponível em: <https://doi.org/10.1007/978-3-642-00164-2_5>.

SUN, D.; LUO, Y.; QIN, D. Integrated control strategy for cvt powertrains with consideration of vehicle drivability. *Chinese Journal of Mechanical Engineering*, v. 25, n. 3, p. 515–523, May 2012. ISSN 1000-9345. Disponível em: <<http://dx.doi.org/10.3901/CJME.2012.03.515>>.

TING, L. W. *Cars on a diet : the material and energy impacts of passenger vehicle weight reduction in the U.S.* Tese (Doutorado), Massachusetts, USA, 2010.

TRANSPORTATION, O. of; QUALITY, A. *Where the Energy Goes: Gasoline Vehicles*. [S.l.], 1995. Disponível em: <<http://www.fueleconomy.gov/feg/atv.shtml>>. Acesso em: 04 jul. 2017.

U.S. ENVIRONMENTAL PROTECTION AGENCY. *Fuel Economy Guide - Model Year 2017*. [S.l.], 2017. Disponível em: <<https://www.fueleconomy.gov/feg/pdfs/guides/FEG2017.pdf>>. Acesso em: 06 jul. 2017.

VOORT, M. van der; DOUGHERTY, M. S.; MAARSEVEEN, M. van. A prototype fuel-efficiency support tool. *Transportation Research Part C: Emerging Technologies*, v. 9, n. 4, p. 279 – 296, 2001. ISSN 0968-090X. Disponível em: <<http://www.sciencedirect.com/science/article/pii/S0968090X00000383>>.

WEIR, D. H.; CHAO, K. C. Review of control theory models for directional and speed control. In: _____. *Modelling Driver Behaviour in Automotive*

Environments: Critical Issues in Driver Interactions with Intelligent Transport Systems. London: Springer London, 2007. p. 293–311. ISBN 978-1-84628-618-6. Disponível em: <https://doi.org/10.1007/978-1-84628-618-6_17>.

WONG, V. W.; TUNG, S. C. Overview of automotive engine friction and reduction trends—effects of surface, material, and lubricant-additive technologies. *Friction*, v. 4, n. 1, p. 1–28, Mar 2016. ISSN 2223-7704. Disponível em: <<https://doi.org/10.1007/s40544-016-0107-9>>.

WU, G.; ZHANG, X.; DONG, Z. Powertrain architectures of electrified vehicles: Review, classification and comparison. *Journal of the Franklin Institute*, v. 352, n. 2, p. 425 – 448, 2015. ISSN 0016-0032. Special Issue on Control and Estimation of Electrified vehicles. Disponível em: <<http://www.sciencedirect.com/science/article/pii/S0016003214001288>>.

XU, S. et al. Instantaneous feedback control for a fuel-prioritized vehicle cruising system on highways with a varying slope. *IEEE Transactions on Intelligent Transportation Systems*, v. 18, n. 5, p. 1210–1220, May 2017. ISSN 1524-9050.

ZHANG, Y.; ZHAO, H. Investigation of combustion, performance and emission characteristics of 2-stroke and 4-stroke spark ignition and cai/hcci operations in a {DI} gasoline. *Applied Energy*, v. 130, p. 244 – 255, 2014. ISSN 0306-2619. Disponível em: <<http://www.sciencedirect.com/science/article/pii/S0306261914005315>>.

ZHENG, C. et al. An energy management approach of hybrid vehicles using traffic preview information for energy saving. *Energy Conversion and Management*, v. 105, n. Supplement C, p. 462 – 470, 2015. ISSN 0196-8904. Disponível em: <<http://www.sciencedirect.com/science/article/pii/S0196890415007128>>.

ZHENG, C. H.; LIM, W. S.; CHA, S. W. Performance optimization of cvt for two-wheeled vehicles. *International Journal of Automotive Technology*, v. 12, n. 3, p. 461–468, 2011. ISSN 1976-3832. Disponível em: <<http://dx.doi.org/10.1007/s12239-011-0054-4>>.

Appendix

APPENDIX A – CHARACTERISTICS OF VEHICLES

Manufacturer	Model	Specification	Transmission	Gears	Mileage [km/ℓ]	CO2 [g/km]
Honda	Fit	DX	CVT	10	12.30	102
Fiat	Punto	Essence Dualogic	MTA	5	9.50	131
Hyundai	HB20	Plus	A	6	9.90	121
MINI	Cooper	SP	A	6	11.60	110
Nissan	New March	SV	CVT	10	11.70	104
Peugeot	208	Griffe	A	4	11.70	109
Peugeot	208	Griffe	A	6	11.00	112
Renault	Sandero	Expression	MTA	5	11.80	108
Toyota	Erios Hatchback	XLS	A	4	11.90	107
VW	Gol	Comfortline 15	MTA	5	11.10	112
VW	Fox	Comfortline I-Motion	MTA	5	11.20	113
AUDI	A1 Sportback	Attraction	DCT	7	12.60	97
BMW	120i	ActiveFlex	A	8	9.60	126
Chevrolet	Cobalt	LTZ	A	6	11.10	108

Chevrolet	Spin	LT ADV(SL)	A	6	10.10	114
Ford	New Fiesta Sedan	SEL	DCT	6	11.10	109
Honda	City	DX	CVT	10	12.30	101
Hyundai	HB20s	Plus	A	6	10.20	120
Lexus	CT200H	CT200H	HCVT	10	15.70	86
Mercedes-Benz	A200 FF		DCT	7	10.80	112
Nissan	New Versa	SV	CVT	10	11.60	106
Renault	Logan	Dynamique	MTA	5	11.80	106
Toyota	Etiós Sedã	XLS	A	4	12.20	100
VW	Up	Cross (I-motion)	MTA	5	13.30	96
Chevrolet	Novo Onix	L7Z	A	6	11.70	105
Citroen	C3	Exclusive	A	4	11.00	115
Fiat	Novo Palio	Sporting Dualogic	MTA	5	11.60	128
VW	Voyage	Comfortline 15	MTA	5	11.20	110
VW	Spacefox	Comfortline I-motion	MTA	5	11.10	111
Volvo	V40	CC T4 Kinetic	A	6	10.40	119
Audi	A3 Cabriolet		DCT	7	9.90	127
Chevrolet	Novo Cruze Turbo	L7Z	A	6	11.20	108
Citroen	C4 Lounge Turbo	THP origine	A	6	10.50	115
Honda	Civic	Sport	CVT	10	10.50	116

Honda	CR-V	EXL 4WD	A	5	9.20	135
Fiat	500	Cult Cabrio Dualogic	MTA	5	11.40	111
Fiat	Mobi	Drive GSR	MTA	5	14.00	89
Kia	Picanto	EX4	A	4	11.30	109
Fiat	Novo Uno	Sporting Dualogic	MTA	5	13.20	98.00
Audi	RS3		DCT	7	8.00	159.00
BMW	225i	CAT Active Flex	A	8	10.20	121.00
Citroen	DS 4 Turbo	So Chic	A	6	9.90	125.00
Fiat	Grand Siena	Essence Dualogic	MTA	5	9.60	129.00
Mercedes-Benz	A250	Sport	DCT	7	10.10	123.00
Mercedes-Benz	AMG A 45 4M		DCT	7	8.40	144.00
Subaru	Imprenza	XV	CVT	10	9.60	130.00
Toyota	Prius	NGA	HCVT	10	18.90	71.00
VW	Golf TSI	Highline	A	6	11.30	109.00
VW	Golf TSI		DCT	6	10.20	122.00
Volvo	V40	T4 Inscription	DCT	6	9.60	127.00

Legend of the Table:

- A: Automatic
- DCT: Dual Clutch
- CVT: Continuously variable Transmission
- HCVT: Hybrid CVT
- MTA: Manual Transmission

APPENDIX B – EQUATIONS FOR THE ENGINE CRANKSHAFT’S DYNAMICS

Consider an internal combustion engine with a reciprocating crank-slide mechanism as shown in Figure 64. The joints are classified according to the method presented by (RÉSHETOV, 1988) in order to identify the mobility of the mechanism.

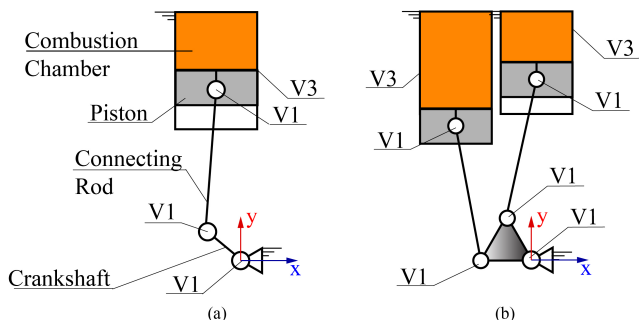


Figure 64 – (a) Structural representation of the crank-slid mechanism of an ICE; (b) Schematic of a plane mechanism for an ICE with 2 cylinders.

From the mechanism's theory, the mobility M of a given structure is defined by

$$M = (n - j - 1) \lambda + j \quad (\text{B.1})$$

where n is the number of elements, j the number of joints and λ the order of the screw system. For a plan mechanism, $\lambda = 3$ and, for both schematics of Figure 64, the mobility yields to 1. This property corresponds to the minimum number of coordinates that are necessary to define the position of all the components and, consequently, to the number of Degrees of Freedom (DoF).

For an ICE, most of the events are functions of the crankshaft angle, e.g. start of injection and spark, which can be used as the minimum coordinate. Adopting the kinematic model described in (MA; PERKINS, 2003), considering the schematic in Figure 12, the following equations are obtained:

- The angle between the connecting rod and vertical direction:

$$\phi = \sin^{-1} \left(\frac{L_c \sin(\theta_c) - h}{L_R} \right) \quad (\text{B.2})$$

- For the position of connecting rod's the center of gravity:

$$\begin{aligned} x_R &= -L_c \sin(\theta_c) + L_{R,G} \sin(\phi) \\ y_R &= L_c \cos(\theta_c) + L_{R,G} \cos(\phi) \end{aligned} \quad (\text{B.3})$$

- For the vertical position of the piston:

$$y_p = L_c \cos(\theta_c) + L_R \cos(\phi) \quad (\text{B.4})$$

In order to obtain the equations of Euler-Lagrange of 2^{nd} kind, it is necessary to describe the kinetic energy of each element of the mechanism. The piston presents only a linear displacement in the vertical direction, therefore, its kinetic energy is given by

$$T_P^* = \frac{1}{2} M_P \dot{y}_p^2 \quad (\text{B.5})$$

where \dot{y}_p is the time derivative of the position of the piston. The connecting rod presents translation in both x and y axes and also rotates around the z axis with respect to its center of mass. Hence, its total kinetic energy is given by

$$T_R^* = \frac{1}{2} \left[M_R \left(\dot{x}_R^2 + \dot{y}_R^2 \right) + J_R \dot{\phi}^2 \right] \quad (\text{B.6})$$

At last, the crankshaft presents only one rotation and its kinetic energy is defined by

$$T_C^* = \frac{1}{2} J_C \dot{\theta}_C^2 \quad (\text{B.7})$$

Hence, the total kinetic energy of the system is described by

$$T_{tot}^* = \frac{1}{2} \left[M_P \dot{y}_P^2 + M_R (\dot{x}_R^2 + \dot{y}_R^2) + J_R \dot{\phi}^2 + J_C \dot{\theta}_C^2 \right] \quad (\text{B.8})$$

Substituting the Equations (B.2), (B.3) and (B.4) into (B.8), with proper arithmetic manipulation, the total kinetic energy becomes a function of a single variable, given by

$$T_{tot}^*(\theta_C) = \frac{1}{2} \dot{\theta}_C^2 (J_c + \tau(\theta_C)) \quad (\text{B.9})$$

where τ is

$$\begin{aligned} \tau = & J_R \left[\frac{(L_c \cos(\theta_c))^2}{L_R^2 - (L_c \sin(\theta_c) - h)^2} \right] + m_R \left[\frac{L_c^2}{L_R^2} \cos^2(\theta_c) (L_{R,G} - \right. \\ & \left. L_R)^2 + L_c^2 \left[\sin(\theta_c) + \frac{L_{R,G} \cos(\theta_c) (L_R \sin(\theta_c) - h)}{L_R \sqrt{L_R^2 - (L_c \sin(\theta_c) - h)^2}} \right]^2 \right] + \quad (\text{B.10}) \\ & M_P L_c^2 \left[\sin(\theta_c) + \frac{\cos(\theta_c) (L_R \sin(\theta_c) - h)}{\sqrt{L_R^2 - (L_c \sin(\theta_c) - h)^2}} \right] \end{aligned}$$

The Equation (B.10) is valid only for engines with a single cylinder and the effects of further components connected to the crankshaft, are neglected. However, the addition of further cylinder requires few changes in the presented formulation. As shown in Figure 65, considering one piston as reference, the further ones present a shift on the crankshaft angle, here defined as

$$\theta_j = \theta_c + S_{\theta,j} \quad (\text{B.11})$$

where θ_c is the reference crankshaft angle and $S_{\theta,j}$ is the shift angle for the cylinder j .

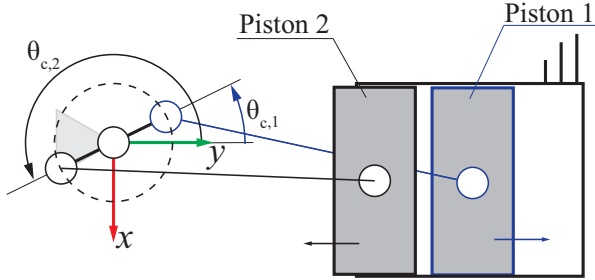


Figure 65 – Schematic of a crank-slide mechanism with multiple prismatic joints and their respective crankshaft angles for a given position.

Summing the contribution of all the N_{cyl} cylinders, the equation for the kinetic energy yields to

$$T_{tot}^* = \frac{1}{2} \dot{\theta}_c^2 \left(J_c + \sum_{j=1}^{N_{cyl}} \tau(\theta_j) \right) \quad (\text{B.12})$$

According to the Euler-Lagrange approach, the lagrangian operator is defined as

$$\mathcal{L} = T_{tot}^* - V_{tot} \quad (\text{B.13})$$

where V_{tot} is the total potential energy of the system. Since the modeled system only presents reservoirs of kinetic energy, the lagrangian corresponds to the total kinetic energy.

The Euler-Lagrange equations of second kind are given by

$$\frac{d}{dt} \frac{\partial \mathcal{L}(Q, \dot{Q})}{\partial \dot{q}_k} - \frac{\partial \mathcal{L}(Q, \dot{Q})}{\partial q_k} = \mathbf{F}_k - \mathbf{D}_k \quad (\text{B.14})$$

where Q is the vector of minimum generalized coordinates q_k , \mathbf{F}_k is the vector of forces and \mathbf{D}_k the dissipation function applied to the element k . Since the

developed model has only one generalized coordinate, the Equation (B.14) applied to the engine can be written as

$$\frac{d}{dt} \frac{\partial T_{tot}^*}{\partial \dot{\theta}_c} - \frac{\partial T_{tot}^*}{\partial \theta_c} = \mathbf{F}_c - \mathbf{D}_c \quad (\text{B.15})$$

Given that $\tau = f(\theta_c(t))$, then

$$\frac{d}{dt} (T_{tot}^*) = \frac{\partial T_{tot}^*}{\partial \theta_c} \dot{\theta}_c \quad (\text{B.16})$$

Hence, the Equation (B.15) can be simplified to

$$\ddot{\theta}_c \left[J_c + \sum_{j=1}^{N_{cyl}} \tau(\theta_j) \right] + \frac{1}{2} \dot{\theta}_c^2 \sum_{j=1}^{N_{cyl}} \left[\frac{\partial \tau(\theta_j)}{\partial \theta_c} \right] = \mathbf{F}_c - \mathbf{D}_c \quad (\text{B.17})$$

where the derivative of τ with respect to the crankshaft angle is given by

$$\begin{aligned} \frac{\partial \tau(\theta_j)}{\partial \theta_c} = 2 L_c^2 \left\{ \frac{J_R \cos(\theta_j)}{L_R^3 \cos^4(\phi_j)} [L_C \cos^2(\theta_j) \sin(\phi_j) - \right. \\ \left. L_R \cos^2(\phi_j) \sin(\theta_j)] + m_R \left[\left[\sin(\theta_j) + \frac{L_{R,G}}{L} \right. \right. \right. \\ \left. \left. \cos(\theta_j) \tan(\phi_j) \right] \left[\cos(\theta_j) + \frac{L_{R,G}}{L_R} \left(\frac{L_C \cos^2(\theta_j)}{L_R \cos^3(\phi_j)} - \right. \right. \right. \\ \left. \left. \left. \sin(\theta_j) \tan(\phi_j) \right) \right] - \cos(\theta_j) \sin(\theta_j) \left[\frac{L_{R,G}}{L_R} - 1 \right]^2 \right] \\ \left. + m_P [\sin(\theta_j) + \cos(\theta_j) \tan(\phi_j)] \left[\cos(\theta_j) - \right. \right. \\ \left. \left. \sin(\theta_j) \tan(\phi_j) + \frac{L_c \cos^2(\theta_j)}{L_R \cos^3(\phi_j)} \right] \right\} \quad (\text{B.18}) \end{aligned}$$

The terms of force and energy dissipation depend on the purpose of the simulation. If the torque is considered as a function of the pressure inside the

combustion chamber, the dissipative forces due to friction and pumping losses have to be considered. However, if the brake torque is considered, the internal power losses are already considered and the term \mathbf{D}_c yields to zero.

In order to verify the consistency of the equations, an equivalent model of a 4-cylinder engine was created using Adams™View, which is shown in Figure 66. The geometric properties were based on the engine "Model 20 Intek", manufactured by Briggs& Stratton, and the inertial specifications calculated directly with ADAMS/View, as listed in Table 19. The crankshaft was suppressed and its inertia added to the flywheel's, in order to simplify the modeling task.

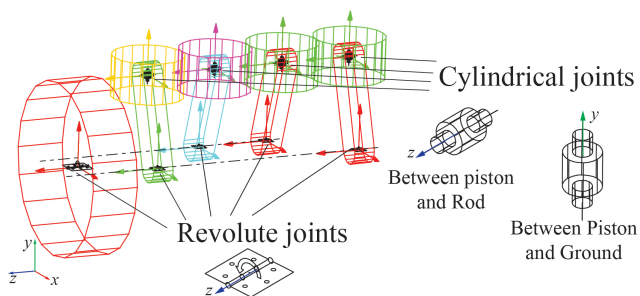


Figure 66 – ADAMS Model

Table 19 – Geometric and inertial properties of the reference engine model

Geometry	Value
Crankshaft radius	33 mm
Connecting Rod length	200 mm
Position of the Rod CG	50%
Piston Radius	39.5 mm
Offset	0 mm
Crankshaft angle shift	0 / -540° / -180° / -360°
Inertial	Value
Inertia of Crankshaft and Flywheel	$5.17 \times 10^{-2} \text{ kg m}^2$
Mass of the Rod	0.628kg
Inertia of the Rod	$8.29 \times 10^{-4} \text{ kg m}^2$

The conditions assumed to simulate the mechanism and configuration

of both solvers are listed in Table 20. In order to verify the dynamic and kinematic responses, the results withdrawn from the simulations are the evolution of the flywheel's angular velocity and the positions of the piston and the connecting rod's center of mass over time.

Table 20 – Parameters adopted for the simulations in Simulink and Adams/View

Conditions	
Constant net torque at the Flywheel	45 N m
Initial angular velocity	83.77 rad/s (800 rpm)
Duration	2.5 s
Simulink Solver Configurations	
Solver	ODE45 (Dormand-Prince)
Maximum allowed time-step	1×10^{-4} s
Type	Variable-step
Adams/View Solver Configurations	
Simulation type	Dynamic
Solver	GSTIFF
Formulation	SI2
Maximum allowed time-step	1×10^{-4} s

As observed in Figure 67, the difference between the results is roughly the same during the simulation, achieving the maximum of 0,85% at 460 rad/s. The shift in the phase of the angular velocity can be explained by the small differences in the values of mass and inertia, since in Adams™ these properties are calculated based on the geometry and material of the parts and the values adopted for the model in Matlab™ were truncated with lower precision. Similarly, both models provided similar results of piston and connecting rod motions, as shown in Figures 68 and 69.

The same procedure was repeated for cases with reduced number of cylinders and the models converged to similar results as well. Besides the difference of behavior in those cases, it was also noticed higher sensibility to variations of the crankshaft's inertia than the case presented above, which was expected, since the contribution of this part becomes more relevant if other components are removed.

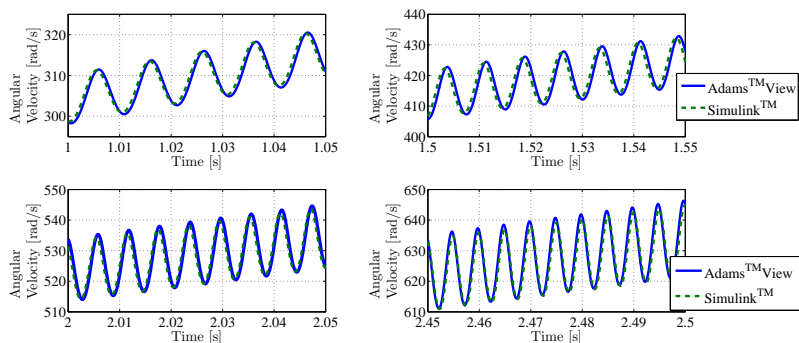


Figure 67 – Results of angular velocity calculated using Adams™View and Simulink™ in different time intervals of the simulation.

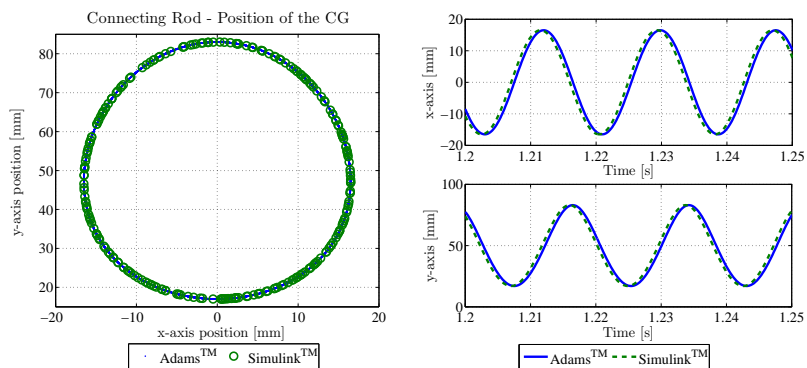


Figure 68 – On the left, the position of the connecting rod's center of gravity is shown as a function of its coordinates. On the right, it is shown the behavior of the coordinates x and y within a time interval

Hence, given the proximity of the presented results, the proposed model is considered capable to represent the dynamics of a reciprocating engine with multiple cylinders. The limitations of the model are the input of force, which was proposed as the torque at the crankshaft, demanding the conversion of the pressure inside the chamber. Furthermore, the power sinks were not explored in this text and, depending on the application, the equations describing the related phenomena should be added to the model.

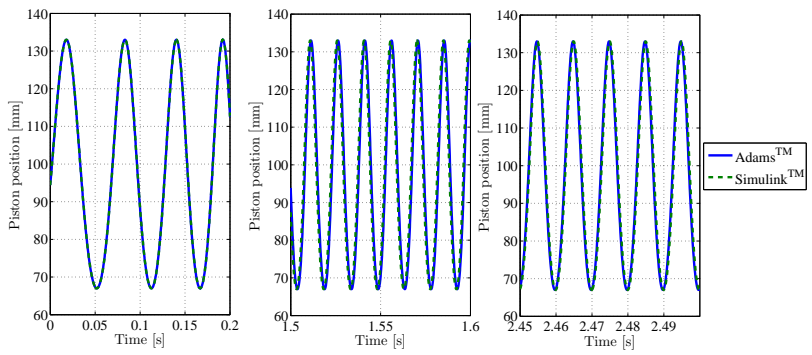


Figure 69 – Position of the piston represented as a function of the simulation time